University of Wisconsin-Madison

Space Science and Engineering Center

NPOESS/IPO Contract 50-SPNA-1-00039

Henry E. Revercomb, PI

Co-Investigators:

Steven Ackerman

Robert O. Knuteson

David C. Tobin

Paolo Antonelli

Fred A. Best

Report

Government Study in Support of a Broad Scope of NPOESS Calibration and Validation Activities

Reporting Period: September 27, 2001 through December 31, 2003

March 24, 2004

Submitted to:

NPOESS Integrated Program Office

United States Department of Commerce, NOAA

8455 Colesville Road, Suite 1450

Silver Spring, MD 20910-3320

Attn: Don Kraus (Don.Kraus@noaa.gov), Contracting Officer

Steve Mango (Stephen.Mango@noaa.gov), COTR

Table of Contents

Government Study in Support of a Broad Scope of NPOESS Calibration and Validation Activities

1. Introduction

This report summarizes the accomplishments from work performed under the Internal Government Study, NPOESS/IPO Contract 50-SPNA-1-00039, for three funding periods including; the initial funding installment extending from 1 October 2001 to 31 May 2002, modification #1 extending from 1 June 2002 to 31 May 2003, and finally modification #2 extending from 1 June 2003 to December 31 2003. For easy reference, the Statements of Work for each of these periods are included as Appendix A.

The report begins with a brief Executive Summary (Section 2) that reviews our project and the key results to date. Section 3 is a more extended description of our accomplishments organized by task category. This more complete section also includes references inside each subsection to relevant papers from our group that were at least partially funded by this contract. In addition, several key papers are included in their entirety in Appendix B, and Appendix C contains a more complete Bibliography of our papers.

A separate document contains our continuation proposal for the period from 1 January 2004 to 31 December 2004. That proposal defines recommendations and planned tasks for further study.

2. Executive Summary

This section summarizes the overall purpose of the effort, describes the basic nature of the study and our connections with other government studies, and concludes with an enumeration of the key results of our work to date. The extensive heritage for our work in this area is described in our proposal and is not repeated here. As outlined in the introduction, more extended information is contained in Section 3, broken down into the eight Task Areas of the original proposal.

2.1 Purpose

Our general goal is to provide expertise to IPO that reduces schedule, cost, and performance risk and leads to the increased positive impact of NPOESS. More specifically, our purpose is to:

1. Make use of broad experience in instrument design, testing, algorithm, and science gained from previous and ongoing UW-SSEC developments to evaluate contractor approaches and results, and to offer alternatives;
2. Provide, maintain, and field high spectral resolution aircraft instruments capable of generating atmospheric data for forward model improvement, calibration and product retrieval algorithm development, development and testing of future instrument enhancement concepts, and NPOESS validation; and
3. Make use of the calibration advantages offered by high spectral resolution to unify NPOESS IR calibration of CrIS, VIIRS & ERBS, among NPOESS platforms, and with other systems.

2.2 Description of the Study

A broad range of NPOESS Calibration and Validation activities for the Cross-track Infrared Sounder (CrIS), with a special focus on applications of the NPOESS Airborne Sounder Testbed (NAST) and the UW Scanning High-resolution Interferometer Sounder (S-HIS) aircraft instruments are encompassed in this study. Activities include providing support for Cal/Val planning, instrument reviews, pre-flight testing and performance evaluation, post-flight radiometric and product performance verification, and Sounder Operational Algorithm Team (SOAT) activities. Both before and after launch, we plan to help conduct aircraft instrument field campaigns, to process data, to analyze results, to provide data for other investigators, and to maintain the calibration of NAST and S-HIS in order to verify and improve analysis techniques, as well as to perform direct CrIS validation. In addition, we plan to help implement a unified NPOESS IR calibration, define future system enhancements, and train the next generation.

These efforts have been closely coordinated with other related Internal Government Studies focusing on the CrIS Sounder, the VIIRS imager, and general forward radiative transfer model work. Special relationships exist with Bill Smith who coordinates the aircraft validation activities and the use of the NAST-I, Dave Staelin who leads the effort with NAST-M, Allen Larar who is the Chair of the Sounder Operational Algorithm Team (SOAT), Paul Menzel and Chris Moeller who are key members of the VIIRS government team, Joe Rice who represents the NIST transfer radiometer (TXT, FTXR) expertise, and with Larrabee Strow and Tony Clough for forward model work.

2.3 Key Accomplishments

We believe that our efforts in this study to date have made major contributions to reducing schedule and cost risk for the NPOESS CrIS program and to ultimately realizing better products. The key results are enumerated below. The contract Task Category defined in Section 3 is referenced in parentheses to make access to the full discussion easier.

1. Discovered a serious CrIS optical design problem that would have led to a large violation of the noise performance spec from vibration related interferometric errors and defined the mechanism based on concepts studied with S-HIS (Task Category 1);
2. Offered possible approaches to fix the problem in 1 through a process with ITT/ABB Bomem and others that resulted in the incorporation of a tilt correction for tilt-induced sample-position errors, and a vibration isolation system (Task Category 6);
3. Defined and implemented several aircraft instrument improvements, including substantial tilt noise reduction on NAST from dynamic alignment adjustments in combination with the UW static tilt electrical adjustment circuit, reduction of aerodynamic buffeting using specially designed closeouts inside pod, tilt correction methods to remove vibration induced interferometric errors (implementation still in progress), reduction of ambient blackbody temperature with addition of fan and cooling fins (Task Category 3);
4. Devised a test of CrIS EDU2 that confirmed the mechanism for a dynamic alignment problem related to displaced reflections from wedged beamsplitter/compensator substrates (Task Category 1);
5. Participated in small group that prepared the initial NPOESS Calibration/Validation plan, and participated in subsequent large group efforts (Task Category 1);

6. Helped conduct six aircraft instrument campaigns, leveraging NASA and DOE field programs to collect data sets for forward model refinements, evaluating performance effects, and developing retrieval and validation techniques (Task Category 2);
7. Established a "data portal" to allow ready access to the extensive data sets from the aircraft field campaigns (Task Category 2);
8. Made forward model improvements to water vapor continua (MT_CKD1.0, where "T" is Tobin) and CO_2 line shapes, which have become part of the CrIS, NAST and S-HIS forward models through joint work with Tony Clough and Larrabee Strow (Task Category 5);
9. Demonstrated the ability to use aircraft observations from S-HIS for highly accurate validation of radiances from AIRS on Aqua (Task Category 4 and Appendix B, first paper);
10. Demonstrated application of AIRS high resolution sounder for accessing MODIS imager Response vs Scan-angle (RVS) dependence, a technique valuable for VIIRS (Task Category 4 and Appendix B, first paper);
11. Developed and demonstrated on-orbit spectral calibration technique for CrIS using S-HIS spectra (Task Category 4);
12. Conducted training and mentoring of a post-doc whose work upgraded our understanding of cavity emissivity modeling (Task Category 7); and
13. Provided in-the-field support for the NAST-I, ongoing blackbody and end-to-end NAST instrument calibration support, and instrument problem solving (Task Category 8).

3. Accomplishments by Task Category

The accomplishments under this Government Study are grouped into eight task categories;

1. CrIS Characterization and Calibration
2. Field Campaign and Analysis
3. Development and Implementation of Aircraft Instrument Performance Improvements
4. Algorithm Develop and Test
5. Forward Model Refinement
6. CrIS Instrument Evaluation
7. Training and Mentoring
8. UW NAST-I Support

The accomplishments within each of these tasks categories are described in detail in the following subsections.

3.1 CrIS Characterization and Calibration (Task Category 1) and CrIS Instrument Evaluation (Task Category 6)

Task categories 1 and 6 are closely related and will be discussed together. Under these tasks we provide consultation and recommendations to IPO on CrIS instrument test plans, results, and radiometric and spectral performance issues, including the establishment of traceability to NIST standards (Task Category 1), and instrument trades and design evolution options as they arise during the design, fabrication, and testing phases (Task Category 6). The overall goal is to provide program risk reduction by making use of our hands-on experience with similar

instruments. This experience, dating back to the development and flight of the High-resolution Interferometer Sounder (HIS) aircraft instrument (1983-1998), continues to grow as described under Tasks 3.2-3.4, thanks to the support of this contract.

Our interaction on these tasks revolves around meetings with the CrIS contractor, ITT/ABB Bomem, and the Sounder Operational Algorithm Team (SOAT). Participation in primary events since the start of the current contract (October 2001) is summarized in Table 1.

Table 1. Primary CrIS Events and Major Contribution Summary

Date	Event	Major Contribution
10, 11 October 2001	Calibration/Validation Plan	Plan definition leadership
22, 23 January 2002	Beamsplitter TIM & SRD CDR	Beamsplitter wedge issues
27, 28 February 2002	Detailed Design Review (DDR)	Tilt Susceptibility Identified
15 March 2002	SOAT	Tilt Presentation
26 June 2002	DDR Action Item Review	Tilt Susceptibility Fixes
13 September 2002	SOAT	Testing team lead- 2 areas
16 October 2002	PMR & Alignment data eval	Defined key test
19 November 2002	ITT Test Reviews-DA fix	
12, 13 June 2003	Calibration/Validation Plan	Plan definition leadership
28, 29 July 2003	SOAT	S-HIS/AIRS Comparisons
12 August 2003	Interferometer CDR	Spectral Cal Techniques
26-28 August 2003	CrIS Critical Design Review	Spectral Cal Techniques
9 December 2003	Calibration/Validation Review	Steps to Calibrate-presented
10 December 2003	EDU3 Test Readiness Review	Non-linearity & Noise

A primary accomplishment under task 3.1 occurred at the CrIS Detailed Design Review in February 2002. A major design problem was identified that would have caused a very large susceptibility to vibration for all off-axis pixels. The problem arose because of placement of the optical aperture stop in the aft telescope, some distance behind the interferometer. This aperture stop location causes the laser beam used for optical path delay (OPD) triggering to be off-center for beams from off-axis pixels, and leads to OPD sampling errors. These errors are linear in mirror tilt and cause much larger radiance errors than typical tilt-induced amplitude modulation errors (that depend on the square of the tilt). Our sensitivity to this issue stemmed directly from our experience with the Scanning HIS aircraft instrument, which employs a novel shared-aperture detector design choice (distinctly different from the NAST and CrIS aft-optics design). The effect is subtle enough that it would likely have been missed until substantially downstream when fixes would have been much more difficult and expensive.

S-HIS experience was also relevant to suggesting possible fixes to the problem (see 15 March 2002 SOAT presentation). Our involvement in instrument changes to deal with this problem fall under Task Category 6. The fixes discussed in June 2002 and later incorporated were: (1) using tilt measurements from the dynamical alignment system to adjust the IR beam time delay to cancel the effect; and (2) incorporating a vibration isolation system. The S-HIS does not have an active correction system, but does make accurate tilt measurements that have been used to demonstrate the principal of this correction approach. Of course, its vibration isolation system is necessary for operation in the high vibration environment of aircraft platforms.

Another CrIS design issue, drift of the dynamically aligned interferometer tilt, was discovered during EDU2 testing in 2002. This design issue was not anticipated and came as a big surprise to everyone who had worked with dynamically-aligned Bomem instruments for years. We became involved in October 2002 when possible explanations were being explored. We defined a test, which conclusively demonstrated that the cause was the suspected multiple reflections from the wedged beamsplitter. Bomem devised a simple fix.

Another theme in Task Category 1 is involvement in planning for Calibration and Validation (Oct 01, June 03, Dec 03). The events in Oct 01 and June 03 were sessions for enlarging the participation in writing the Government Cal/Val Plan, the first draft of which started with the efforts of a small group that we participated in.

These Cal/Val activities are very important for CrIS, both before and after launch. Before launch, activities include collecting atmospheric data and establishing a direct radiance connection to NIST-maintained standards, in addition to the normal interaction with the calibration/characterization of the instrument by the contractor. Acquiring atmospheric data sets is important for making sure that refined products are available soon after CrIS is in orbit. Field campaigns (Task Category 2) are conducted with the NAST and the S-HIS in conjunction with many other observations to collect the required atmospheric data for validation of the forward model (Task Category 5) and for refinement of approaches used in product derivation (Task Category 4). After launch, these same tools will be used to provide observations with higher spatial and spectral resolution to validate CrIS data and products directly. The long-term stability of CrIS for climate can be tested by periodically involving NIST in the validation of these aircraft instruments.

Results from evaluating S-HIS and NAST field experiment data sponsored by our IPO effort have already led to some significant contributions to the CrIS instrument work. The best example is the approach we have demonstrated for establishing the absolute spectral calibration from atmospheric data itself, a method which was raised at the Interferometer and overall CrIS CDRs (August 2003). Our results are being used to show that the CrIS absolute calibration will be excellent (<< 1 ppm from averaging many atmospheric comparisons with a single-sample standard deviation of about 1 ppm), and to model the techniques that will be used in CrIS processing. Other examples include the techniques we have developed for evaluating the impact of tilt on NEN and for non-linearity testing.

Clearly the activities under these tasks have made significant contributions to CrIS risk reduction and provide strong evidence for the value of our continuing Scanning HIS and NAST activities.

3.2 Field Campaign and Analysis

This Government Study conducted several aircraft instrument campaigns that leveraged NASA and DOE field programs to collect data sets for forward model refinements, evaluating performance effects, and developing retrieval and validation techniques. Table 2 shows the field campaigns for which UW provided support during the period of contract performance. The 2004 campaigns are in the planning stages.

Table 2.

NAST/S-HIS Field Campaigns

Year	Field Campaign	Location	IPO	NASA	DOE-ARM	Other
2002	IHOP	SGP	N	M S		
	CRYSTAL-FACE	Florida	N	M N		
	UAV-SGP	SGP	S		M S	
	TX-2002	SGP/ Gulf-Mex	N	M S		
2003	Pacific THORPEX	Hawaii	N S	M		
	Atlantic THORPEX	Maine	N S	M		
2004 plan	INTEX	Wallops Island	N S	M		
	ADRIEX	Italy	N S			M
	EAQUATE	UK	M N S			M
	MPACE	Alaska	S		M	

M = Mission, N = NAST support, S = S-HIS support

Description of activities and major results

a) IHOP 2002

The International H2O Project (IHOP-2002) is a field experiment that took place over the Southern Great Plains (SGP) of the United States from 13 May to 25 June 2002. The chief aim of IHOP-2002 was improved characterization of the four-dimensional (4-D) distribution of water vapor and its application to improving the understanding and prediction of convection. The region was an optimal location due to existing experimental and operational facilities, strong variability in moisture, and active convection." The IHOP project was organized by Dave Parsons of NCAR (among many others) with participation by NOAA NWS, NASA LaRC and Goddard, and the Department of Energy ARM program.

The UW participated both in support of NAST on the Proteus aircraft and under a NASA contract to fly the Scanning-HIS instrument onboard the NASA DC-8 aircraft to collect coincident observations with the NASA LaRC LASE dial lidar instrument. The summary of data collected by the S-HIS during eight IHOP missions is given in Table 3.

Table 3.

SUMMARY OF DATA COLLECTION DURING IHOP Scanning High-resolution Interferometer Sounder (SHIS)					
Flight Date (yymmdd)	**Sortie**	**Mission**	**Data Start (UTC)**	**Data End (UTC)**	**Flight Length (Hours)**
020523	02-0204	Ferry to Oklahoma City	1713	1940	2.5
020524	02-0205	Convective Initiation (CI)	1717	2244	5.5
020530	02-0206	ABL Water Vapor Heterogeneity and Water Vapor Budget	1722	2235	5.3
020602	02-0207	Nocturnal Low Level Jet (LLJ)	0224	0656	4.4
020603	02-0208	Convective Initiation (CI)	1740	2244	5.1
020609	02-0209	Nocturnal Low Level Jet (LLJ) & Convective Initiation (CI)	1329	2114	7.75
020611	02-0210	Convective Initiation (CI)	1640	2157	5.33
020614	02-0211	Boundary Layer Evolution and Transit to Dryden	1307	2126	8.25
				Total Flight Hours:	**43.13**

A key asset of the IHOP data set is the coincident Dial lidar water vapor profiling from the LASE instrument on the DC-8 with S-HIS.

More information on IHOP is available on the web.
The S-HIS homepage for this experiment can be found at http://deluge.ssec.wisc.edu/~shis/IHOP/. The official IHOP homepage can be found at http://www.atd.ucar.edu/dir_off/projects/2002/IHOP.html. Also, further information about the Scanning-HIS campaign during IHOP can be obtained from the following conference paper:

Knuteson, R., P. Antonelli, F. Best, S. Dutcher, W. Feltz, and H. Revercomb, 2003: Scanning High-resolution Interferometer Sounder (S-HIS) measurements during the International Water-Vapor Project (IHOP), *Proceedings of the 6th International Symposium on Tropospheric Profiling: Needs and Technologies*, September 14-20, 2003, Leipzig, Germany.

b) CRYSTAL-FACE
The UW participation under this contract during the NASA CRYSTAL-FACE mission involved the support of the NAST-I instrument data processing. This effort is described under "UW NAST-I Support", Section 3.8.

c) UAV-SGP

A unique dataset for validation technique and algorithm testing was collected in the fall of 2002 during the Unmanned Airborne Vehicle (UAV) campaign at the Department of Energy (DOE) Atmospheric Radiation Measurement (ARM) Southern Great Plains (SGP) site in North Central Oklahoma. The primary validation result was a very good comparison of S-HIS to the AIRS on Aqua on 16 November 2002. This contract supported analysis of the data from the campaign (support for conducting this field campaign was provided by the DOE ARM program).

This was the first deployment of the S-HIS instrument on the Scaled Composite's Proteus aircraft. The S-HIS was installed in a specially fabricated wing pod which allow uplooking zenith views to be intermixed with the normal downlooking cross-track scan. This uplooking data is proving very helpful in constraining the absolute calibration knowledge of the S-HIS instrument since the emission in the uplooking "microwindows" is very close to zero. An example of the observations from the uplooking and downlooking S-HIS from 14 km altitude is shown in Figure 1 below.

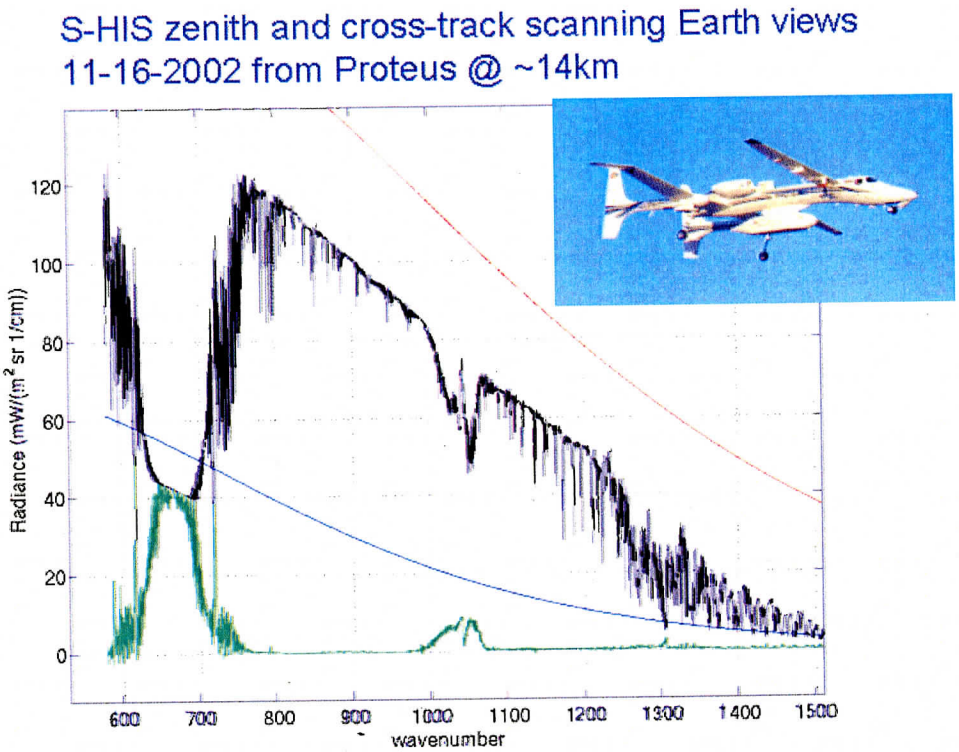

Figure 1. Scanning-HIS observations of up and down infrared emission at 14 km altitude.

d) TX-2002

The Terra-aqua eXperiment 2002 (TX-2002) was conducted from the former Kelly AFB in San Antonio, Texas from November 20 to December 13, 2002 to assess MODerate resolution Imaging Spectroradiometer (MODIS) and Atmospheric Infrared Sounder (AIRS) L1B and science products from the Terra and Aqua satellites. The S-HIS web page for this campaign is http://deluge.ssec.wisc.edu/~shis/tx2002/. Table 4 contains a summary of the data collection during TX-2002

Table 4.

SUMMARY OF DATA COLLECTION DURING TX2002 Scanning High-resolution Interferometer Sounder (SHIS)					
Flight Date	**Sortie**	**Mission**	**Data Start (UTC)**	**Data End (UTC)**	**Flight Length (Hours)**
021121	03-9013	AIRS validation-Gulf of Mexico	17:52	20:50	3
021122	03-9014	CART Site Flight	15:54	19:03	3
021123	03-9015	LA Coast Geomorphology Flight	16:23	21:05	4.6
021124	03-9016	Cirrus Flight - Following Terra Orbit	15:21	19:07	3.6
021127	03-9017	Cirrus Flight - Texas	16:11	17:55	1.8
021129	03-9018	Single Layer Cirrus Flight - CART site	14:54	18:36	3.5
021206	03-9019	Gulf of Mexico-Night Flight	05:37	08:33	3
021207	03-9020	Oklahoma CART Site	17:01	20:26	3.5
				Total Flight Hours:	26

An excellent validation of AIRS radiance spectra was obtained with S-HIS from the 21 November 2002 flight on this campaign (1st paper, Appendix B).

e) Pacific THORPEX (PTOST)

THORPEX objectives are to: 1) evaluate the potential of various in situ and remote sensing observation systems to provide the observations needed to accelerate improvements in operational weather predictions, 2) evaluate model sensitivity studies and test the impact of targeted observations by participant systems on the performance of those operational models, and 3) begin to acquire the observational data needed to develop intelligent observing systems and the models and data assimilation systems that will interact dynamically with those observing systems. The S-HIS web page for this campaign can be found at http://deluge.ssec.wisc.edu/~shis/thorpex/index.html

Table 5 contains a summary of the data collection during Pacific THORPEX.

Table 5.

SUMMARY OF DATA COLLECTION DURING PACIFIC THORPEX Scanning High-resolution Interferometer Sounder (SHIS)					
Flight Date	**Sortie**	**Mission**	**Data Start (UTC)**	**Data End (UTC)**	**Flight Length (Hours)**
030219	036013	Ferry from Dryden, CA			
030221	036014	Characterize atmosphere across a midlatitude jet streak in Pacific Ocean in coordination with G-4 flight. Search for signatures of turbulence.	2100	0320	6.3
030222	036015	Characterize atmosphere across a midlatitude jet streak near 20 N, 147 W in Pacific Ocean in coordination with G-4 flight (dropsondes and profiling).	2140	0430	6.9
030224	036016	Collect ER-2 based observations for validating Aqua MODIS L2 Cloud Science Products including Cloud Top Height and Cloud Particle Phase. Collect data to evaluate AIRS atmospheric profiles. Aqua overpass at 2356 UTC.	2138	0300	5.4
030226	036017	Collect ER-2 based observations of multilayer thin to thick high clouds for validating Aqua (2342 UTC) MODIS L2 Cloud Science Products including Cloud Top Height and Cloud Particle Phase. Underfly ICESat satellite (0120 UTC) with GLAS 1064nm band viewing scenes of thin and thick high cloud.	2200	0320	5.3
030301	036018	Collect ER-2 based observations of clear to partly cloudy (low cloud) conditions for validating Aqua (0010 UTC) MODIS and AIRS L1B and L2 Atmospheric Profiles products. Underfly ICESat satellite (0154 UTC) with GLAS 1064nm band viewing clear and partly cloudy scenes.	2230	0305	4.5
030303	036019	Collect ER-2 based observations of clear to partly cloudy (low cloud) conditions for validating Aqua (2358 UTC) MODIS and AIRS L1B and L2 Atmospheric Profiles products. Overfly Kilaeua volcano.	2155	0110	3.1
030310	039031		2150	0415	6.4

030311	039032	Flew to the northeast and then flew a cube pattern. 15 dropsondes.	2100	0405	7.1
030312	039033	Good day for both SHIS & NASTI. 8 dropsondes along the path plus AQUA overpass	2100	0415	7.3
				Total Flight Hours:	6.7

This campaign provided excellent data sets for comparisons of NAST, S-HIS, and AIRS retrievals under conditions with elevated temperature inversions, allowing vertical resolution comparisons (see Appendix B, Antonelli, et al., 2003). Also, it provided some opportunities to intercompare NAST and S-HIS, although cloud conditions made detailed comparisons difficult.

f) Atlantic THORPEX (AtREC or "ATOST")

THORPEX objectives are: 1) to evaluate the potential of various in situ and remote sensing observation systems to provide the observations needed to accelerate improvements in operational weather predictions, 2) to evaluate model sensitivity studies and test the impact of targeted observations by participant systems on the performance of those operational models, and 3) to begin to acquire the observational data needed to develop intelligent observing systems and the models and data assimilation systems that will interact dynamically with those observing systems. The S-HIS web page for this campaign is at http://deluge.ssec.wisc.edu/~shis/atost/index.html. Table 6 contains a summary of the data collection during ATOST.

Table 6.

SUMMARY OF DATA COLLECTION DURING Atlantic-TOST Scanning High-resolution Interferometer Sounder (SHIS)					
Flight Date	**Sortie #**	**Mission Summary**	**Data Start (UTC)**	**Data End (UTC)**	**Flight Length (Minutes)**
11/03/2003	N/A	Lab Test	18.9	19.3	24
11/06/2003	04-6013	First Checkout flight over California	1925	2115	115
11/13/2003	04-6014	Second Checkout Flight over California	1715	1855	100
11/14/2003	04-6015	Pilot Proficiency Flight	1715	1915	120
11/17/2003	04-6016	Ferry from Dryden to Bangor	1500	2100	360
11/19/2003	04-6017	AQUA Overpass, multi-layer clouds	1555	2111	316

11/28/2003	04-6018	Racetrack pattern over Montreal/Mirabel	1500	2005	305
12/02/2003	04-6019	Coordination with Citation south from St. John's Island	1323	1944	381
12/03/2003	04-6020	AQUA Underflight mission. Variable cloud conditions.	1335	1923	348
12/04/2003	04-6021	AIRS-II "icing" mission over Mirabel	1432	1828	236
12/05/2003	04-6022	Flight supported all three objective of ATREC, AQUA satellite validation, and AIRS-II	1521	2149	388
12/08/2003	04-6023	AQUA underflight. Night mission.	2205	0319	219
12/10/2003	04-6024	ATReC support flight to eastern areas (~40W)	1558	2221	379
12/11/2003	04-6025	AIRS-II mission to Mirabel	1628	1940	192
12/14/2003	04-6026	Aqua underflight centered on eastern tip of Cape Cod	1600	2200	360
12/17/2003	04-6027	Ferry from Bangor, Me to DFRC, CA	1600	2205	365
			Total Flight Hours:		70.13

ATOST provided many good opportunities (including especially the ferry flight from Dryden to Bangor, Maine) of retrievals demonstrating water vapor relative humidity retrieval skill around and beneath broken clouds (see Figure 10).

Status of the data processing

The UW is responsible for processing the aircraft (S-HIS and NAST-I) interferometric data to create calibrated radiance datasets. A major improvement was made in the S-HIS ground data processing procedures during this contract period. Table 7 summarizes the status of the instrument data processing (to the level of radiances):

All of the data has been processed in-the-field to produce a "preliminary" data product. These products are used in creating quicklooks and for near-realtime analysis. After the experiment, data is reprocessed to produce a "final" dataset suitable for public release. These data are made available to the NPOESS/IPO through a data portal described below. The point of contact for data processing questions is robert.knuteson@ssec.wisc.edu.

Table 7.

Campaign	Status (as of March 2004)
IHOP	Prelim; (final processing upon demand)
CRYSTAL-FACE	Prelim; Final; On-line
UAV-SGP	Prelim; (final processing upon demand)
TX-2002	Prelim; (final processing upon demand)
Pacific THORPEX	Prelim; Final; On-line
Atlantic THORPEX	Prelim; Final; On-line

Data Portal

The UW has established a "data portal" to provide access to the calibrated radiances and data products generated under this Government Study. The data portal has a web page front end with hyperlinks to the general experiment information. For example, the hyperlink to the Pacific THORPEX 2003 data portal can be found on the web page at http://thorpex-data.ssec.wisc.edu/. This data portal concept will be expanded to both past and future field campaigns. A paper was presented at the annual AMS meeting in January 2004 (Seattle) on this topic. The reference to this paper is given in the bibliography as Dutcher (2004).

3.3 Development and Implementation of Aircraft Instrument Performance Improvements

Several important improvements have been developed and implemented on the S-HIS aircraft instrument under this contract. Whenever applicable, the plan is to implement corresponding changes on the NAST instrument. Figure 2 shows NAST being inter-compared to the S-HIS and AERI instruments at UW after being worked on in 2001.

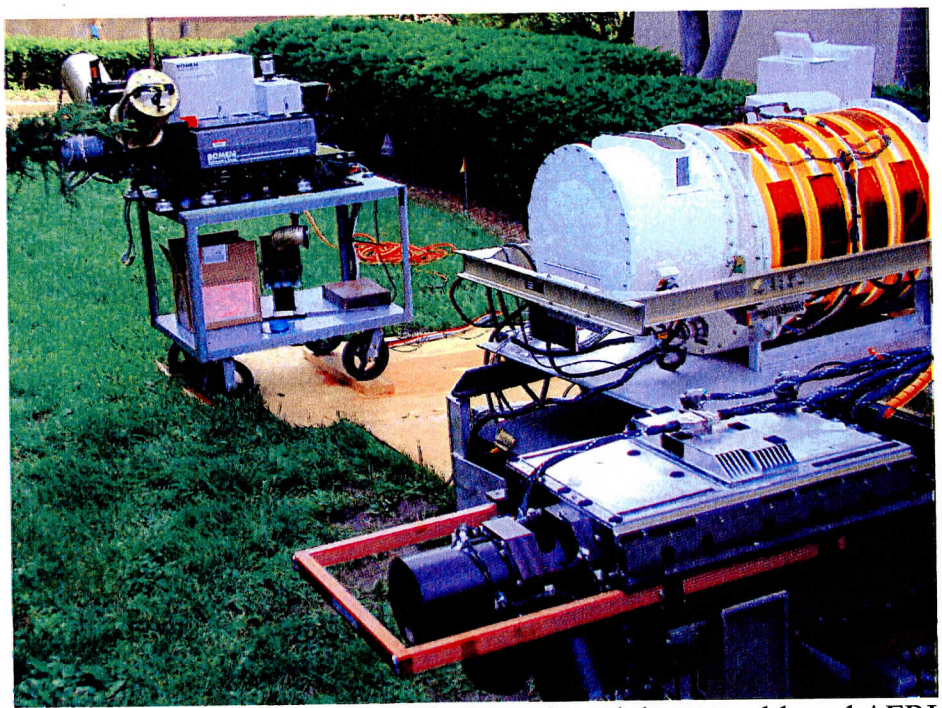

Figure 2. Scanning HIS (foreground), NAST-I (center), and the ground-based AERI instrument.

One of the most important impacts on NAST has been a significant reduction of vibration-induced tilt noise. This vibration-induced tilt noise for NAST is characterized by low resolution spectral amplitude variations caused by uncompensated tilts between the two Michelson flat mirrors induced by aircraft vibration. The specific effort under this contract involved tuning the dynamic alignment subsystem based on experience with S-HIS. The large impact resulted because of the combined effect of this specific change with the low level of static tilt made possible by an electronic static-tilt alignment circuit integrated into the NAST earlier in 2001 (based on a S-HIS development).

Other improvements that were made to the S-HIS include: a) integrating an aerodynamic closeout at the aircraft pod viewing aperture b) adding electronic filters to reduce the electro-magnetic interference that was intermittently degrading the interferogram signal; c) upgrading the interferometer tilt correction algorithm to be used in post processing; and d) lowering the temperature of the ambient blackbody to provide improved radiometric performance.

This effort, in which the S-HIS has been a pathfinder for NAST, is important to refine the both instruments as validation tools for CrIS.

Aerodynamic Close-out of the S-HIS Pod Viewing Aperture on the ER-2

During the transit flight of the S-HIS on-board the ER-2 to the SAFARI mission out of Africa, the viewing aperture of the instrument pod was closed-off with a metal cover to prevent data collection over Brazil – a security request from that government. The data from this flight had significantly less noise than flights with an open aperture, leading to the conclusion that in the normal flight configuration aerodynamic effects were inducing vibrations into the interferometer. To reduce these effects a closeout structure was designed and fabricated at UW, and installed into the ER-2. As shown in Figure 3 the closeout structure effectively seals the region between the pod skin and the S-HIS interferometer front-end hexagon structure that contains the scene mirror and blackbodies. In order to allow free motion of the interferometer on its shock mounts, the closeout structure seals to the front-end hexagon structure with compliant foam. A dramatic improvement in noise performance that was achieved after the aerodynamic closeout was installed.

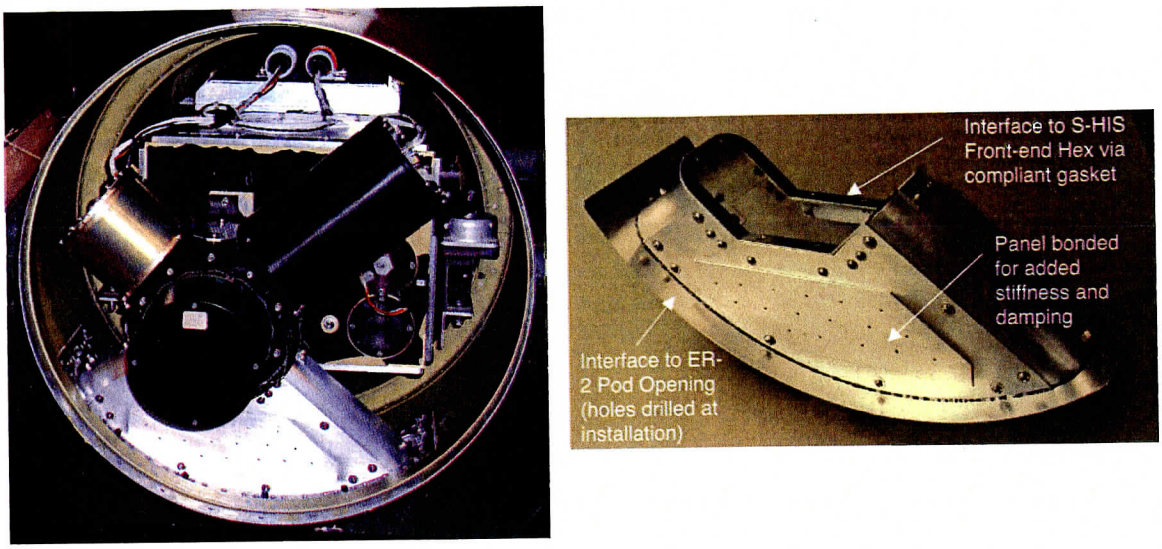

Figure 3. The aerodynamic closeout structure that effectively seals the S-HIS pod viewing aperture to the hexagon front-end structure of the interferometer.

Reduction of Electro-magnetic Interference Sensitivity

The sensitivity to electro-magnetic interference on the S-HIS when flying on the ER-2 has been significantly reduced. A noise problem that manifested itself in the interferograms at the equivalent of 10 and 40 Hz, was found only during flight and only on the ER-2. To reduce the electro-magnetic interference sensitivity of the S-HIS, Ferrite beads were installed on all the lines going into the interferometer box. Additionally, the new aerodynamic insert is thought to provide added protection.

Improvements in the Interferometer Mirror Tilt Correction Algorithm

We have shown that vibration induced tilt modulation errors in a Michelson interferometer can be corrected in post processing using tilt angles measured during an interferometer scan. The tilt correction has been shown to remove most of the tilt induced modulation error and to reduce the correlated errors by a factor of five over much of the spectrum and by as much as 15 at some wavenumbers. Progress has been made on improving and implementing the algorithm. Initially, problems were encountered in correctly reversing the numeric filtering process that is carried out in the S-HIS science data processor. To get a clean data set for application of the algorithm, the instrument controller and science data processor software were modified to enable the collection of both numeric filtered and unfiltered data. The unfiltered data is now being used to implement and validate the algorithm. The algorithm will then be extended so it can be used with filtered data.

Figure 4 shows the improvements that can be achieved using the correction algorithm. The figure shows both random and correlated (tilt related) errors for the S-HIS flight on August 6, 2000, using forward scans. Over most of the spectrum, the tilt correction algorithm reduces the residual correlated noise to significantly below level of the random detector noise.

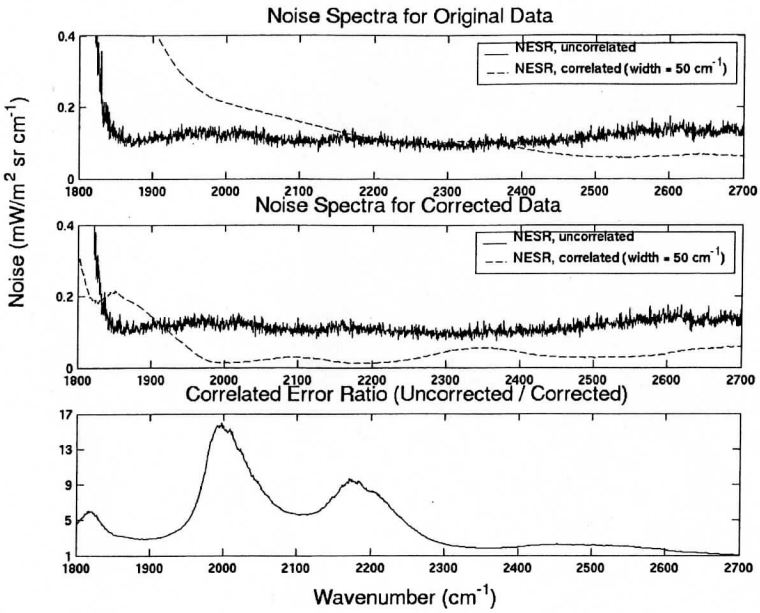

Figure 4. Reduction of correlated (tilt related) noise in the hot blackbody with the modulation error correction. The top plot shows the random and correlated errors for the uncorrected data while the middle plot shows the same thing for the corrected data. The bottom plot is the factor by which the correction improves the correlated errors.

A summary of the results of vibration induced tilt correction can be found in the following reference (which is also attached in Appendix B):

Olson, E. R.; Revercomb, H. E.; Knuteson, R. O.; Howell, H. B.; LaPorte, D. D.; Ellington, S. D.; Werner, M. W.; Garcia, R. K., and Best, F. A. Vibration induced tilt error model for aircraft interferometer data. *International Symposium on Remote Sensing, 9th*, Athens, Greece, 2 September 2002 (proceedings). *Within the Sensors, Systems, and Next Generation Satellites Conference, 8th* (proceedings). Bellingham, WA, SPIE-The International Society for Optical Engineering, 2002. Reprint #3197.

S-HIS ER-2 Ambient Blackbody Thermal Coupling

A new thermal design for the ambient blackbody was implemented to improve S-HIS instrument radiometric performance. In its original configuration, the ambient blackbody was somewhat thermally decoupled from the instrument and pod temperatures in order to improve the effectiveness of the heaters that are designed to keep the cavities above the dew point during descent. During flight at altitude, this decoupling prevented the ambient blackbody from reaching the low temperatures required for the desired radiometric performance, especially at low scene temperatures. Figure 5 shows the radiometric performance that can be realized with different ambient blackbody temperatures, assuming S-HIS flight conditions on the ER-2. The temperature of the ambient blackbody in its original configuration was about 260 K. The new blackbody thermal coupling illustrated in Figure 6 allowed the blackbody to get down to between 230 and 240 K during flight. As shown in the figure, calibration brightness temperature errors are significantly reduced with the new configuration. In the shortwave, for the old blackbody

configuration, only scene temperatures above 235 K had brightness temperature errors under 0.2 K, whereas in the new configuration, scene temperatures down to 207 will be under 0.2 K. A similar improvement is demonstrated in the longwave where scene temperatures with lower than 0.2 K errors went from 245 K to 218K.

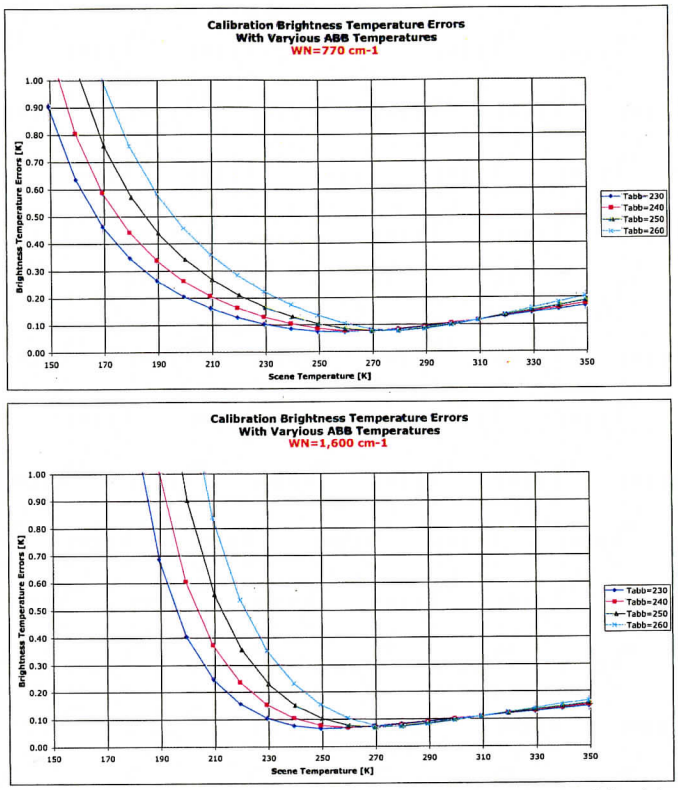

Figure 5. The radiometric performance is improved with a lower ambient blackbody temperature. Originally, the ambient blackbody was running near 260 during flight. After the improved thermal coupling scheme was implemented, this blackbody is running between 230 and 240 K, offering much improved radiometric performance at lower scene temperatures.

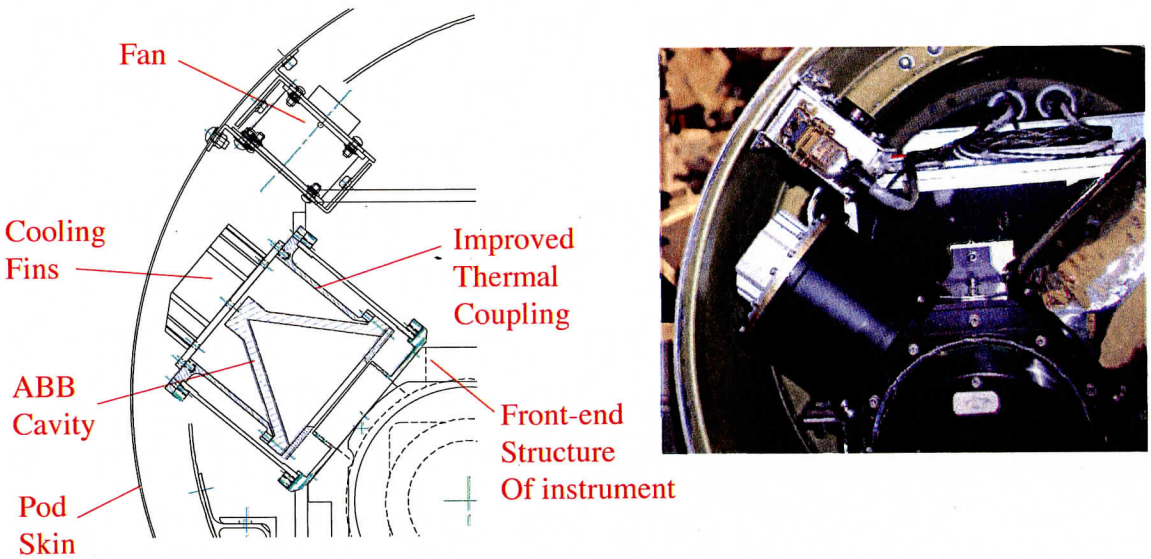

Figure 6. New configuration of the S-HIS Ambient Blackbody that provides better thermal coupling to the pod ambient temperature through conductive and forced heat transfer.

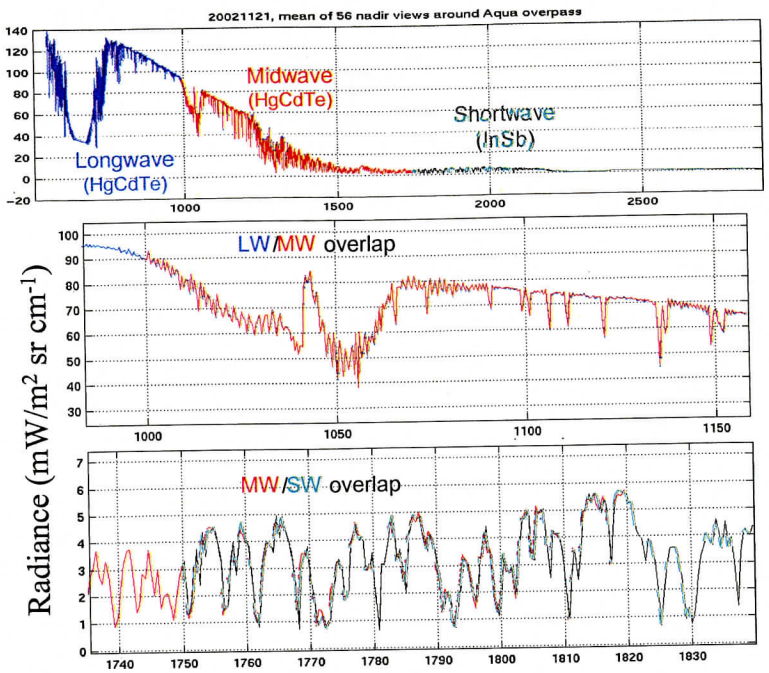

Figure 7. Scanning HIS radiance spectra collected over the Gulf of Mexico on 21 November 2002 from the NASA ER2 at 20 km altitude during the Terra-Aqua Experiment (TX-2002). The three separate spectral bands of S-HIS are illustrated, along with the good agreement between spectra from neighboring bands where they overlap.

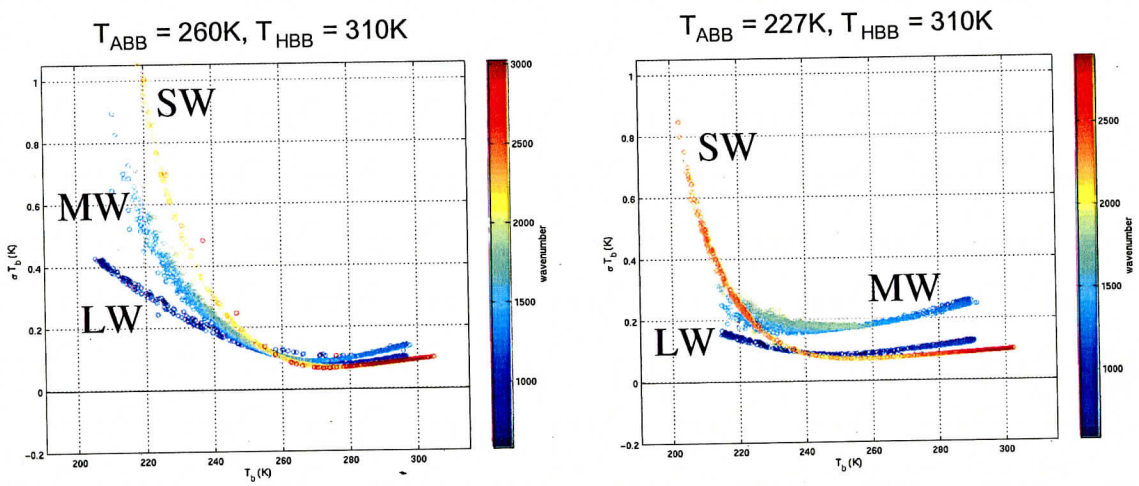

Figure 8. Three-sigma calibration accuracy estimates for Scanning HIS with two different ambient blackbody temperatures. Conditions apply to AIRS validation flights on 21 November 2002 on the ER2 over the Gulf of Mexico (left) and 16 November 2002 on Proteus over the DOE Atmospheric Radiation Measurement (ARM) site in Oklahoma (right). TABB and THBB are the ambient and hot blackbody temperatures.

b) Spectral Calibration using Earth Scene Spectra

Spectral calibration is the process of accurately determining the wavenumber scale to assign to the measured spectrum. The CrIS ATBD specifies that neon lamp sources will be co-aligned with the metrology laser, and laser fringe counts of the neon views, along with the known wavelength of the neon lamp, will be used to determine the wavelength of the metrology laser and the resulting wavenumber scale. An alternate method of performing spectral calibration is to use known features in the upwelling Earth scene data as the reference. We have recently performed an analysis of how well this type of spectral calibration can be performed using a large ensemble of clear sky S-HIS cases collected during AFWEX. The basic technique is shown in Figure 9 and the results are presented in Tobin 2003. Using this technique, the S-HIS spectral calibration can be determined with an uncertainty of 0.3 ppm (3-sigma). Based on the success of this approach and recent concerns about the neon lamp implementation, CrIS is evaluating the Earth view technique for its spectral calibration approach.

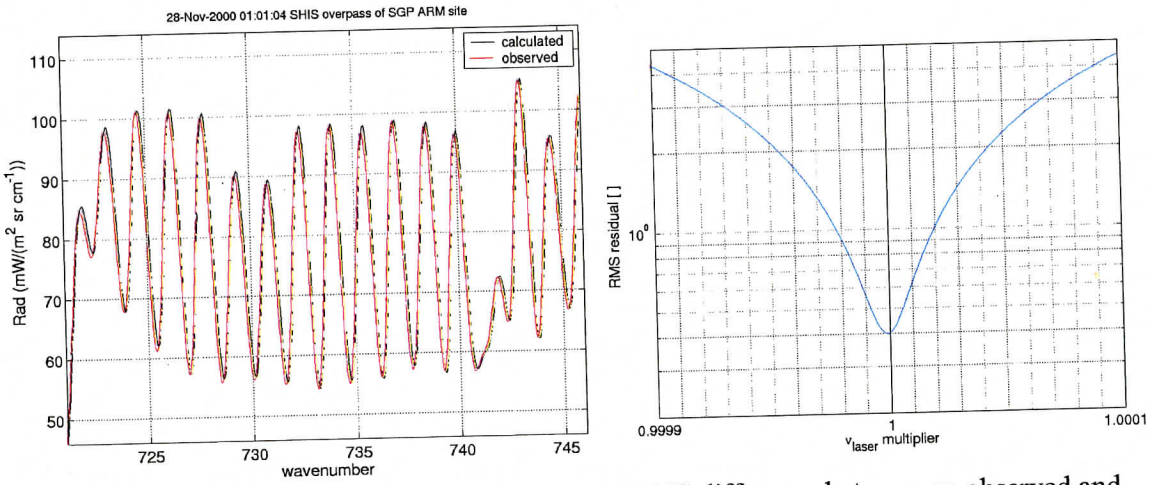

Figure 9. An example SHIS spectral calibration. The RMS difference between an observed and calculated nadir spectrum (left panel) is summed over the 730 to 740 wavenumber range. This metric is computed for a range of possible effective laser wavenumbers, corresponding to a range of observed spectrum wavenumber scales (right panel), and the optimum spectral calibration is obtained where the residual is a minimum.

Tobin, D. C., H. E. Revercomb, R. O. Knuteson, 2003: On-orbit Spectral Calibration of the Geosynchronous Imaging Fourier Transform Spectrometer (GIFTS). Proceedings of CALCON 2003, Characterization and Radiometric Calibration for Remote Sensing, Space Dynamics Laboratory / Utah State University, Logan, Utah, 15-18 September 2003.

2. Level 2+ product retrieval algorithms

The generation of Level 2 (environmental) products from the calibrated radiances is being pursued under this Government Study. Three areas have been investigated; performance of the Smith algorithm for temperature and water vapor retrieval, improvements in cloud top pressure retrieval using a variant of CO2 slicing, carbon monoxide column retrieval, and land surface infrared emissivity and effective temperature retrieval. The main focus has been in the development of a temperature and water vapor retrieval methodology for use with Scanning-HIS

radiances in close coordination with Bill Smith and Dan Zhou (NASA LaRC) who have successfully applied the same retrieval technique to NAST-I data.

a) Temperature and Water Vapor Retrieval from High Spectral Resolution Infrared Data

The temperature and water vapor retrieval methodology used in the processing of Scanning-HIS data is outlined in the figure below from a paper by Antonelli et al. (2003). This technique relies upon a "training set" of pre-computed radiances in order to develop regression coefficients that relate observed radiances to vertical profiles of temperature and water vapor mixing ratio along the line of sight. The key to the current technique is the inclusion of a cloud "proxy" in the training set which causes the retrieved temperature below clouds to become isothermal. This causes a "discontinuity" in the retrieved temperature profile which can be used to determine cloud top altitude. Investigation and validation of the performance of this algorithm is an ongoing activity.

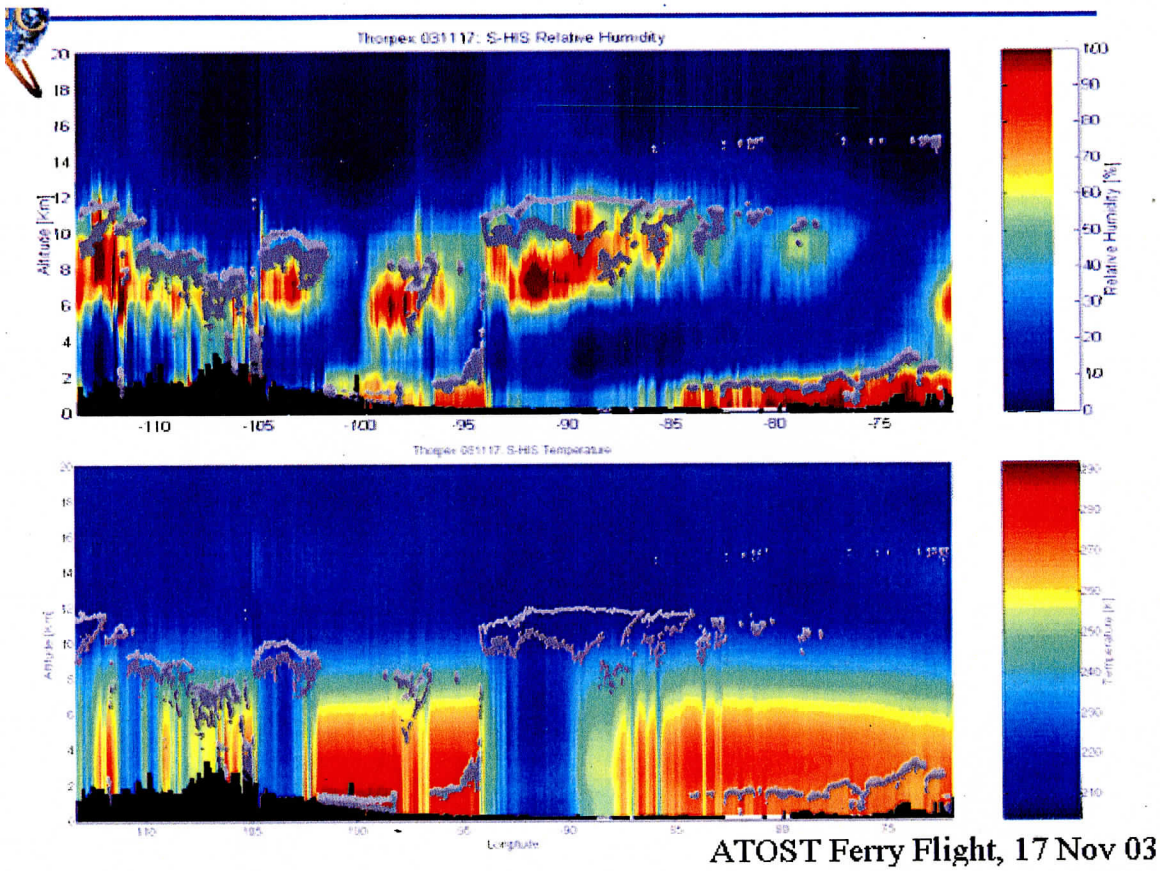

Figure 10. Time cross-section of Scanning-HIS retrieval of relative humidity (upper) and air temperature (lower panel). Overlaid on the image are the locations of cloud top from the NASA Cloud Physics Lidar (CPL).

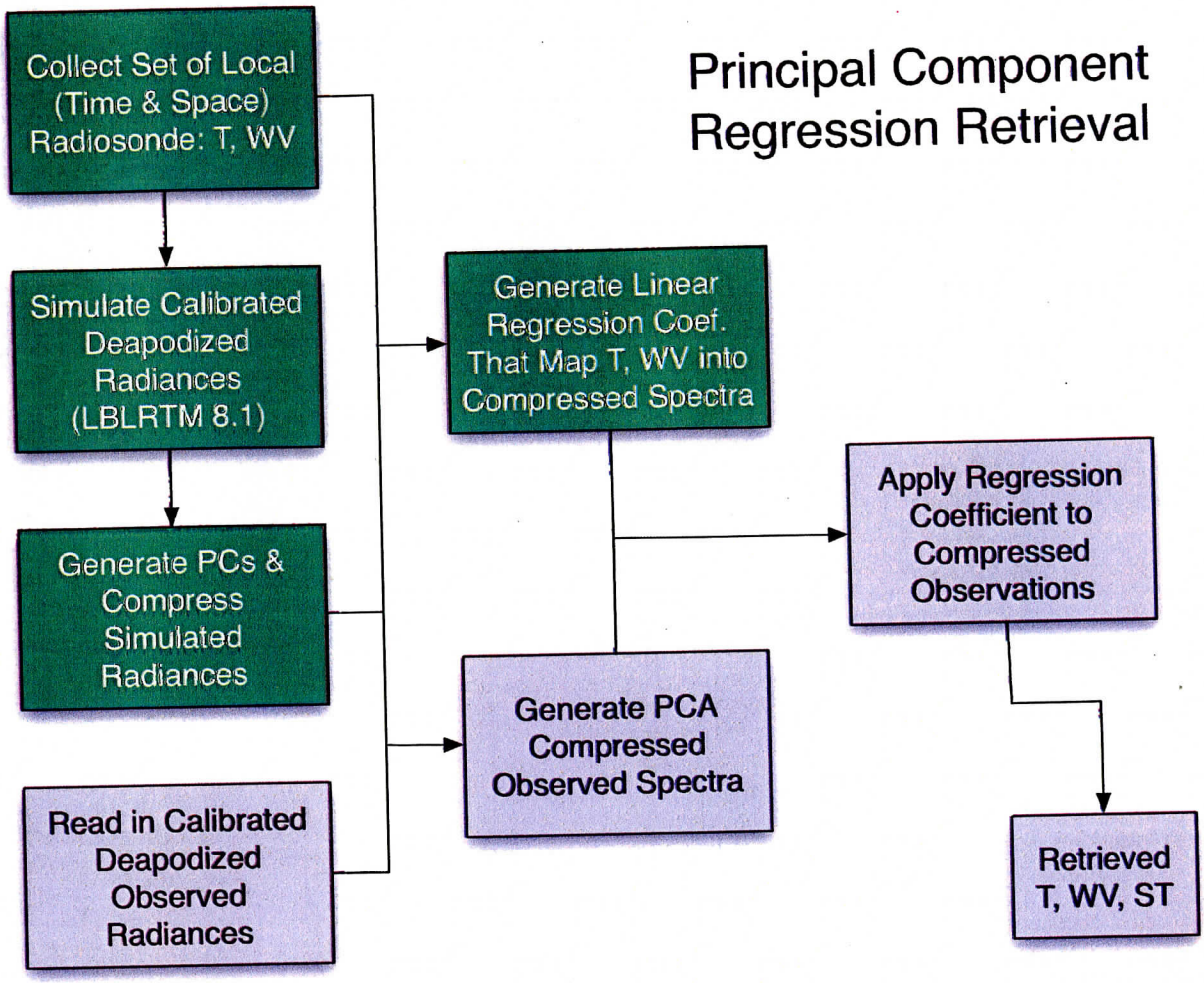

Figure 11. Scanning-HIS retrieval methodology (following Zhou et al.)

An illustration of the retrieval of moisture (relative humidity) down to thick clouds and through broken and "thin" clouds is given in Figure 10, using S-HIS data from Atlantic THORPEX (17 Nov 2003). The retrieval methodology (Figure 11) is that defined by Bill Smith and implemented by Paolo Antonelli of UW-SSEC with assistance from Dan Zhou of NASA Langley. A summary paper of the results of this study can be found in the following reference (which is also attached in Appendix B):

Antonelli, P. et al., 2003: Validation and Comparison of S-HIS and NAST-I Retrievals for THORPEX-2003, *Intl. TOVS Study Conference - XIII*, Ste. Adele, Canada, 29 October - 4 November 2003.

b) Surface Temperature and Emissivity

For this task, we developed an approach for the validation of NPOESS land surface characterization products. In particular, land surface emissivity and temperature products derived from aircraft observations will be compared with ground-based measurements made in the vicinity of a ground truth site. The results of this study are being published in the journal

Advances in Space Research. The reference is given below for the paper and several conference proceedings:

Knuteson, R., F. Best, D. DeSlover, B. Osborne, H. Revercomb, and W. Smith, Sr., 2004: Infrared land surface remote sensing using high spectral resolution aircraft observations. *Adv. Space Res.*, Vol. 33, (in press).

Knuteson, Robert; Osborne, Brian; Revercomb, Henry; Tobin, David, and Smith, William L., 2001: Infrared land surface emissivity retrieval from high-spectral resolution upwelling radiance. *Conference on Satellite Meteorology and Oceanography, 11th*, Madison, WI, 15-18 October 2001 (preprints). Boston, MA, American Meteorological Society, pp688-691.

Knuteson, Robert O.; DeSlover, Dan H.; Larar, Allen M.; Osborne, Brian; Revercomb, Henry E.; Short, John F.; Smith, William L., and Tanamachi, Robin, 2003: Infrared land surface remote sensing using high spectral resolution observations. Multispectral and Hyperspectral *Remote Sensing Instruments and Applications*, Hangzhou, China, 25-27 October 2002. Bellingham, WA, International Society for Optical Engineering, (SPIE), pp24-35.

Knuteson, R., B. Osborne, H. Revercomb, W. Smith, and D. Tobin, 2003: Validation of Satellite AIRS LST/LSE Products Using Aircraft Observations, *Intl. TOVS Study Conference - XIII*, Ste. Adele, Canada, 29 October - 4 November 2003.

Knuteson, R., H. Revercomb, D. Tobin, B. Osborne, 2003: Land Surface Product Validation Using the DOE ARM Southern Great Plains Site, *Eos Trans. AGU*, 84(46), Fall Meet. Suppl., Abstract B21E-0751, 2003.

c) Carbon Monoxide (CO) Column Retrieval

We developed an approach for retrieving column CO from aircraft data as a prelude to application to satellite sensors. In particular, time cross-sections of CO were made using Scanning-HIS and NAST-I radiance data. The results of this study were presented at several conferences referenced below:

Vinson, Kenneth H.; Revercomb, Henry E.; Howell, H. Benjamin; Knuteson, Robert O., and Smith, William L., 2003: Carbon monoxide and methane column retrieval from the Scanning High Resolution Interferometer Sounder (S-HIS) and National Polar-orbiting Operational Environmental Satellite System Airborne Sounder Testbed- Interferometer (NAST-I). *Optical Remote Sensing of the Atmosphere and Clouds III*, Hangzhou, China, 25-27 October 2002. Bellingham, WA, International Society for Optical Engineering, (SPIE), pp472-482.

Vinson, Kenneth; Revercomb, Henry; Howell, H. Ben, and Knuteson, Robert, 2001: CO and CH4 column retrieval from the Scanning High-resolution Interferometer Sounder (S-HIS). *Conference on Satellite Meteorology and Oceanography, 11th,* Madison, WI, 15-18 October 2001 (preprints). Boston, MA, American Meteorological Society, pp666-669.

d) Cloud Top Pressure Retrieval

We investigated improvements to the traditional CO_2 slicing method using high spectral resolution infrared data. The use of passive infrared cloud top remote sensing remains the only method that can be applied to operational sensors in the NPOESS era. This Government Study is leveraging the collection of aircraft infrared sounder data (Scanning-HIS and NAST-I), which is coincident (on the same aircraft) with nadir viewing lidar systems. In particular, the NASA Goddard Cloud Physics Lidar (CPL) is being used to validate cloud top pressure retrieval algorithms. This work is being conducted by a graduate student, (advised by S. Ackerman), in the University of Wisconsin-Madison Department of Atmospheric and Oceanic Sciences. An example of recent intercomparisons is shown in Figure 12. The reference to this work is given below:

Holz, R.E., et al., 2004: A Comparison of High Spectral Resolution Infrared Cloud Top Pressure Algorithms using S-HIS Data. *Fourteenth ARM Science Team Meeting*, Albuquerque, New Mexico, 22-26 March 2004.

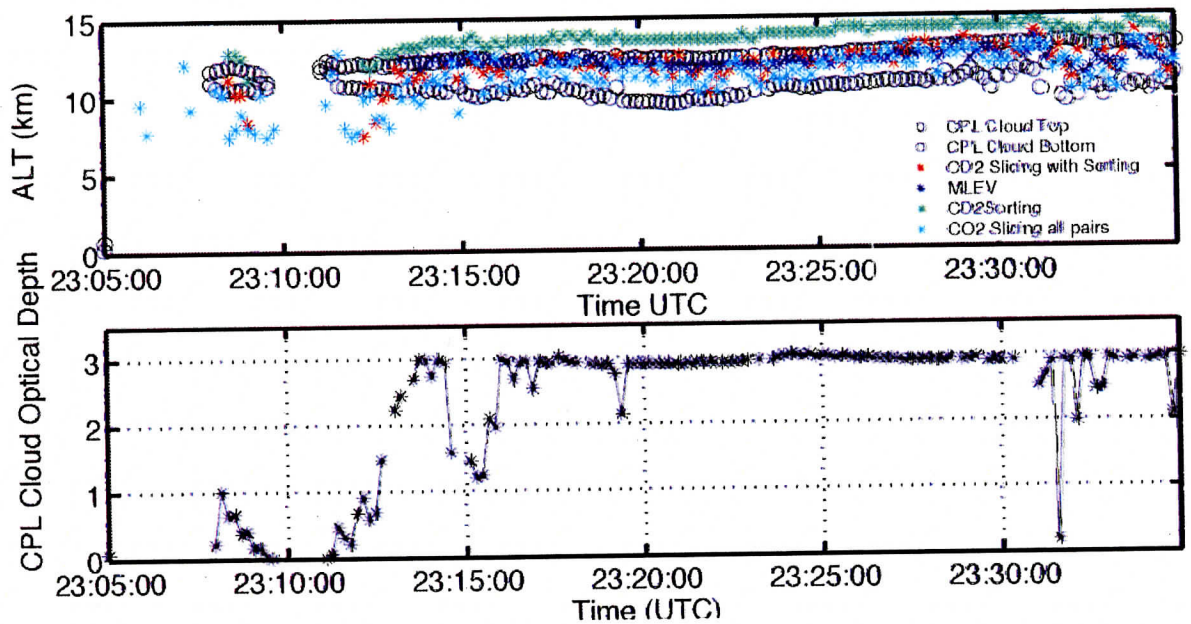

Figure 12. Scanning-HIS cloud top altitude detection during the Pacific THORPEX experiment. Three retrieval algorithms are compared: CO2 slicing, MLEV, and a new hybrid algorithm that combines CO2 sorting with CO2 slicing.

e) Cloud Optical Depth and Particle Size

We focus our study of cloud properties in spectral regions located between gaseous absorption lines within the 8-12 μm infrared atmospheric window. This focus provides a number of spectral measurements in the cleanest portion of the measured spectrum. The measured radiance represents the downwelling (AERI; upwelling S-HIS and NAST-I) column clear sky (molecular) radiance and any contribution from aerosol (e.g., cloud) emission.

The measured downwelling radiance is broken up into layers: clear sky below cloud, cloud layer, and clear sky above cloud. Line-by-line radiative transfer model (LBLRTM) calculations, using radiosonde atmospheric state measurements as input, are used to determine the atmospheric clear

sky transmittance. Cloud reflectance is parameterized based on a two-stream model, to account for reflected upwelling terrestrial and atmospheric radiation. The remaining unknown, cloud transmittance, is inverted from the radiative transfer equation to yield the cloud absorption optical depth. Lidar measurements are used to indicate cloud boundaries. LBLRTM transmittance profiles are then calculated for each MWR-scaled radiosonde measurement. Radiosonde temperature and LBLRTM transmittance profiles are then interpolated to derive clear sky column radiance for each measurement.

Spectral variations in measured absorption optical depth are used to infer effective radius of ice particles within the cirrus. Figure 13 (top panel) shows variation in absorption optical depth for various effective radii assuming hexagonal column ice crystals, where each curve is normalized to an absorption optical depth of 1.0 at 900 cm^{-1}. Note that the sensitivity decreases with increased particle size, such that the retrieval capability diminishes at an effective radius of about 30 to 40 μm. An example is given for ground-based AERI measurements on 29 November 2002 in Figure 13. The top panel shows model calculations for 5, 15, and 50 μm effective radii (open symbols) and a sample AERI measurement (asterisks) applied to each microwindow. The bottom panel illustrates a best fit to the measurement using both Mie ice spheres and hexagonal column crystals. Both ice spheres and hexagonal columns yield a similar spectral fit; however, the derived effective radius is roughly 10 percent larger when assuming spheres.

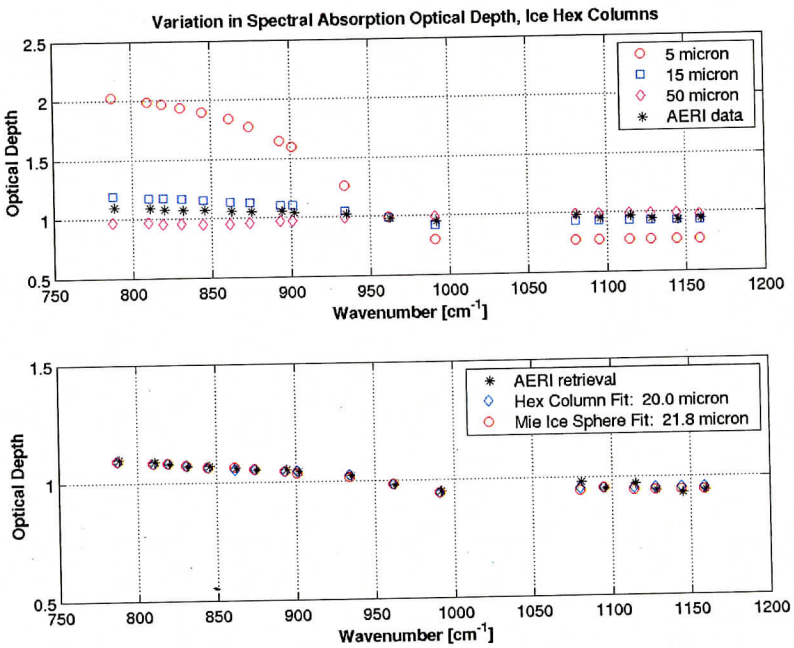

Figure 13. Theoretical absorption optical depth spectra for 5, 15, and 50 μm effective radius (top panel) with an example AERI spectrum. A best fit to the AERI spectrum (bottom panel) using both ice spheres and hexagonal columns yields the effective ice particle radius in the cloud.

The remainder of this cloud properties section describes a case study using Texas 2002 (TX2002) data. TX2002 was conducted to assess MODerate resolution Imaging Spectroradiometer (MODIS) and Atmospheric Infrared Sounder (AIRS) L1B and science products from the Terra and Aqua satellites. Results from a cirrus case, which occurred on 29

November 2002, will be presented here. Figure 14 shows GOES IR imagery at 1715 UTC with the ER2 flight track overlay for this case (with hourly timestamps). The event consisted of mostly uniform, single-layer cirrus. The ER2 was airborne between 1445 and 1900 UTC, and hourly ER2 location markers are indicated on the image. Figure 14 represents the time when the ER2 was over the Atmospheric Radiation Measurement (ARM) Central Research Facility (CRF) site—located near the 1700 UTC timestamp. Overall, four flight overpasses over the CRF were used to simultaneously analyze the cirrus from above and below the cloud.

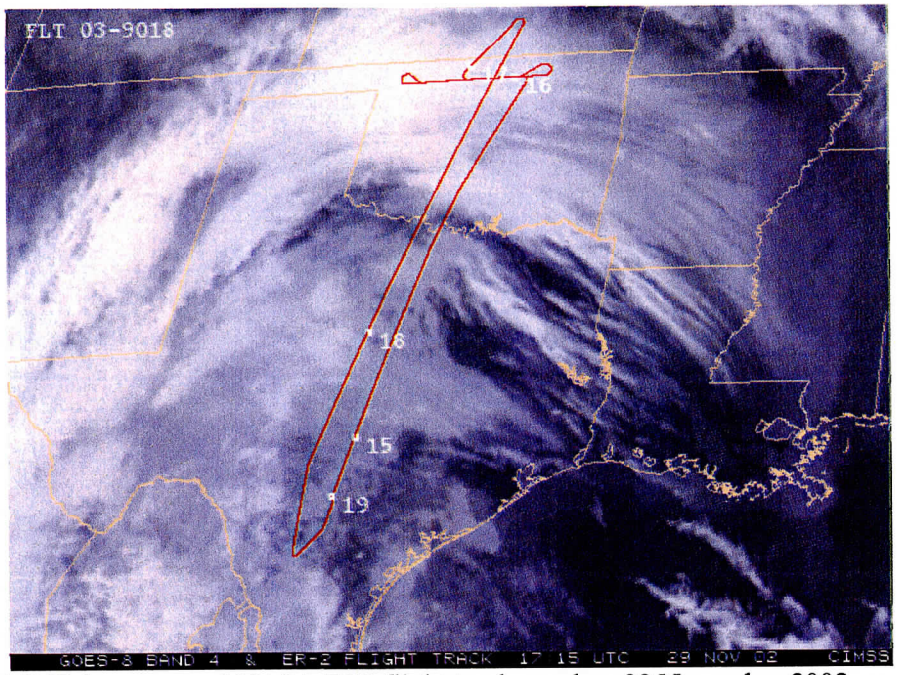

Figure 14. GOES IR imagery and NASA ER2 flight track overlay, 29 November 2002.

The general approach to cloud optical depth retrieval utilizes an average cloud base and cloud top altitude, derived from lidar data, during the AERI scene dwell time. Radiosondes are released several times during the day, which provide atmospheric state information required to calculate the clear sky radiance contribution and atmospheric transmissivity between the surface and cloud base. S-HIS measurements were used when the aircraft latitude/longitude was within a box defined by ± 0.1 degrees of the AERI surface instrument location. This approach was also used because an airborne lidar was not available. Therefore, the cloud boundaries for the aircraft-based cloud retrievals were also determined by the ground-based lidar measurements.

The four ER-2 overpasses of the CART site occurred between 1600 and 1720 UTC. Mean aircraft-based S-HIS absorption optical depth measurements are shown in Figure 15, relative to mean ground-based AERI results, for each individual overpass. Note that the AERI was operating in rapid-sample mode; such that an atmospheric scene was acquired roughly every 30 seconds (nominal AERI sampling occurs every 7-8 minutes). Data times correspond to aircraft presence within a 0.1 degree lat/lon box, specific to the AERI surface location. Retrieved mean cloud particle effective radius (μm) is also shown in each panel. The error bars and uncertainty given in the figure are associated with the standard deviation relative to the mean values shown, determined from all spectra which fall within the spatial "box."

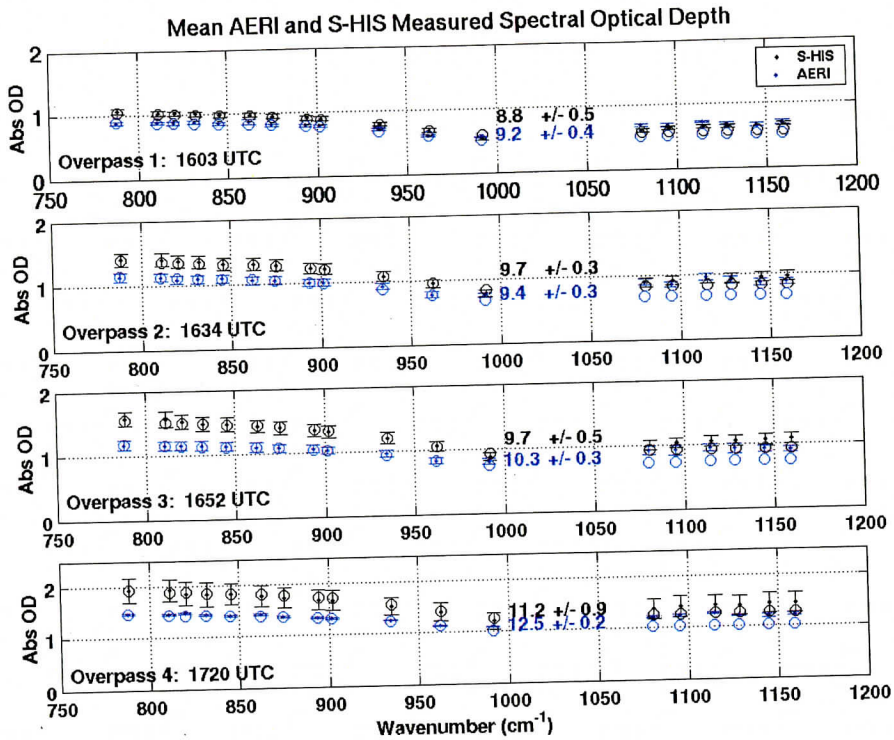

Figure 15. Absorption optical depth spectra from simultaneous AERI, ground-based, and S-HIS, aircraft-based, measurements. Results are shown for four separate overpasses of the ARM CRF. Some disagreement is expected given the large scale variability of cloud cover with the instruments' field of views. The retrieved effective radius (μm) is shown in the middle of each panel.

Results from 0000 through 0018 UTC are illustrated in Figure 16. CART Raman Lidar (CARL) measured cloud boundaries are given in the upper panel. The middle panel shows cloud optical depth for all AERI microwindows, CARL, 900 cm^{-1} S-HIS microwindow, and GOES measurements (using the CERES algorithm). Note that the dropouts in lidar data are a result of system self-calibration. Also, lidar cloud boundaries are determined from depolarization measurements which have greater sensitivity than the nitrogen channel data used to infer optical depth (OD); hence, CARL OD results are underestimated after 1700 UTC. Retrieved cloud particle effective radius is shown in the lower panel for AERI, S-HIS, and GOES data. Both AERI and GOES data are noisy from 0400 to 1100 UTC (GOES due to nighttime measurements, AERI due to small OD). The results are well correlated from 1400 UTC. The retrieved size increases as the cloud base decreases, which is expected as particles grow then gravitationally settle.

Figure 16 shows results for the 29 November 2002 cirrus case. The top panel represents lidar measured cloud boundaries as a function of time (shown from 0000 to 1800 UTC). The cirrus are single layer and uniform throughout most of the day, with a small break between 1100 and 1400 UTC, and then increasing in geometrical thickness by 1800 UTC. The middle panel shows the cloud optical depth from both the CARL (solid black line) and AERI (thin lines) for the entire time period. One feature of particular interest occurs between 0800 and 1000 UTC, where it appears a wave cloud has advected over the site. This is readily apparent in the AERI data which

shows a significant oscillation in optical depth – ranging between 0 and 2 – over this duration. This is a striking feature, and a direct result of rapid-sample operation. The lidar data has a several minute running average, which smears the oscillation. Aircraft measurements coincided with the gradual increase in cloud geometrical, and optical, thickness from 1500 UTC to 1800 UTC. The circles represent the S-HIS 900 cm^{-1} microwindow optical depth and are consistent with the ground-based measurements. Also shown are GOES (squares) cloud optical depths (visible data, not valid prior to 1200 UTC) which agree well with the other results (converted to infrared optical depths for the comparison). Note that the dropout in CARL (and AERI, due to a lack of cloud boundaries) optical depths just after 1700 UTC were due to CARL instrument calibration. The bottom panel shows cloud particle effective radius as a function of time. The decrease in scatter after 1400 UTC in the AERI results are not related to diurnal (i.e., daylight) variations, which is true for the GOES results. Rather, the AERI-based cloud particle size retrieval depends on the spectral variation in optical depth. The relatively small cloud optical depth (measured radiance dominated by atmospheric water emission), coupled with rapid oscillation in cloud optical depth evident in the middle panel, contributed to the difficulty in retrieved particle size. As the cloud optical depth increases monotonically (after 1400 UTC), the retrieved particle size exhibits very little variation and increases as the cloud base decreases, which would be consistent with gravitational settling of larger cloud particles. The S-HIS (circles) and GOES (squares) show similar results for measurements from above the cloud. A slight bias is expected from the above-cloud results, due to sensitivity to smaller particles near the cloud top.

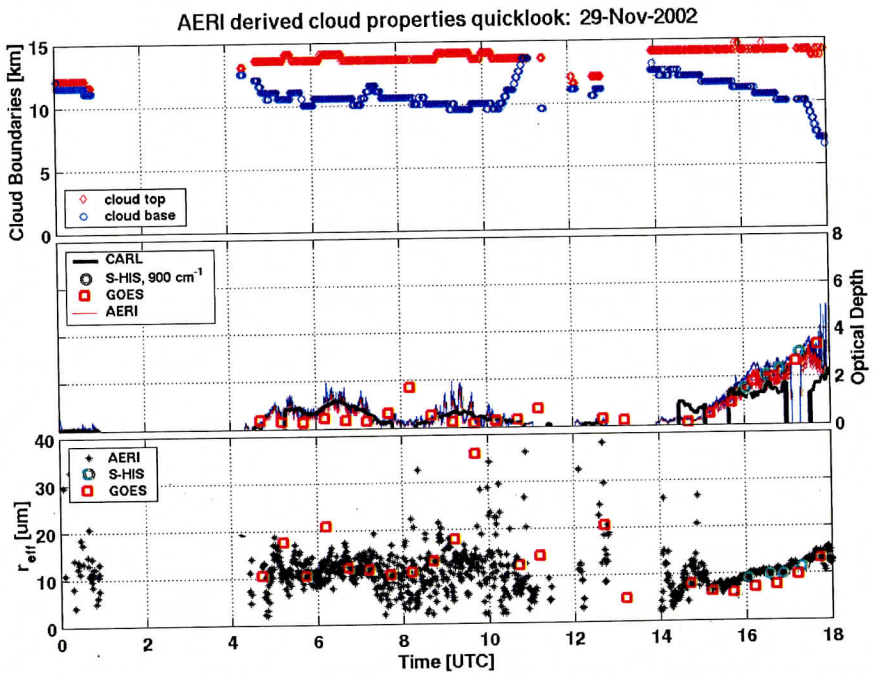

Figure 16. Results from TX2002 cirrus case on 29 November 2002. Lidar (CARL) measured cloud boundaries are shown in the top panel. Ground- (AERI and CARL), aircraft- (S-HIS), and satellite-based (GOES) measurements of cloud optical depth (middle panel) and particle size (bottom panel) are consistent from both above and below the cloud. Note that GOES measurements are based on visible imagery and are ineffective during night-time observations.

3.5 Forward Model Refinement

Significant progress had been made in the area of clear sky forward modeling. This effort is funded through a combination of projects including this IPO contract, Atmospheric Radiation Measurement (ARM) Program involvement, and the Atmospheric Infrared Sounder (AIRS) project involvement. This work has included close collaborations with Tony Clough's group at AER, Inc. and Larrabee Strow's group at the University of Maryland Baltimore County. These collaborations are significant in that these two groups represent and maintain the two state-of-the-art forward models, LBLRTM and kCARTA, respectively. Our forward modeling effort can be divided into four main categories:

1. Improvements in ARM atmospheric state measurements and characterization of their uncertainties
2. Analysis of downwelling Atmospheric Emitted Radiance Interferometer (AERI) spectra
3. Development of a new water vapor continuum model, MT_CKD
4. Validation of improved forward modeling using ground, aircraft, and satellite based observations

Progress in each area is described in the following sections. In the past several years, through this effort and those of others, the forward models are approaching the accuracy levels required for remote sensing. For our ground based (e.g. AERI) and satellite based (e.g. AIRS) validations, maximum residuals (observed minus calculated) across the spectrum are less than ±0.5 K, with few exceptions. Emphasis is placed on temperature and water vapor sounding channels.

Improvements in ARM atmospheric state measurements and characterization of their uncertainties

A necessary ingredient when using atmospheric data to refine and validate a forward model is the accurate characterization of the relevant atmospheric state parameters. For our work, we use the ARM Cloud and Radiation Testbed (CART) sites which are the some of the most heavily instrumented ground based atmospheric state and radiation measurement sites in the world. Water vapor accuracy, especially in the upper levels, has traditionally been the limiting factor in using atmospheric data for this purpose. Through a series of extensive field campaigns, we have led the effort to characterize the ARM water vapor measurements. Conclusions from these efforts are summarized in following papers:

Revercomb, H. E., D. D. Turner, D. C. Tobin, R. O. Knuteson, W. F. Feltz, J. Barnard, J. Bosenberg, S. Clough, D. Cook, R. Ferrare, J. Goldsmith, S. Gutman, R. Halthore, B. Lesht, J. Liljegren, H. Linne, J. Michalsky, V. Morris, W. Porch, S. Richardson, B. Schmid, M. Splitt, T. Van Hove, E. Westwater, and D. Whiteman, 2003: The ARM Program's Water Vapor Intensive Observation Periods: Overview, Initial Accomplishments, and Future Challenges. *BAMS*, **84**, 217-236.

Turner, D. D., B. M. Lesht, S. A. Clough, H. E. Revercomb, D. C. Tobin, 2003: Dry Bias and Variability in Vaisala RS80-H Radiosondes: The ARM Experience. *J. Atmos. Oceanic Tech*, **20**, 117-132.

Ferrare, R. A., E.V. Browell, S. Ismail, S. Kooi, L.H. Brasseur, V.G. Brackett, M. Clayton, J. Barrick, G. Diskin, J. Goldsmith, B. Lesht, J. Podolske, G. Sachse, F.J. Schmidlin, D. Turner, D. Whiteman, D. Tobin, H. Revercomb, L. Miloshevich, 2003: Characterization of upper troposphere water vapor measurements during AFWEX using LASE. Submitted to *J. Atmos. Oceanic Tech.*, **27**, October 2003.

D. C. Tobin, H. E. Revercomb, D. D. Turner, 2003: Radiosondes: The ARM and AIRS Perspectives. Workshop to Improve the Usefulness of Operational Radiosonde Data, Asheville, NC, 11-13 March 2003.

Metrics for water vapor accuracy required for remote sensing and climate applications have been developed. To characterize the downwelling flux at the surface to ~1W/m^2, and forward model issues relevant in the atmospheric window regions, the total column water vapor must be known to ~2%. Similarly, to characterize the Outgoing Longwave Flux at the top of atmosphere to ~1W/m^2 requires the top-most 0.1mm of water vapor in the profile to be known to 10%. Under clear sky conditions, ARM MicroWave Radiometer (MWR) measurements at 22.8 Ghz combined with an accurate forward model have been shown to provide total column water vapor measurements (PWV) with absolute accuracy of ~2% for PWV greater than ~1 cm. A sample comparison of PWV measurements from eleven sensors during the Water Vapor Intensive Operating Period (WVIOP) 2000 is shown in Figure 17.

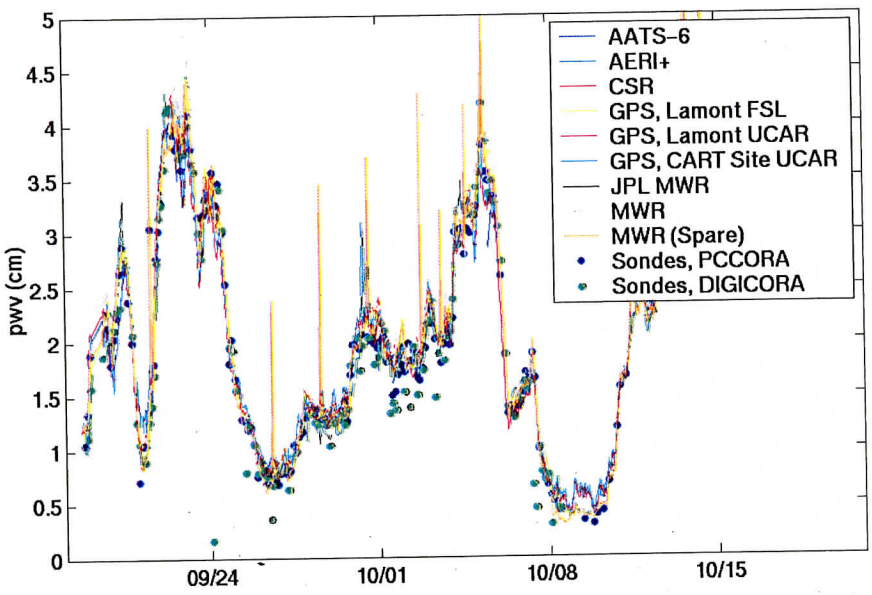

Figure 17. A time series of various total column water vapor measurements from one of the ARM WVIOPs which were conducted to establish the absolute accuracy of the ARM MicroWave Radiometers (MWR).

The accuracy of ARM upper level water vapor measurements with the ARM CART Raman Lidar and Vaisala radiosondes were investigated during the ARM/FIRE Water Vapor Experiment (AFWEX), conducted in December 2000. This experiment included aircraft based reference water vapor sensors. Numerous overpasses of the ARM site were made during

Ferrare, R. A., E.V. Browell, S. Ismail, S. Kooi, L.H. Brasseur, V.G. Brackett, M. Clayton, J. Barrick, G. Diskin, J. Goldsmith, B. Lesht, J. Podolske, G. Sachse, F.J. Schmidlin, D. Turner, D. Whiteman, D. Tobin, H. Revercomb, L. Miloshevich, 2003: Characterization of upper troposphere water vapor measurements during AFWEX using LASE. Submitted to *J. Atmos. Oceanic Tech.*, **27**, October 2003.

D. C. Tobin, H. E. Revercomb, D. D. Turner, 2003: Radiosondes: The ARM and AIRS Perspectives. Workshop to Improve the Usefulness of Operational Radiosonde Data, Asheville, NC, 11-13 March 2003.

Metrics for water vapor accuracy required for remote sensing and climate applications have been developed. To characterize the downwelling flux at the surface to ~1W/m^2, and forward model issues relevant in the atmospheric window regions, the total column water vapor must be known to ~2%. Similarly, to characterize the Outgoing Longwave Flux at the top of atmosphere to ~1W/m^2 requires the top-most 0.1mm of water vapor in the profile to be known to 10%. Under clear sky conditions, ARM MicroWave Radiometer (MWR) measurements at 22.8 Ghz combined with an accurate forward model have been shown to provide total column water vapor measurements (PWV) with absolute accuracy of ~2% for PWV greater than ~1 cm. A sample comparison of PWV measurements from eleven sensors during the Water Vapor Intensive Operating Period (WVIOP) 2000 is shown in Figure 17.

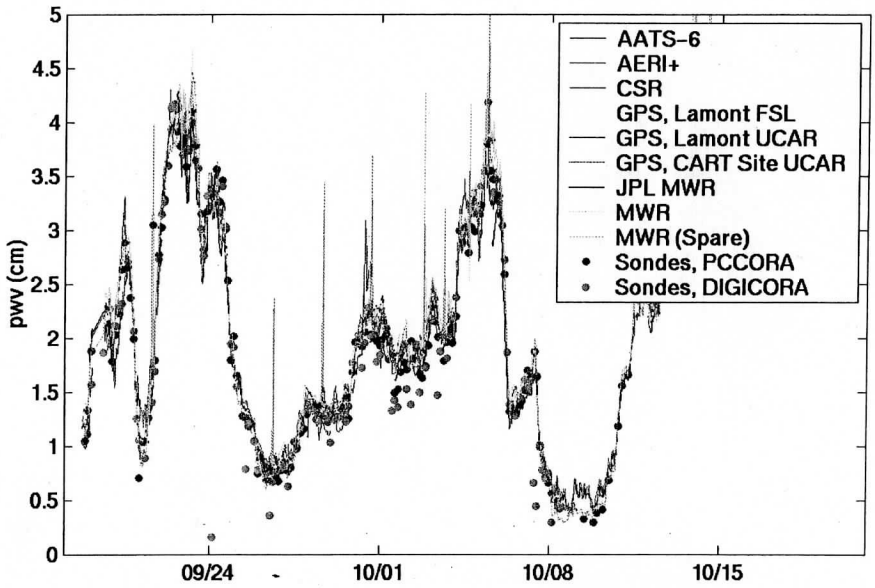

Figure 17. A time series of various total column water vapor measurements from one of the ARM WVIOPs which were conducted to establish the absolute accuracy of the ARM MicroWave Radiometers (MWR).

The accuracy of ARM upper level water vapor measurements with the ARM CART Raman Lidar and Vaisala radiosondes were investigated during the ARM/FIRE Water Vapor Experiment (AFWEX), conducted in December 2000. This experiment included aircraft based reference water vapor sensors. Numerous overpasses of the ARM site were made during

coincident Raman lidar measurements and radiosonde launches. After incorporating various physical corrections to the Raman Lidar calibrations and to the Vaisala RS-80 calibrations, agreement in upper level water vapor between several of the reference sensors, the Raman Lidar, and radiosondes on the <5% level was found.

Analysis of downwelling Atmospheric Emitted Radiance Interferometer (AERI) spectra
The ground based AERI instruments at the ARM sites measure the downwelling infrared spectra with high radiometric and spectral accuracy. Using collocated accurate measurements of the lower troposphere temperature and water vapor, we have compiled a large ensemble of clear sky AERI residuals (observed minus calculated). This dataset is very useful for refining the representation of the water vapor continuum absorption, particularly in the atmospheric window regions. Based on this data, adjustments to the strength of the water continuum absorption coefficients in the longwave window regions have been determined. AERI residuals for an atmospheric "microwindow" at 900 wavenumbers versus PWV is shown in Figure 18.

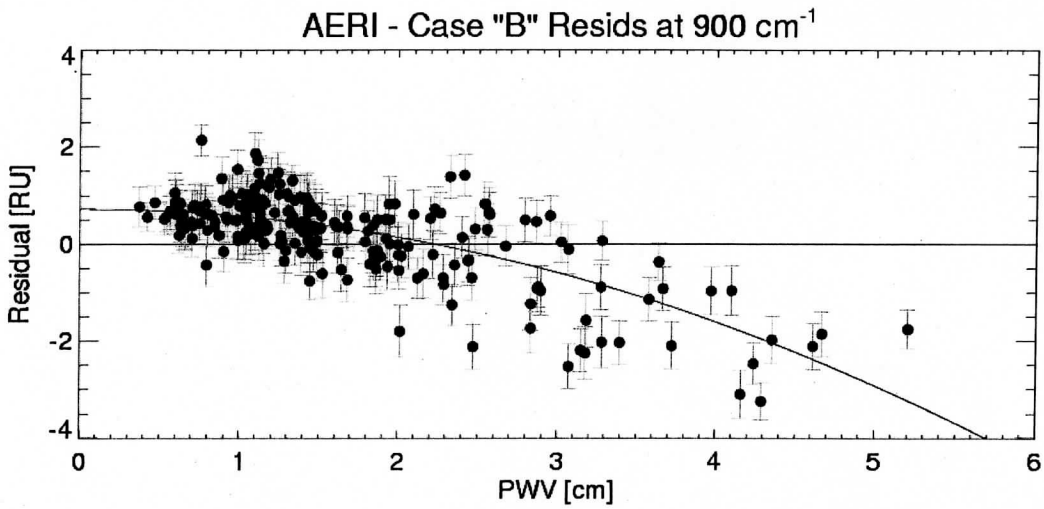

Figure 18. AERI observed minus calculated differences at 900 wavenumbers for the Southern Great Plains clear sky ensemble using the CKDv2.4 water vapor continuum model. The decrease in residual with increasing PWV is the signal that the water vapor continuum absorption used in the model calculations is too large.

The dataset has also been used to derive new water continuum coefficients in the shortwave window region (Strow, October 2003 AIRS Science Team Meeting). This has reconciled differences that were previously seen between the longwave and shortwave spectral regions in the AIRS clear sky residuals.

Also, this AERI dataset has been used to derive a new representation of the carbon dioxide far wing lineshape in LBLRTM. This has improved the residuals by ~1K in the main 15 micron temperature sounding channels. Publications which summarize our AERI related forward model work include:

Turner, D. D., D. C. Tobin, S. A. Clough, P. D. Brown, R. G. Ellingson, E. J. Mlawer, R. O. Knuteson, H. E. Revercomb, T. R. Shippert, W. L. Smith, and M. Shepard, 2003: The QME

AERI/LBLRTM: A closure experiment for downwelling high spectral resolution infrared radiance. In review, *J. Atmos. Sci.*, June 2003.

Tobin, D. C., D. D. Turner, H. E. Revercomb, 2002: Analysis of the AERI / LBLRTM QME. Twelfth ARM Science Team Meeting, St. Petersburg, FL, 8-12 April 2002.

Shephard et al., 2003: Validation of CO2 line parameters used in temperature retrievals. Optical Society of America ORS/FTS Topical Meeting, Quebec City, 3-6 February 2003.

Shaphard, M. W., S. A. Clough, D. C. Tobin, H. E. Revercomb, R. O. Knuteson, J. Worden, R. Beer, L. Brown, A. Goldman, and C. P. Rinsland, 2003: Radiative Transfer Modelling for TES. ASSFTS (Atmospheric Science from Space using Fourier Transform Spectrometry) 11 Workshop, Bad Wildbad (Black Forest), Germany, 8-10 October 2003.

Development of a new water vapor continuum model, MT_CKD

A significant achievement is the development and release of a new water vapor continuum model. This work was led by Tony Clough's group at AER, Inc. The first water vapor continuum model, called CKDv0, was released in 1989. This was an empirical model of the non-lorentzian water vapor lineshape, which had various adjustable parameters. These parameters were adjusted to obtain best agreement with various water vapor continuum measurements which were available at the time. Since then, based on new measurements, there have been many modifications to the CKD continuum coefficient, but without tracing the differences back to the underlying water vapor lineshape. To address this, a revised formulation for the water vapor lineshape, called MT_CKDv0, has been developed and released. This model is based primarily on the ARM AERI ensemble, on AERI-ER measurements of the far-IR emission from the Arctic ARM site, and from various aircraft based case studies (e.g. SHIS, NAST-I). The advantage of having a continuum model which has an underlying lineshape is that the model can be extended to spectral regions where direct measurements of the continuum are not available. MT_CKD extends continuously from 0 to 20,000 wavenumbers. MT_CKD has since been subject to many forward model validation studies, which is discussed in the next section. Publications regarding the development of MT_CKD include:

E. J. Mlawer, S. A. Clough, D. C. Tobin, 2003: The MT_CKD Water Vapor Continuum: A Revised Perspective Including Collision Induced Effects. ASSFTS (Atmospheric Science from Space using Fourier Transform Spectrometry) 11 Workshop, Bad Wildbad (Black Forest), Germany, 8-10 October 2003.

E. J. Malwer, D. C. Tobin, S. A. Clough, 2003: A New Water Vapor Continuum Model: MT_CKD_1.0. Thirteenth ARM Science Team Meeting, Broomfield, CO, 31 March - 4 April 2003.

Figure 19 shows results from working with MT_CKD.

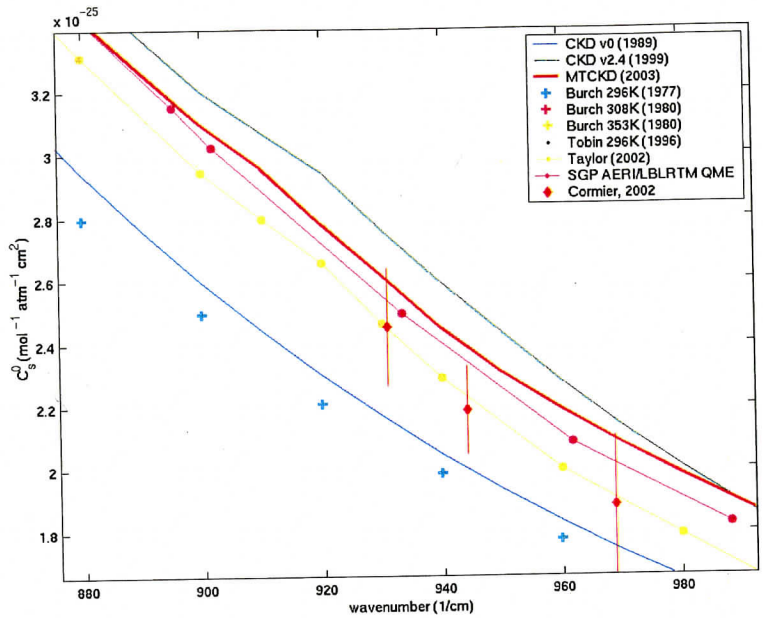

Figure 19. Comparison of various measurements and models of the self broadened water vapor continuum in the longwave window. The solid red curve is our new continuum model, MT_CKD.

Validation of improved forward modeling using ground, aircraft, and satellite based observations

We have used real atmospheric observations from AERI, SHIS, NASTI, and AIRS to validate the various aspects of the clear sky forward models. This work results in a significant risk reduction for CrIS. As mentioned previously, these validations show that the forward models have attained or are approaching the required accuracies. Example validations using Scanning-HIS and AIRS data are shown in Figures 20 and 21. Publications relevant to these efforts are:

H. Revercomb, D. Tobin, R. Knuteson, F. Best, and J. Li, 2003: Testing ARM Longwave QME with AIRS on the NASA Aqua Platform and Water Vapor Messages. 2003 ARM Instantaneous Radiative Flux (IRF) Working Group Meeting, SUNY, Albany, New York, 21-23 October 2003

D. C. Tobin, 2003: ARM Site Atmospheric State Best Estimates and AIRS Observed minus Calculated Spectra. AIRS Science Team Meeting, JPL, Pasadena, CA, May 2003.

L. L. Strow, S. E. Hannon, S. De Souza-Machado, H. E. Motteler, and D. C. Tobin, 2003: An Overview of the AIRS Radiative Transfer Model. *IEEE Transactions on Geoscience and Remote Sensing*, **41**, pp303-313.

Clough et al., 2003: Radiation Models for ARM: Updates, Validations and Rapid Models for the Shortwave. Thirteenth ARM Science Team Meeting, Broomfield, CO, 31 March - 4 April 2003.

Clough et al., 2004: Atmospheric Radiative Transfer Modeling: A Summary of AER Codes. Fourteenth ARM Science Team Meeting, Albuquerque, New Mexico, 22-26 March 2004.

Shephard et al., 2003: Validation of CO2 line parameters used in temperature retrievals. Optical Society of America ORS/FTS Topical Meeting, Quebec City, 3-6 February 2003.

M. W. Shaphard, S. A. Clough, D. C. Tobin, H. E. Revercomb, R. O. Knuteson, J. Worden, R. Beer, L. Brown, A. Goldman, and C. P. Rinsland, 2003: Radiative Transfer Modelling for TES. ASSFTS (Atmospheric Science from Space using Fourier Transform Spectrometry) 11 Workshop, Bad Wildbad (Black Forest), Germany, 8-10 October 2003.

Tjemkes, S. A., T. Patterson, R. Rizzi, M. W. Shephard, S. A. Clough, M. Matricardi, J. Haigh, M. Hopfner, S. Payan, A. Trotsenko, N. Scott, P. Rayer, J. Taylor, C. Clerbaux, L. L. Strow, S. DeSouza-Machado, D. Tobin, R. Knuteson, 2003: ISSWG Line-by-line Intercomparison Experiment, *JQSRT*, **77**, 433-453.

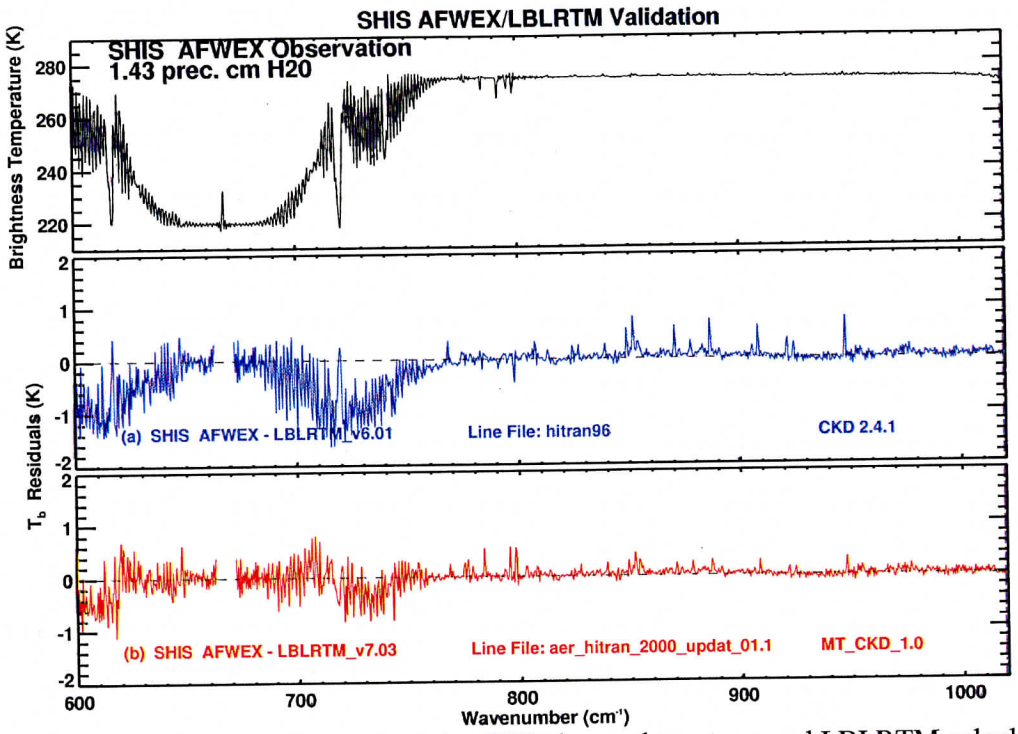

Figure 20. A comparison of a clear sky Scanning-HIS observed spectrum and LBLRTM calculations using LBLRTM versions 6.01 and 7.03. Version 7.03 includes improvements to the far wing carbon dioxide lineshape based on AERI data.

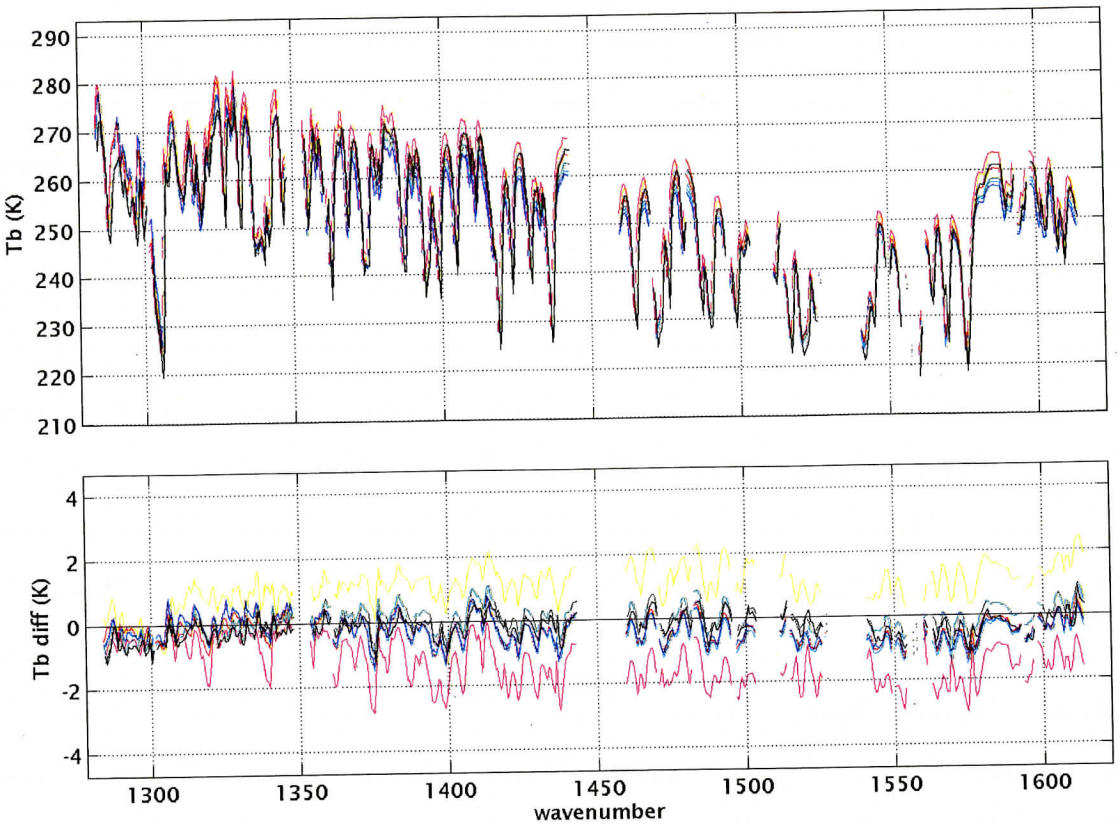

Figure 21. Mean AIRS clear sky spectra and residuals (observed minus calculated) for upper level water vapor channels using various validation dataset ensembles. The ensembles include the NASA GSFC Raman Lidar (yellow), Radiosonde launches from the Chesapeake Lighthouse (purple), research grade frost point hygrometers of Voemel et al. (black) and our ARM SGP night (green) and day (red) and ARM TWP night (blue) and day (cyan) "best estimate" profiles. The Voemel measurements are considered to be the most accurate sensors available for this purpose. Using the Voemel or ARM ensembles, the AIRS residuals are less than a few tenths K for all but the highest peaking channels. For the highest peaking channels, the Voemel and ARM residuals are suggestive of a dry bias in the water vapor measurements, or of a water vapor near wing lineshape issue, or some combination of both.

3.6 CrIS Instrument Evaluation

The accomplishments under this section are described in Section 3.1.

3.7 Training and Mentoring

This Government Study support two main activities in the area of training and mentoring: support of a post-doctoral student and the development of specialized course material for an undergraduate course in satellite remote sensing.

The UW hired a post-doc from France named Yao Te, who had been working in the Paris group lead by Claude Camy-Peret, the joint-chairman of the IASI Sounding Science Working Group (ISSWG). Dr. Te completed just over one year of his post-doctoral study before returning to Paris with a teaching position. Dr. Te worked with the PI and co-Is of this study to further the

understanding of the absolute calibration of the S-HIS and NAST-I aircraft instruments. In particular, he investigated the use of monte carlo modeling to numerically compute the emissivity of the UW on-board reference cavities. Dr. Te also successfully applied techniques for carbon monoxide retrieval from the IASI balloon borne simulator (also an FTS instrument) to NAST-I data.

Course material was developed by the PI for use in a student workshop conducted in Maratea, Italy in 22-31 May 2003. The web link for the workshop is given at http://barrage.ssec.wisc.edu/%7Epaoloa/teaching/Maratea2003/html/index.html The title of the presentation was "High Spectral Resolution IR Observing & Instruments." The meeting was supported by CNR-IMAA(Potenza) & EUMETSAT(Darmstadt). This project also indirectly supported a workshop on Soundings from High Spectral Resolution Infrared Observations in Madison, Wisconsin from 6-8 May 2003. This "sounding" workshop brings together experts from the government, academia, and industry to discuss current topics of interest to the sounding community.

3.8 UW NAST-I Support

This task provides support for the NAST-I instrument and includes the following:

Field Campaign Support
The UW provided in-the-field support for the NAST-I radiance calibration data processing during the IHOP, CRYSTAL-FACE, Pacific THORPEX 2003 and Atlantic THORPEX 2003 campaigns. Support was also provided during the TX-2002, although the NAST-I was having significant instrument problems and did not collect any useable data. Data from each NAST-I mission has been processed in the field and the data transferred to a "data warehouse" at the University of Wisconsin Space Science and Engineering Center. This NAST-I data warehouse is mirrored to a computer system at NASA Langley so that as data is added in Wisconsin it appears on the system at LaRC the next day. The data processing for each mission was completed within 30 days of each experiment. The NAST-I web page has a link for database access through a UW web site: http://deluge.ssec.wisc.edu/~nasti/.

A significant activity under the later portion of this contract period was the evaluation of instrument problems with the NAST-I sensor. The NAST-I instrument performed well during IHOP and CRYSTAL-FACE but failed during the TX-2002 mission and was in a non-optimal configuration for both THORPEX missions (Pacific and Atlantic 2003). There were problems with noise performance, spectral calibration, and linearity experienced with the longwave detector. The data reprocessing to handle some of these anomalous instrument conditions is still in progress.

Calibration Support
During this reporting period the NAST blackbodies were recalibrated and the 3 sigma drift over the 34 month period since their original calibration was found to be 20 mK for the ambient blackbody and 15 mK for the hot blackbody. This is well within the allowable drift and less than the uncertainty in the Guildline Temperature Standard (+/- 30 mK) that is used for the absolute temperature calibration of the blackbody thermistors.

Additional coarser level "sanity" checks of blackbody temperatures during flight were carried out by looking at the temperature of the hot blackbody compared with the set point temperature, and by looking at the relative difference of the ambient blackbody thermistors. The average of the "top" and "bottom" thermistors in the hot blackbody should be within 0.1 K of the set point temperature, and typically, this average has been running within 0.07 K—indicating healthy thermistors. It should be noted that the temperature that the hot blackbody runs with respect to the set point is not critical; it is the knowledge of temperature that is important. This is why the absolute accuracy of the set point was designed to be somewhat looser than the thermistor temperature accuracy (which is typically better than 0.05 K). Checks of the ambient blackbody thermistors during flight show that the maximum gradient between them is less than 0.1 K. This measurement is well within the expected value of 0.2 K, and indicates that all three ambient blackbody thermistors are behaving well.

Science Coordination Support

The radiative properties of clouds has been an active area of investigation lead by Prof. Bill Smith working closely with a UW researcher, Dan DeSlover. Examples of significant work have been included under the "clouds" discussion of section 3.4 and one technical paper is included in the appendix. A list of literature citations is included here:

DeSlover, Daniel H.; Nasiri, Shaima; Knuteson, Robert O., and Revercomb, Hank E. Measurement of cirrus cloud optical properties from ground- and aircraft-based high spectral resolution interferometry. *Remote Sensing of Clouds and the Atmosphere VI*, Toulouse, France, 17-20 September 2001. Bellingham, WA, International Society for Optical Engineering, (SPIE), 2001, pp1-7. Reprint #3358.

DeSlover, DH, RO Knuteson, DD Turner, DN Whiteman, and WL Smith. 2002. "AERI and Raman Lidar Cirrus Cloud Optical Depth Retrieval to Validate Aircraft-Based Cirrus Measurements." In *Proceedings of the Twelfth ARM Science Team Meeting*, Ed. by D. Carrothers, U.S. Department of Energy, Richland, WA.

DeSlover, Daniel H.; Knuteson, Robert O.; Osborne, Brian; Zhou, Daniel K., and Smith, William L. Validation of aircraft-measured land surface emissivity. *Optical Remote Sensing of the Atmosphere and Clouds III,* Hangzhou, China, 25-27 October 2002. Bellingham, WA, International Society for Optical Engineering, (SPIE), 2003, pp384-391. Reprint #3475.

DeSlover, D. H., D. D. Turner, D. N. Whiteman, and W. L. Smith (2002): Ground-based measurement of cirrus cloud optical properties as validation to aircraft- and satellite-based cloud studies. In *Proceedings from the 9th International SPIE Symposium on Remote Sensing: Remote Sensing of the Clouds and Atmosphere VII*, Crete, Greece.

DeSlover, D. H., D. D. Turner, D. N. Whiteman, and W. L. Smith (2002): Ground- and aircraft-based cirrus cloud measurements using lidar and high spectral resolution FTS during the AFWEX 2000 field campaign. In *Proceedings from the 47th Annual SPIE meeting: Atmospheric Radiation Measurements and Applications in Climate*, Seattle, WA.

Design Support for the NAST-2

UW provided continuous support to help formulate top-level requirements and preliminary design concepts for the follow-on NAST instrument, currently referred to as NASTER. We supported the NASTER kick-off meeting held at NASA LaRC in July 2003, with presentations related to radiometric calibration and lessons learned from other interferometer-based aircraft instruments. In support of NASTER activities we created a table that breaks down the instrument development into 26 components and that identifies: a) the organizations were responsible for these program components for past instrument developments; the organizations that now have capability in each area; and several scenarios that could be considered for the NASTER development. The development scenario is presented in Table 8.

Table 8. NASTER Development Scenarios.

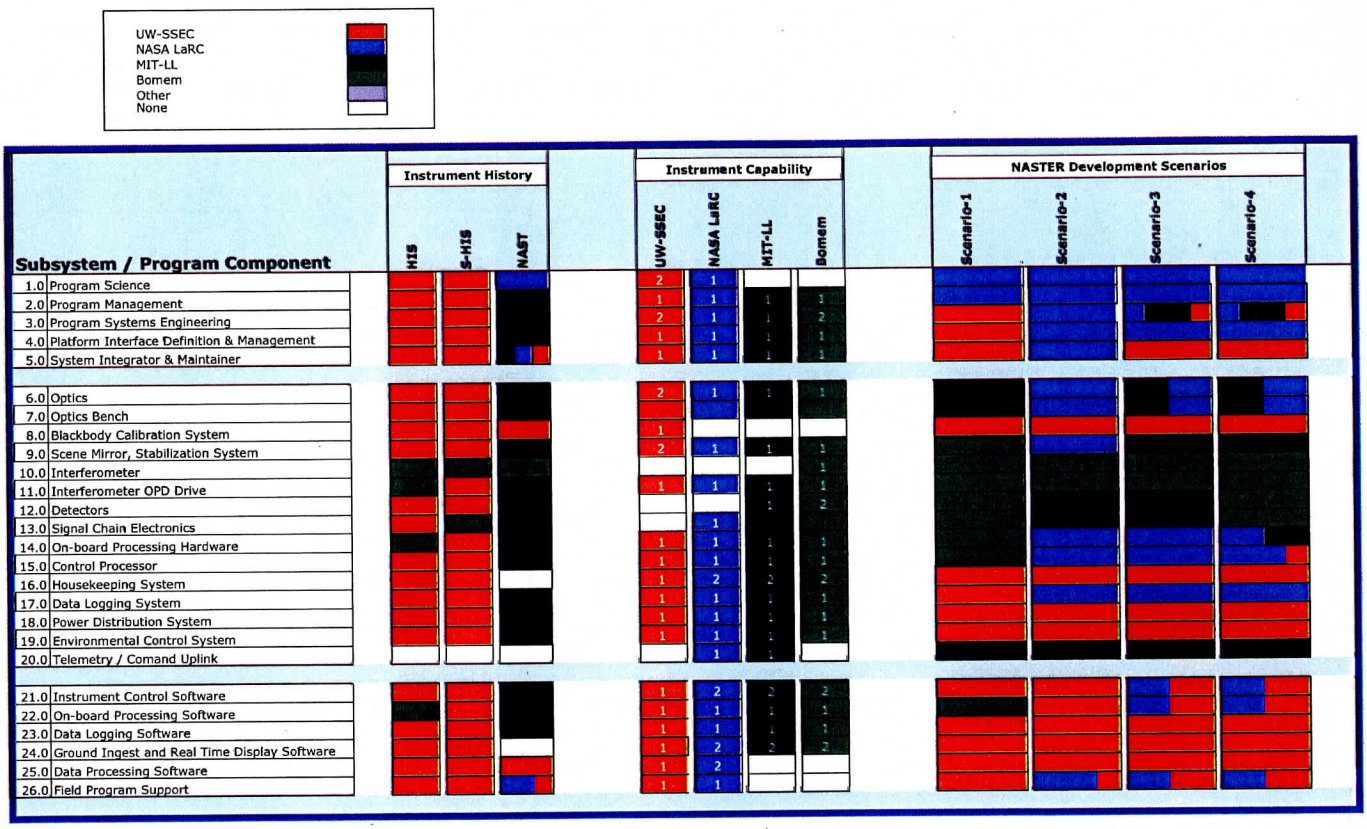

As a result of the Kick-off meeting, UW was assigned 5 trade studies defined in Table 9 with the key questions that are to be addressed. An outline of each study was sent to the project office at LaRC in early October of 2003, and a draft version was completed in late November. The studies are expected to be complete soon.

During the month of December 2003, UW also supported several LaRC costing exercises related to the NASTER development.

Table 9. UW NASTER Trade Studies.

Study #	Study Name	Key Questions
2	**Mirror design: Corner cube vs. flat**	What type of mirror design would best meet the noise performance requirement across the various platform environments?
10	**Zenith View and 3rd Blackbody**	Identify the benefits from a zenith view and or use of 3rd blackbody source. What is the cost in terms of weight, size, and power. What is the benefit in regards to the calibration accuracy requirement?
11	**Spectral resolution and coverage**	Identify feasible spectral resolution ranges and spectral coverage.
15	**Data storage and archive system**	Identify feasible data storage and archive systems that will handle the expected data rates and be maintenable over the instrument lifetime.
16	**Software Architecture and Design for Flight and Support Systems**	Identify software architecture and design for flight OS and flight software. This includes data acquisition and instrument control functionality.

Appendix A: Contract Statement of Work

Date of SOW: Original Proposal 7-01
Period of Performance: 10-01 through 5-02
Budget: $235,000

(1) Cross-track Infrared Sounder (CrIS) Characterization and Calibration Participation
During the first year we will evaluate current plans for fundamental radiometric performance testing of the CrIS instrument. Several aspects of these tests are specific to the interferometer design for CrIS, which we are quite familiar with from the development of the UW HIS and Scanning HIS, plus work with the NAST-I. As part of this effort, we will review plans for NIST participation in the testing. [Plans for government participation in the CrIS prelaunch testing are discussed in the NPP Calibration and Validation Plan.]

(2) Field Campaign Participation to Collect Atmospheric Data Sets for Validation Technique and Algorithm Testing
Part of any field campaign involves preparing and characterizing the data sets to make them useful for further studies and to allow them to be used by other parties. During the first year we will prepare the data set from the Scanning HIS participation in the NASA Clams mission, to be conducted during July and August of 2001. This mission will offer opportunities for validation demonstrations using the Terra spacecraft and for Scanning HIS intercomparisons with NAST-I. This data set will be added to the existing data catalog and made available on-line via the internet from a dedicated data server.

(3) Development and Implementation of Aircraft Instrument Performance Improvements
This task is aimed at further investigations to reduce the aerodynamically induced forcing on the Scanning HIS for ER2 applications. Several approaches will be investigated, probably including aerodynamic changes to the pod on the ER2 to reduce the forcing, and interferometer modifications (electrical and beamsplitter-compensator) to reduce the alignment static tilt. We need to make the effort to bring the performance on the ER2 up to the level of performance realized on the ground and recently proven achievable under special conditions in the air. This effort is important to refine the Scanning HIS as an important validation tool, but it will also point to the way to bring the NAST performance up to this level.

(4) Validation Algorithm Development and Testing
This task includes developments related to three important products for aircraft validation.

a) Cloud Radiative Properties:
This task is to develop techniques for deriving cloud radiative properties from aircraft observations that can be used to validate NPOESS cloud products. In the first year, a case study will be performed from a recent field experiment to demonstrate the ability of the high spectral resolution infrared observations to detect and identify cloud radiative properties.

b) Temperature and Water Vapor Sounding:
This task is to refine the technique for deriving atmospheric temperature and water vapor vertical profiles from the aircraft observations of upwelling spectral radiance. In the first year, a retrieval formalism will be implemented for use with Scanning-HIS and/or NAST-I data. Comparison will be made with in situ validation sources to verify the software implementation of the approach.

c) Surface Temperature and Emissivity:
This task is to develop an approach for the validation of NPOESS land surface characterization products. In the first year, data from recent field programs will be used to develop the algorithms for deriving surface properties from aircraft data and to demonstrate the capabilities of existing in situ measurements in the validation of this data. In particular, land surface emissivity and temperature products derived from aircraft observations will be compared with ground-based measurements made in the vicinity of a ground truth site.

(5) Forward Model Refinement
This task is to create validation cases of high spectral resolution observations and atmospheric state data specifically designed to test forward radiative transfer equation models and to compare those data set results against reference calculations. This task includes participation in the international comparison of forward RTE models organized by EUMETSAT for the IASI Sounder Science Working Group (ISSWG). During the first year, a validation case will be created for use in RTE validation.

(6) CrIS Instrument Trade-offs and Evolution Evaluation
We will evaluate instrument trades and evolution options as they arise during the design, fabrication, and testing phases, and provide IPO consultation and recommendations.

(7) Training and Mentoring
Involve an undergraduate and graduate student or young scientist in the SSEC IPO project to accomplish mentoring, while efficiently accomplishing other tasks.

Date of SOW: 7 Feb 02
Period of Performance: 6-02 through 5-03
Budget: $522,744 (Mod #1)

(1) Cross-track Infrared Sounder (CrIS) Characterization and Calibration Participation
This task includes participation in the CrIS pre-launch ground testing as outlined in the NPP Calibration and Validation Plan.

(2) Field Campaign Participation
This task will continue the effort to collect atmospheric data sets for validation technique and algorithm testing. Possible campaigns include the NASA CRYSTAL experiment in Florida and the NASA TX-2002 experiment in the Southern Great Plains.

(3) Development and Implementation of Aircraft Instrument Performance
This task is to continue the incremental improvements to the airborne instruments used in validation of the NPOESS products. This includes an effort to reduce sensitivity to Electro-Magnetic Interference on the ER-2 high altitude aircraft platform.

(4) Validation Algorithm Development and Testing
This task is to continue to refine the algorithms for deriving information from the high spectral resolution aircraft observations in preparation for the use of these techniques for validation of future NPOESS products. Specific techniques to be addressed are cloud property determination, temperature and water vapor retrieval, and surface property characterization.

(5) Forward Model Refinement
This task is to continue the effort to generate case studies to address areas of uncertainty in forward radiative transfer modeling and to collaborate with research groups working in this important area.

(6) CrIS Instrument Trade-offs and Evolution Evaluation
This task will continue the evaluation of trade studies and other issues that arise during the period of design, fabrication, and test. This task will support the role of consultation and the provision of recommendations.

(7) Training and Mentoring
This task will continue the support of training and mentoring of undergraduate students, graduate students, and/or young scientists in the area of atmospheric remote sensing with the long-term objective of fostering the next generation of scientists and engineers.

Date of SOW: 19 May 03
Period of Performance: 6-03 through 12-03
Budget: $660,457 (Mod #2)

(1) Cross-track Infrared Sounder (CrIS) Characterization and Calibration Participation
This task includes planning and participation in the CrIS pre-launch ground testing as outlined in the NPP Calibration and Validation Plan. Under this task, CrIS design reviews will be supported by key UW-SSEC personnel.

(2) Field Campaign Participation
Under this task we will continue to collect atmospheric data sets for validation technique and algorithm testing. In FY 03/04, this task will include the analysis of the data collected by the Scanning HIS on the Proteus at the SGP in the fall of 2002. The support for conducting this field campaign was provided by the DOE ARM program. This task also involves conducting a field program with the Scanning HIS on the ER-2 at THORPEX, including, instrument preparation and calibration, instrument integration and test flights at NASA Dryden prior to deployment to Hawaii, four weeks in the field in Hawaii, and the initial phase of the post deployment data analysis.

(3) Development and Implementation of Aircraft Instrument Performance
Under this task we will continue the incremental improvements to the airborne instruments used in validation of the NPOESS products. There are two sub-tasks included under this task:

a) *Improvement in the interferometer mirror tilt correction algorithm.* Under this task efforts will be continued to compare an implementation of the mirror tilt correction algorithm with theoretical expectations of the error characteristics, and to develop a data set for use in model validation.

b) *Improve S-HIS ER-2 Ambient Blackbody Thermal Coupling.* During flight there is a desire to have the passively cooled S-HIS Ambient Blackbody (ABB) run at a colder temperature – closer to the pod ambient temperature. Lowering the ABB temperature will improve calibration accuracy. The current configuration of the S-HIS Ambient Blackbody is somewhat decoupled, thermally, from the pod environment. This allows the ABB descent heaters to raise the cavity temperature above the dew point as the ER-2 traverses from higher (colder) altitudes to the ground (warm moist conditions). A new design will be implemented that will improve thermal coupling to the pod environment during normal flight by using a high altitude fan blowing on a redesigned ABB aft end that incorporates cooling fins. The fan will be commanded off during descent, providing the decoupling necessary to allow proper cavity heating during that phase of the mission.

(4) Validation Algorithm Development and Testing
This task is to continue to refine the algorithms for deriving information from the high spectral resolution aircraft observations in preparation for the use of these techniques for validation of future NPOESS products. Specific techniques to be addressed are noise filtering, surface property characterization, and statistical regression dataset development.

(5) Forward Model Refinement
This task is to continue the effort to generate case studies to address areas of uncertainty in forward radiative transfer modeling and to collaborate with research groups working in this important area.

(6) CrIS Instrument Trade-offs and Evolution Evaluation
This task will continue the evaluation of trade studies and other issues that arise during the period of design, fabrication, and test. This task will support the role of consultation and the provision of recommendations.

(7) Training and Mentoring
This task will continue the support of training and mentoring of undergraduate students, graduate students, and/or young scientists in the area of atmospheric remote sensing with the long-term objective of fostering the next generation of scientists and engineers. In particular, we have included a full time Post Doctoral scientist to work closely with the senior science staff on all aspects of the program.

(8) Project Planning and Reporting
Under this task planning and reporting for the project is conducted. Travel for presentations at Washington, DC is also included under this task.

9) Support of NAST
This task provides support for the NAST-I instrument and includes the following:

a) *THORPEX Support.* Provide field support in Hawaii, data analysis and post-field reprocessing, and S-HIS/NAST-I instrument inter-comparison analysis.

b) *Texas 2002 Support.* Provide field support in Texas, data analysis, post-field reprocessing and S-HIS/NAST-I instrument inter-comparison analysis.

c) *Calibration Support.* Provide ongoing blackbody and end-to-end NAST instrument calibration support.

d) *Science Coordination Support.* Provide the PI with continued science coordination support.

e) *Design Support for the NAST-2.* Provide continuous support to help formulate top level requirements and preliminary design concepts.

Appendix B: Attached Papers of Significant Work

- Validation of AIRS Spectral Radiances with the Scanning HIS Aircraft
  Henry E. Revercomb, David C. Tobin, Robert O. Knuteson, Fred A. Best, William L. Smith, Paul van Delst, Daniel D. LaPorte, Scott D. Ellington, Mark W. Werner, Ralph G. Dedecker, Ray K. Garcia, Nick N. Ciganovich, H. Benjamin Howell, Steven Dutcher, and Joe Taylor

- Validation and Comparison of S-HIS and NAST-I Retrieval for THORPEX 2003
  P. Antonelli, H. E. Revercomb, R. O. Knuteson, D. C. Tobin, S. Dutcher, W. L. Smith, and D. Zhou

- Vibration Induced Tilt Error Model for Aircraft Interferometer Data
  E. R. Olson, H. E. Revercomb, R. O. Knuteson, H. B. Howell, D. D. LaPorte, S. D. Ellington, M. W. Werner, R. K. Garcia, and F. A. Best

- Validation of Satellite AIRS LST/LSE Products Using Aircraft Observations
  Robert O. Knuteson, Brian J. Osborne, Henry E. Revercomb, David C. Tobin, and William L. Smith, Sr.

Validation of Atmospheric InfraRed Sounder (AIRS) Spectral Radiances with the Scanning High-resolution Interferometer Sounder (S-HIS) aircraft instrument

Henry E. Revercomb, David C. Tobin, Robert O. Knuteson, Fred A. Best, William L. Smith*, Paul van Delst, Daniel D. LaPorte, Scott D. Ellington, Mark W.Werner, Ralph G. Dedecker, Ray K. Garcia, Nick N. Ciganovich, H.Benjamin Howell, Steven Dutcher, and Joe K. Taylor

University of Wisconsin-Madison, Space Science and Engineering Center
1225 West Dayton Street, Madison Wisconsin, 53706
* NASA Langley Research Center

ABSTRACT

The ability to accurately validate high spectral resolution IR radiance measurements from space using comparisons with aircraft spectrometer observations has been successfully demonstrated. The demonstration is based on a 21 November 2002 under-flight of the AIRS on the NASA Aqua spacecraft by the S-HIS on the NASA ER-2 high altitude aircraft and resulted in brightness temperature differences approaching 0.1K for most of the spectrum!

Aircraft comparisons of this type provide a mechanism for periodically testing the absolute calibration of spacecraft instruments with instrumentation for which the calibration can be carefully maintained on the ground. This capability is especially valuable for assuring the long-term consistency and accuracy of climate observations, including those from the NASA EOS spacecrafts (Terra, Aqua and Aura) and the new complement of NPOESS operational instruments. The validation role for accurately calibrated aircraft spectrometers also includes application to broadband instruments and linking the calibrations of similar instruments on different spacecraft.

Both the AIRS and the S-HIS calibrations are expected to be very accurate (formal 3-sigma estimates are better than 1 K brightness temperature for a wide range of scene temperatures), because high spectral resolution offers inherent advantages for absolute calibration and because they make use of high emissivity cavity blackbodies as onboard radiometric references. AIRS has the added advantage of a cold space view, and the S-HIS calibration has benefited from the availability of a zenith view from high altitude flights on the Proteus aircraft. The S-HIS has also benefited from calibration techniques developed over many years in conjunction with the original HIS aircraft instrument and with the Atmospheric Emitted Radiance Interferometer (AERI) instruments developed for the DOE ARM Program. The absolute radiometric calibration is traceable to NIST, and in the future, we plan to check the calibration directly by inter-comparison to a NIST-maintained sensor (the TXR radiometer).

It is expected that aircraft flights of the S-HIS and its close cousin the NPOESS Atmospheric Sounder Testbed (NAST) will be used to check the long-term stability of AIRS and the NPOESS operational follow-on sounder, the Cross-track Infrared Sounder (CrIS), over the life of the mission.

1. Introduction

The need for higher accuracy and more refined error characterization of radiance measurements from space (and corresponding geophysical products) to improve both weather forecasting and climate change monitoring has led to a new emphasis on conducting direct tests of in-orbit performance, referred to as "validation". Validation involves collecting higher quality reference data from specially maintained airborne and ground-based facilities that can support refined analyses of a controlled set of well-understood measurements, instead of statistical analyses of data having inconsistent pedigree and unknown error characteristics. This is a positive trend that will help take full advantage of our satellite systems.

The validation activities initiated for the NASA Earth Observing System (EOS) platforms, which are well underway for the Terra and Aqua platforms and will soon be initiated for Aura, are setting the stage for enhanced validation of new observational satellite systems. Extensive plans for validation of the National Polar Orbiting Environmental Satellite System (NPOESS) and future geosynchronous systems are also underway. The Scanning High-resolution Interferometer Sounder (S-HIS) aircraft instrument discussed in this paper is an important validation tool that is currently being used for both EOS and NPOESS. For NPOESS, S-HIS use is coordinated with the NPOESS Airborne Sounder Testbed (NAST) to optimize payload compatibility with joint field campaigns and for critical inter-comparison tests of accuracy.

2. The Scanning High-resolution Interferometer Sounder (S-HIS)

The Scanning HIS is an airborne Michelson Interferometer follow-on to the original University of Wisconsin HIS (Smith, et al., 1989; Revercomb, et al., 1988a) that was flown successfully on the NASA ER2 from 1986 to 1998. The original nadir-only spatial sampling of the HIS has been replaced by cross-track coverage with similar 2-km footprints, while at the same time S-HIS is smaller and much easier to operate (Revercomb, et al., 1996, 1998). In addition to the NASA ER2, it has been successfully flown on the NASA DC8 and on the Scale Composites Proteus, as shown in Figure 1. As illustrated, the Proteus implementation also provides a zenith view to augment calibration information and as a valuable capability for studying upper level water vapor.

Typical S-HIS radiance spectra are shown in Figure 2. The overlapping regions of the three spectral bands are used to constrain the non-linearity correction required for the longwave and midwave bands that use photo-conductive HgCdTe detectors. The shortwave band uses an InSb detector and its expected linearity is confirmed by the lack of telltale out-of-band contributions. As with the original HIS (Revercomb, et al., 1988b, 1989, 1997; Best, et al., 1997), accurate calibration has been a major goal for the S-HIS. Figure 3 shows the 3-sigma radiometric performance expected for S-HIS. Note that for scene temperatures above 220 to 240 K, the 3-sigma absolute calibration accuracy is less than 0.3 K! For carefully calibrated IR spacecraft instruments, the accuracy will be even better for cold scene temperatures, because space provides a well-known cold reference.

The zenith viewing option was first implemented in November 2002. Up and down-looking observations from 14 km altitude are shown in Figure 4. Note the accurate zero determined from the warm and intermediate temperature blackbody spectra shown, even for the non-linear longwave and midwave bands. The zenith view adds an important constraint on the S-HIS non-linearity correction algorithm (Revercomb, 1994).

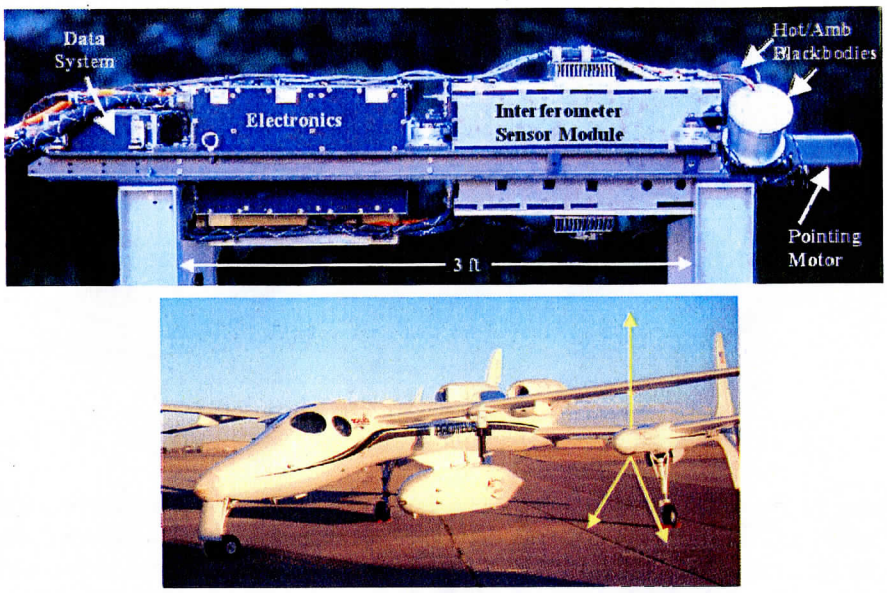

Figure 1. Scanning HIS instrument and illustration of cross-track and zenith viewing from the Proteus aircraft. S-HIS has been configured to fly on the NASA DC8 and ER2 aircraft as well as the Proteus.

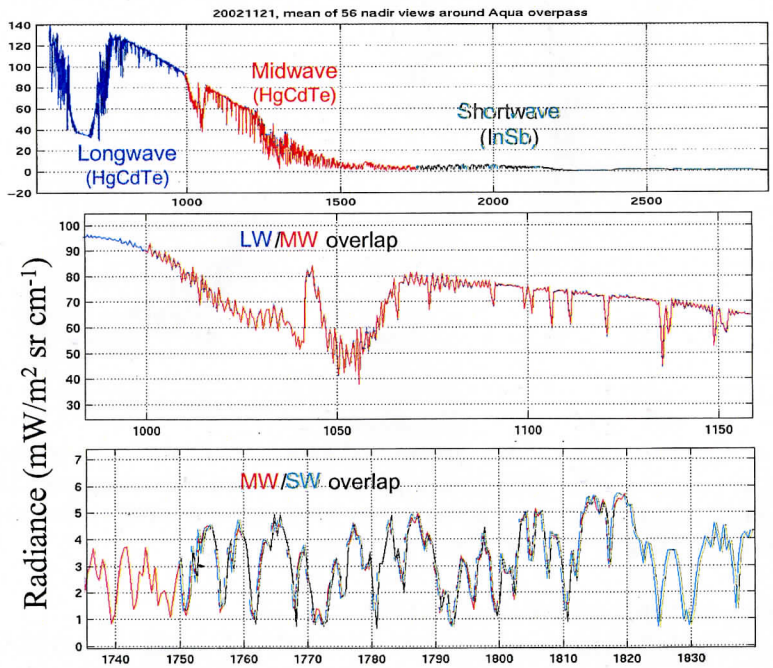

Figure 2. Scanning HIS radiance spectra collected over the Gulf of Mexico on 21 November 2002 from the NASA ER2 at 20 km altitude during the Terra-Aqua Experiment (TX-2002). The three separate spectral bands of S-HIS are illustrated, along with the good agreement between spectra from neighboring bands where they overlap.

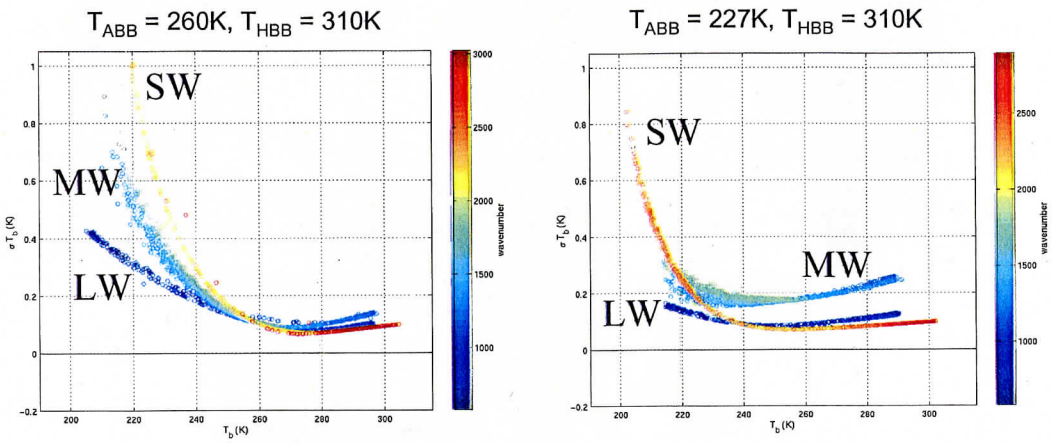

Figure 3. Three-sigma calibration accuracy estimates for Scanning HIS with two different ambient blackbody temperatures. Conditions apply to AIRS vadiation flights on 21 November 2002 on the ER2 over the Gulf of Mexico (left) and 16 November 2002 on Proteus over the DOE Atmospheric Radiation Measurement (ARM) site in Oklahoma. T_{ABB} and T_{HBB} are the ambient and hot blackbody temperatures.

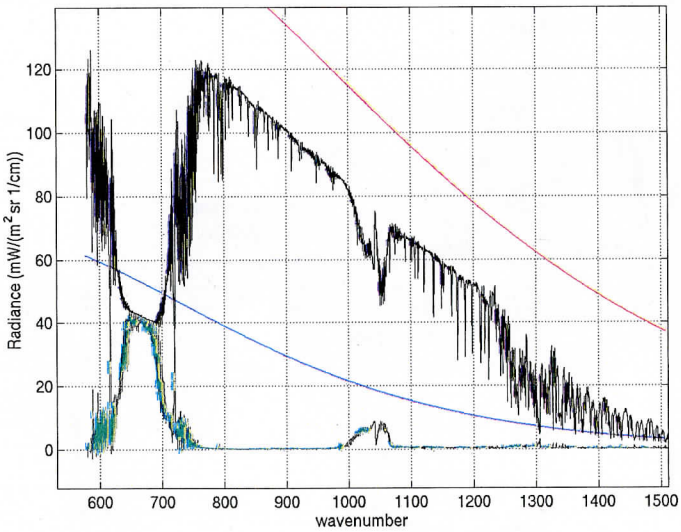

Figure 4. Comparison of zenith (green) and nadir (black) radiance spectra from the Proteus at 14 km over the DOE Atmospheric Radiation Measurement (ARM) program Southern Great Plains site on 16 November 2002. Spectra of the reference blackbodies used for calibration are shown in red and blue.

3. Validation of AIRS with Scanning HIS

The Atmospheric Infrared Sounder (AIRS) on the NASA Aqua spacecraft launched on 20 May 2002 is a cryogenic cross-dispersed grating spectrometer (Aumann et al., 2003). It employs 7 different orders of dispersion to map the spectrum onto 12 detector modules with a total of 15 linear arrays. A single spatial footprint is detected at a time, with the field being focused on the grating to minimize the impact of non-uniform cloudy scenes on spectral calibration.

The differences in spatial and spectral sampling that need to be accounted for in making accurate comparisons of AIRS and S-HIS are illustrated in Figure 5. The technique selected for doing this is to make use of calculations that account for the actual spectral and spatial characteristics of each instrument. The calculated spectra allow the observation-minus-calculation residual for each instrument to be compared, avoiding the first-order effects of these differences. To improve this comparison even further, the residuals are each convolved with the Instrument Line Shape (ILS) of the other. This is equivalent to eliminating grating contributions from optical path differences larger than measured by S-HIS and weakly apodizing S-HIS to match the effect of the AIRS ILS.

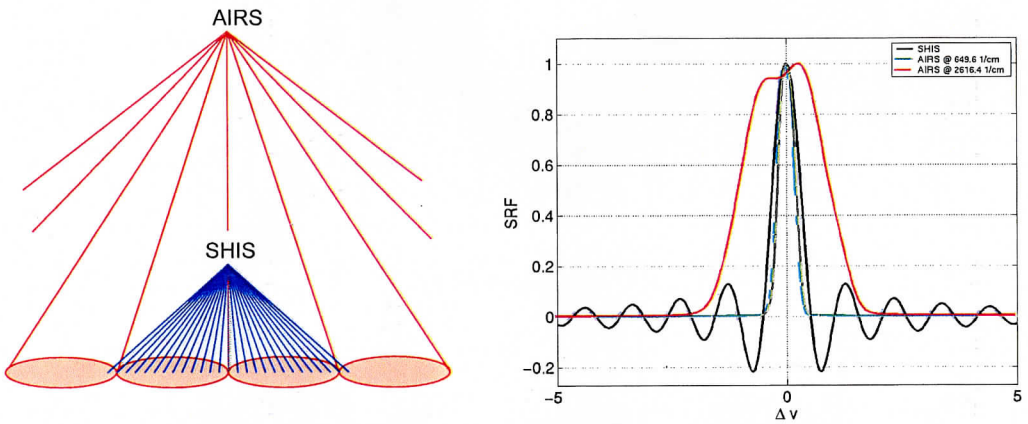

Figure 5. Illustration of the differences between AIRS and S-HIS spatial viewing conditions (left) and spectral Instrument Line Shape (ILS) functions that need to be accounted for in making detailed radiance comparisons.

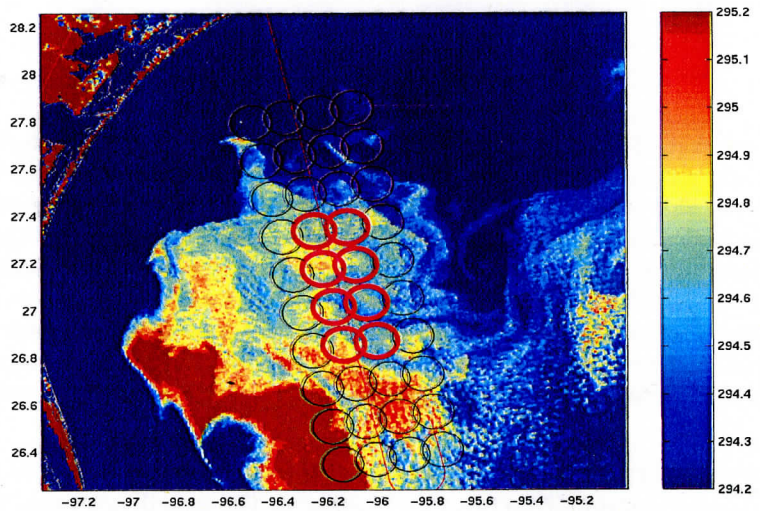

Figure 6. Aqua MODIS 12 micron band image over the Gulf of Mexico on 21 November 2002, illustrating the aircraft sub-track (narrow line) and the 8 near nadir AIRS footprints (~15 km diameter) chosen for comparison based simultaneity and scene uniformity (peak-to-peak brightness temperature variations of about 0.5 °C).

The best conditions for validation of AIRS with Scanning HIS to date were encountered over the Gulf of Mexico on 21 November 2002 as part of the Terra Aqua Experiment (TX 2002). The excellent scene uniformity is illustrated in Figure 6, and the first-order spectral comparison is shown in Figure 7. For this first-order comparison, the spectra from each instrument have been noise filtered using principle component techniques, and averaged over common spatial footprints.

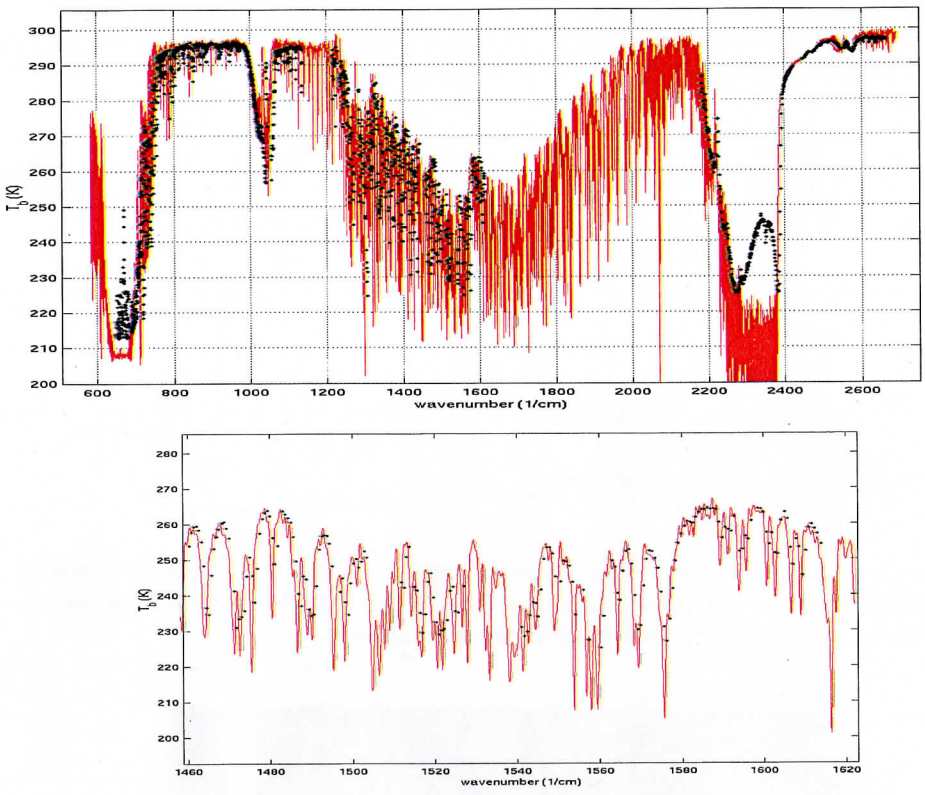

Figure 7. Average of Scanning HIS spectra (red) from inside 8 AIRS footprints (see Figure 6) compared to AIRS spectral channels (black +'s) averaged over the 8 footprints. For this comparison, nothing has been done to account for the different spectral characteristics or altitudes of the two platforms. The portions of the AIRS spectra in the middle of the 15 and 4-micron carbon dioxide bands are sensitive to altitudes above the ER2 altitude of the S-HIS and should not be expected to agree. However, the spectrum from near the middle of the 6.3-micron water vapor band (lower blow-up) is a region where the effective spectral resolutions are comparable, and where the major contributions come from below the ER2. Note the excellent agreement in this region.

The final comparison between S-HIS and AIRS radiances is shown in Figure 8 as the difference of spectrally normalized obs-calc residuals. The excellence of the agreement is demonstrated by the histograms for each module, as discussed in the caption. Note that while the small residual differences are not just for window regions, but extend deeply into the 15-micron carbon dioxide band and also into the 6.3-micron water vapor band. The analysis also identified a spectral scale error in one AIRS module (Figure 9).

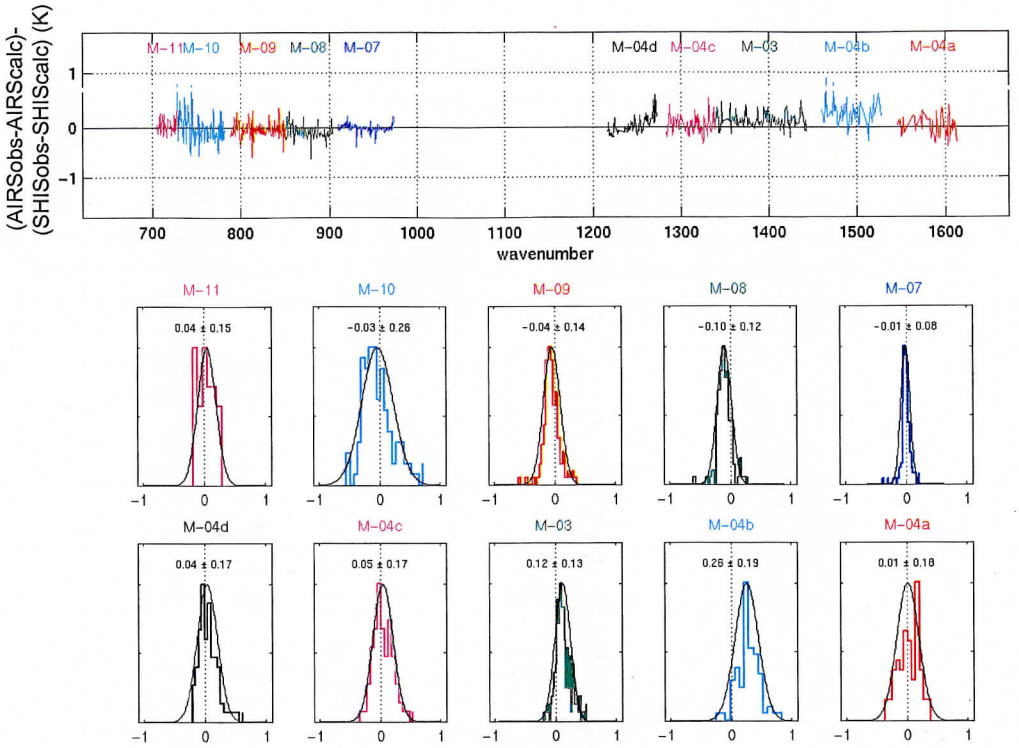

Figure 8. Summary of final AIRS to Scanning HIS comparison with elimination of channels with significant sensitivity above the ER2. The colors distinguish different detector modules of the AIRS instrument (separate linear detector arrays), with corresponding color coded histograms of differences. Note the excellent agreement! The mean agreement over most modules is order 0.1 °C or less (M-04b is the one exception with a mean of 0.26 °C). Also, the standard deviations are with one exception less than 0.2°C.

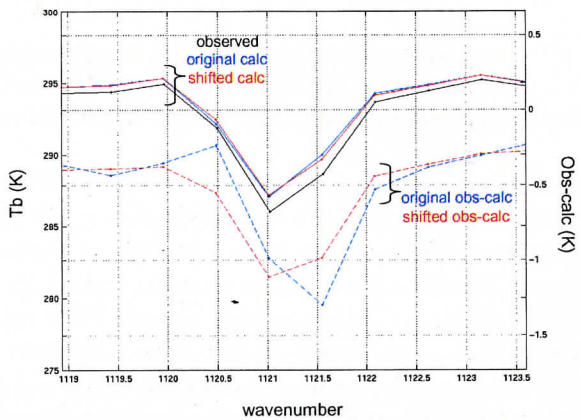

Figure 9. Evidence for very small shift in the spectral calibration of AIRS channels (3% of spectral resolution) from module M-05 discovered with S-HIS. The original shift has now been confirmed with direct comparisons of calculated spectra with AIRS and the spectral response functions adjusted to remove it.

4. Assessment of MODIS Calibration from AIRS

Having validated AIRS with S-HIS, it is useful to consider the implications for other infrared instruments. Since the AIRS provides reasonably high spectral resolution, it can be used to simulate the radiance of lower resolution instruments, such as the EOS MODIS imager, by convolving the AIRS spectrum with the normalized MODIS spectral resolution function for each of the 15 MODIS IR bands. A sample AIRS spectrum is compared to MODIS spectral response functions in Figure 10. Note that there are some gaps in the AIRS spectrum that create significant convolution errors, unless they are accounted for.

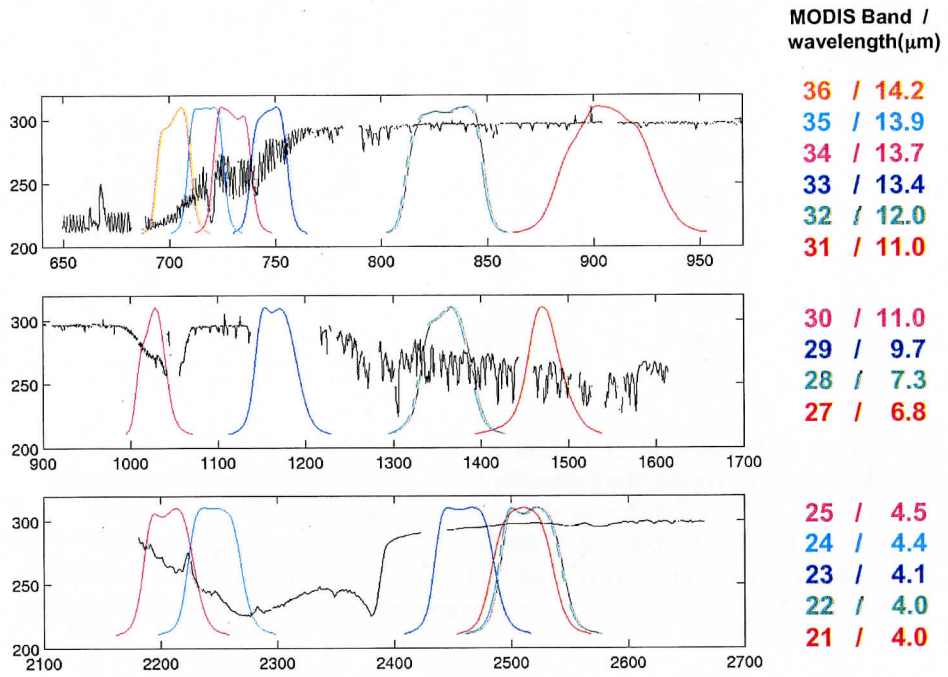

Figure 10. Comparison of AIRS spectrum and MODIS spectral response functions for its overlapping IR bands. It is clear that most MODIS bands can be simulated with AIRS by convolving the AIRS spectra with the MODIS spectral response functions.

The results of comparing co-located AIRS and MODIS for a large selection of global samples, chosen from reasonably uniform AIRS footprints is shown in Figure 11. Note that the numbers of comparisons range from a few 100,000 for window channels and the ozone channel to almost 2 million for the most opaque channel 36. The distributions of AIRS-MODIS differences shown in blue for each band are the final results with corrections for convolution errors determined from a standard atmosphere. The blue bars give an estimate of the convolution errors and are centered at the mean AIRS-MODIS difference. Given the excellent agreement between AIRS and S-HIS, it is expected that the largest part of these differences are issues with MODIS. The most significant differences occur for the most opaque 15-micron CO2 bands (34-36) and for water vapor (27, 28).

Red=without accounting for convolution error
Blue=accounting for convolution error with mear
correction from standard atmospheres

p-p Convolution Error (CE) Estimate

Band	Diff	CE	Diff	Std	N
21	0.10	-0.01	0.09	0.23	187487
22	-0.05	-0.00	-0.05	0.10	210762
23	-0.05	0.19	0.14	0.16	244064
24	-0.23	0.00	-0.22	0.24	559547
25	-0.22	0.25	0.03	0.13	453068
27	1.62	-0.57	1.05	0.30	1044122
28	-0.19	0.67	0.48	0.25	1149593
30	0.51	-0.93	-0.41	0.26	172064
31	0.16	-0.13	0.03	0.12	322522
32	0.10	0.00	0.10	0.16	330994
33	-0.21	0.28	0.07	0.21	716940
34	-0.23	-0.11	-0.34	0.15	1089663
35	-0.78	0.21	-0.57	0.28	1318406
36	-0.99	0.12	-0.88	0.43	1980369

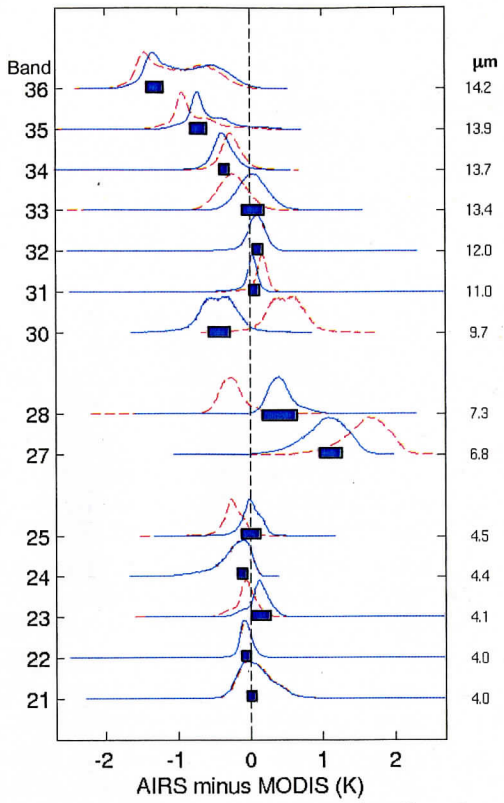

Figure 11. Distributions of brightness-temperature differences between AIRS and MODIS for a large number of samples (N) taken from scenes with reasonably small spatial non-uniformity. An spectral shift in the MODIS spectral response functions could account for most of these differences. It has been demonstrated that a single spectral shift would make the differences small for a wide range of scene brightness temperature conditions.

5. Summary

These initial results of comparing AIRS in orbit on the Aqua platform to aircraft observations from S-HIS illustrate the substantial advantages of high spectral resolution observations for accurate calibration applications.

The basic conclusions are listed below:

1. The calibration uncertainty of advanced high spectral resolution infrared observations are approaching the 0.1 K desired for climate applications,
2. High spectral resolution observations from airborne instruments (S-HIS & NAST) are now proven tools for the detailed validation of satellite based observations,
3. AIRS is providing high quality global radiances for atmospheric sounding & climate applications, and a calibration reference for other IR instruments, and
4. High spectral resolution Aircraft comparisons provide a way to periodically test the absolute calibration of spacecraft instruments with instrumentation that can be carefully re-calibrated with reference standards on the ground, which is especially valuable for assuring the long-term consistency and accuracy of weather and climate observations.

Acknowledgements
We gratefully acknowledge the support of the Integrated Project Office (IPO), contract 50-SPNA-1-00039 and of NASA contract NAS5-31375 for support of S-HIS instrument refinement, field deployment, and data analysis for this work. Integration of S-HIS to the Proteus and early development was supported by the DOE ARM Program.

References

Aumann, H.H., Chahine, M.T., C. Gautier, M.D. Goldberg, E. Kalnay, L.M. McMillan, H. Revercomb, P.W. Rosenkranz, W.L. Smith, D.H. Staelin, L.L. Strow, and J. Susskind, 2003: AIRS/AMSU/HSB on the Aqua Mission: Design, Science Objectives, Data Products, and Processing Systems. IEEE Transactions on Geoscience and Remote Sensing, 41, p 253-264.

Best, F.A.; Revercomb, H.E.; LaPorte, D.D.; Knuteson, R.O., and Smith, W.L, 1997: Accurately calibrated airborne and ground-based Fourier transform spectrometers II: HIS and AERI calibration techniques, traceability, and testing. In: Proceedings of the Council for Optical Radiation measurements (CORM) 1997 Annual Meeting, National Institute of Standards and Technology (NIST), Gaithersburg, MD

Revercomb, H.E., D.D. LaPorte, W.L. Smith, H. Buijs, D.G. Murcray, F.J. Murcray, and L.A. Sromovsky, 1988a: High-Altitude Aircraft Measurements of Upwelling IR Radiance: Prelude to FTIR from Geosynchronous Satellite. Mikrochimica Acta [Wien], II, 439-444.

Revercomb, H.E., H. Buijs, H.B. Howell, D.D. LaPorte, W.L. Smith, and L.A. Sromovsky, 1988b: Radiometric Calibration of IR Fourier Transform Spectrometers: Solution to a Problem with the High Resolution Interferometer Sounder. Applied Optics, 27, 3210-3218.

Revercomb, H.E., H. Buijs, H.B. Howell, R.O. Knuteson, D.D. LaPorte, W.L. Smith, L.A. Sromovsky, and H.W. Woolf, 1989: Radiometric Calibration of IR Interferometers: Experience from the High-resolution Interferometer Sounder (HIS) Aircraft Instrument. RSRM '87:Advances in Remote Sensing Retrieval Methods, A. Deepak, H. Fleming, J. Theon (Eds.). A. Deepak Publishing, Hampton, Virginia

Revercomb, H. E., 1994: Techniques for Avoiding Phase and Non-linearity Errors in Radiometric Calibration: A Review of Experience with the Airborne HIS and Ground-based AERI. Keynote Address, Proceedings of the 5th International Workshop on Atmospheric Science from Space using FTS, p 353-378, Tokyo, Japan, 30 November -2 December.

Revercomb, H. E., W. L. Smith, F. A. Best, J. Giroux, D. D. LaPorte, R. O. Knuteson, M. W. Werner, J. R. Anderson, N. N. Ciganovich, R. W. Cline, S. D. Ellington, R. G. Dedecker, T. P. Dirkx, R. K. Garcia, and H. B. Howell, 1996: Airborne and ground-based Fourier transform spectrometers for meteorology: HIS, AERI and the new AERI-UAV. Proceedings SPIE Optical Instruments for Weather Forecasting, edited by G.W. Kamerman, 2832, 106-117.

Revercomb, H. E., F. Best, D. LaPorte, R. Knuteson, W. Smith, N. Ciganovich, R. Dedecker, T. Dirkx, R. Garcia, R. Herbsleb, J. Short, and H. Howell, 1997: Accurately Calibrated Airborne and Ground-based Fourier Transform Spectrometers I: HIS and AERI Instrument Design, Performance, and Applications for Meteorology and Climate. Council for Optical Radiation Measurements (CORM) 1997 Annual Meeting, National Institute of Standards and Technology (NIST), Gaithersburg, Maryland, 29 April.

Revercomb, H.E., D. C. Tobin, V.P. Walden, J. Anderson, F.A. Best, N.C. Ciganovich, R.G. Dedecker, T. Dirkx, S.C. Ellington, R.K. Garcia, R. Herbsleb, H.B. Howell, R.O. Knuteson, D. LaPorte, D. McRae, and M. Werner, Recent Results from Two New Aircraft-based Instruments: the Scanning High-resolution Interferometer Sounder (S-HIS) and the NPOESS Atmospheric Sounder Testbed-Interferometer (NAST-I), Proceedings of the Eighth International Workshop on Atmospheric Science from Space using Fourier Transform Spectrometry (ASSFTS8), Toulouse, France, 16-18 November, 1998; sponsored by Meteo-France, CNES, CNRS; p 249-254.

Smith, W.L., H.M. Woolf, H.B. Howell, H.-L. Huang, and H.E. Revercomb, 1989: The Simultaneous Retrieval of Atmospheric Temperature and Water Vapor Profiles - Application to Measurements with the High-resolution Interferometer Sounder (HIS). RSRM '87:Advances in Remote Sensing Retrieval Methods, A. Deepak, H. Fleming, J. Theon (Eds.). A. Deepak Publishing, Hampton, Virginia.

Validation and Comparison of S-HIS and NAST-I Retrievals for THORPEX 2003

P. Antonelli*, H. E. Revercomb*, R. O. Knuteson*, D. C. Tobin*, S. Dutcher*, W. L. Smith+ and D. Zhou+

*University of Wisconsin, Madison, Wisconsin; +NASA Langley Research Center, Hampton, VA

Abstract

The Scanning High-resolution Infrared Sounder (S-HIS) and the NPOESS Aircraft Sounding Test-bed Interferometer (NAST-I) have flown simultaneously on the same platform during the 2003 THORPEX Observing System Test (PTOST) campaign. Both the instruments are Michelson interferometers and possess very high spectral and spatial resolution. The results of several airborne missions exploited in the past years have shown that the absolute accuracy of the spectral radiances measured with these instruments is excellent. This paper aims to take advantage of the simultaneous observations collected by the two interferometers and by the other instruments such as the Cloud Physics Lidar (CPL), the MODIS Airborne Simulator (MAS) and Dropsondes, involved in the mission, to show: a) the observation capabilities of S-HIS, b) the relative accuracy of the S-HIS derived products with respect to those derived by the other instruments c) the differences in the vertical and horizontal structure of the retrieved temperature fields between S-HIS and NAST-I.

Introduction

The S-HIS participation to the THORPEX program was aimed to answer the following questions: 1) What can be retrieved, in terms of vertical and horizontal resolution, from S-HIS observations? 2) How do the S-HIS observing capabilities compare to those of other instruments involved in the experiment? 3) How do we make the information about the atmospheric state embedded in the Fourier Transform Spectrometers data available to Numerical Weather Prediction (NWP) models? 4) Which impact do the FTS data have on NWP model analysis and forecast?

The work done for PTOST and presented in this paper focuses the first two questions, leaving the third and the fourth one to future work. The paper is divided in two main parts, the first one describes the THORPEX program and its first experiment (PTOST) and the second one describes the results (temperature retrievals) obtained for a specific case study and their validation. A short section dedicated to the conclusions closes the paper.

THORPEX

Overview

THORPEX is a 10 year international research program under the auspices of the World Meteorological Organization/World Weather Research Program (WMO/WWRP) deigned to accelerate improvements in short range (up to 3 days), medium range (3-7 days) and extended range (two week) weather forecast. THORPEX tries to asses the potential to produce significant quantitative and qualitative improvements in forecasts of high impact weather by addressing and examining issues related to predictability and observing system design. The program builds upon ongoing advances within the basic-research and operational-forecasting communities, and aims to enhance the international collaboration between these communities and with users of forecast products. The 2003 Pacific THORPEX Observing System Test (PTOST) is the first in the 10 year series of Pacific and Atlantic observation campaigns in support of the WWRP/USRP THORPEX Program.

Platforms and Instruments

PTOST was conducted from February 18 to March 15, 2003. The campaign focused on the characterization of high-impact weather in the North Pacific north of Hawaii, within the context of the overall objectives of THORPEX. It had objectives regarding tropical cloud characteristics and ocean thermal properties, as well as complimentary satellite validation and aviation weather objectives. The observing platforms and systems used for PTOST/2003 are the NASA ER-2 Aircraft equipped with:

- S-HIS (Infrared) a 0.5 cm-1 resolution Fourier transform spectrometer;
- NAST-I (Infrared) a 0.25 cm-1 resolution Fourier transform spectrometer;
- CPL (visible), measures backscatter cross-sections of cloud and aerosol particles at 1.064 and 0.532 microns, providing cloud and aerosol backscatter quick-looks, depolarization ration quick looks, optical depth and cloud boundaries;
- MAS (visible, infrared) a 50-channel multi-spectral imager Fast Ozone Photometer - high altitude /in situ/ ozone concentration.

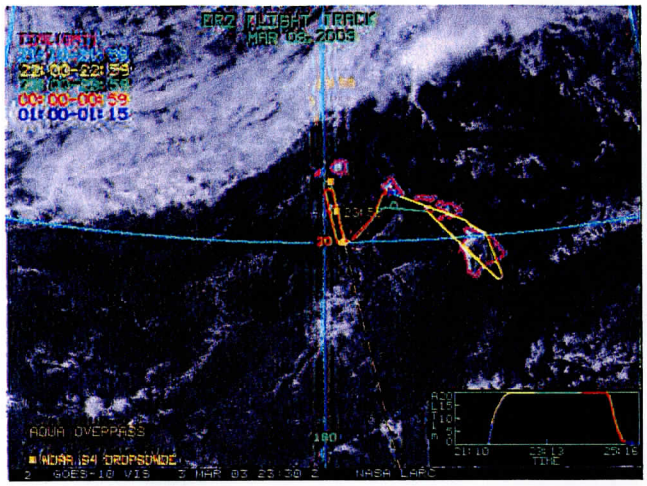

Figure 1: 03 March 2003: ER-2 Flight Track. The yellow squares indicate the locations where dropsondes were released by the G-4.

and the NOAA/G-4 Aircraft, coordinated with the ER-2 and equipped with:

- AVAPS high-density dropsonde system (simultaneous monitoring of 8 dropsondes).
- NOAA Aeromomy Laboratory measurements of ozone and carbon monoxide.
- Flight-level thermodynamic, wind velocity, and turbulence measurements.

The Science Objectives of the PTOST/2003 were: the inter-comparison of forecast skill using NOAA/G-4 dropsonde profiles in observationally sensitive regions versus ER-2 thermodynamic profiles from the S-HIS and NAST-I which are essentially a future sounder simulator (such as GIFTS or HES); the impact of cloud-top temperatures on data assimilation and forecasts given cloud-top heights from the ER2 airborne LIDAR combined with AIRS (Airborne Infra red Sounder) satellite data S-HIS and NAST cloud-top temperature and water vapor phase data.

Case Study

To answer the questions 1 and 2 in the introduction we selected as case study for this paper March 3rd, 2003 (030303). Data were collected between 23:40 and 00:00 UTC of the following day. The ER-2 took off from Honolulu (21:10 UTC) , flew South-East, over Big island (22:30 UTC), North-West toward Kaua'i and then it completed 2 loops (*race tracks*) South of Kaua'i (00:00 UTC) see figure 1. Four dropsondes were released along the *race track*, South of Kaua'i, by the G-4 (between 23:40 and 00:40 UTC), and one radiosonde was lunched from Lihue at 00:00 UTC.

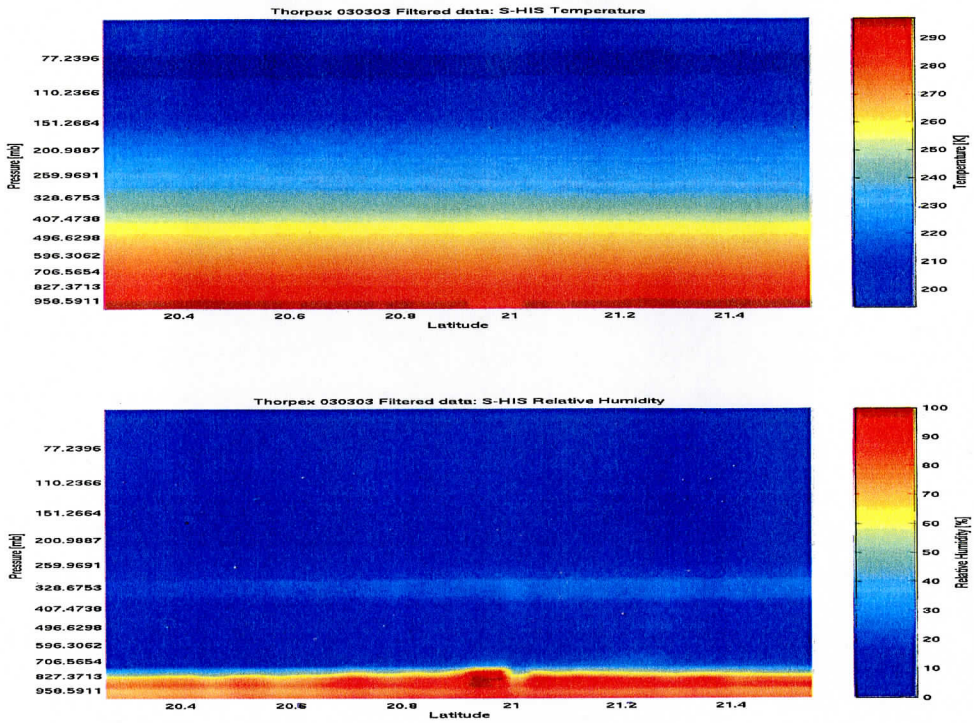

Figure 2: S-HIS VCS for Temperature (top) and Relative Humidity (bottom). The retrieved VCS refer to the flight segment South of Kaua'i between 23:48 and 00:03 UTC.

S-HIS Participation to THORPEX

S-HIS participation to PTOST aimed to provide atmospheric Temperature ($T(p)$) and water vapor Mixing Ratio, or Relative Humidity ($MR(p)$, $RH(p)$) profiles and cloud micro and macro-physical properties. The results showed in this paper focus only on the profiling capabilities of S-HIS. The atmospheric temperature and water vapor fields (figure 2) are retrieved from S-HIS observations using a statistical regression approach described in [Zhou et al. 2002, Huang and Antonelli] .

Validation

The S-HIS retrieved profiles have been validated against the radiosonde launched at Lihue on March 4th, at 00:00 UTC. Figure 3 shows the comparison between the retrieved profiles and the radiosonde. The first plot on the left shows the comparison of the temperature profiles as functions of pressure. The second and third plots show the comparison between the water vapor mixing ratio and relative humidity profiles. The forth plot shows how S-HIS retrieved profiles and of the radiosonde are relatively close in time and space. The comparison of the profiles shows good accuracy of the S-HIS retrieval for both temperature and water vapor.

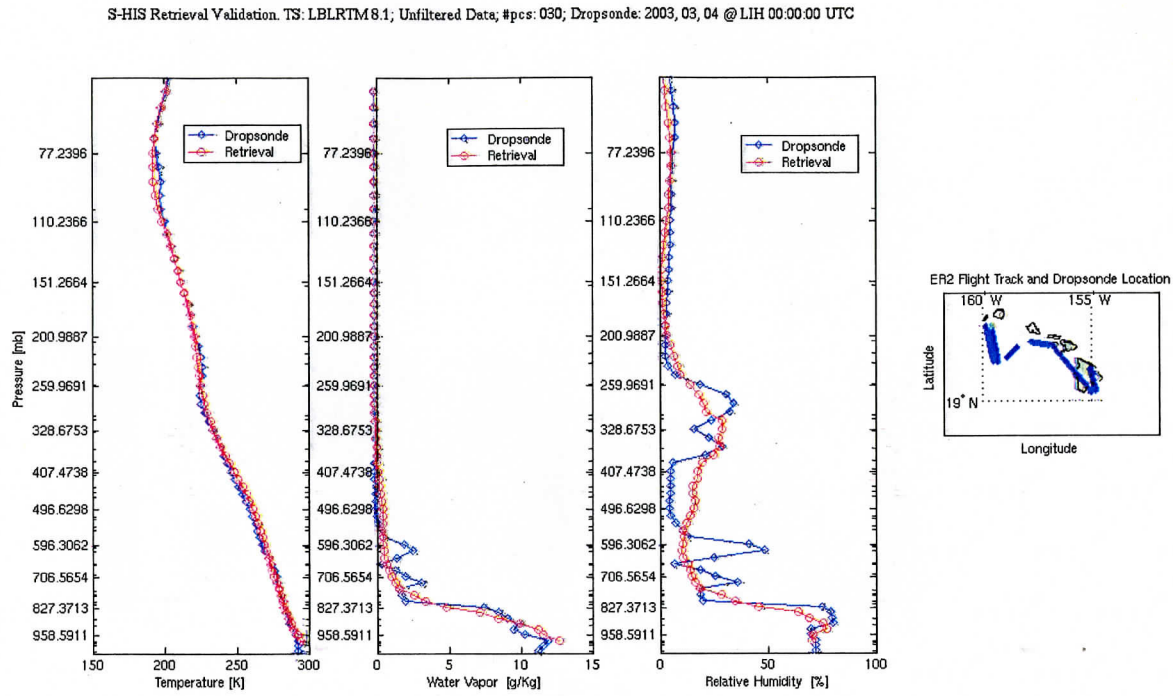

Figure 3: Validation of S-HIS derived temperature and water vapor mixing ratio profiles (red curves). The profiles have been validated against the radiosonde profiles observed at Lihue at 00:00 UTC (blue curves). Starting from the left side the first plot shows the comparison of the temperature profiles as functions of pressure. The second and third plots show the comparison between the water vapor mixing ratio and relative humidity profiles. The forth plot shows the location of the S-HIS retrieved profiles and of the radiosonde. The comparison of the profiles shows good accuracy of the S-HIS retrieval for both temperature and water vapor.

The profiles have been also validated against the dropsondes released by the G-4 South of Kaua'i. The top plot, in figure 4, shows a Vertical Cross Section (VCS) of the temperature deviation field, obtained interpolating spatially the deviation of 3 dropsonde temperature profiles from their mean. The plot shows an horizontal temperature gradient of about 7 K at 250 hPa. The bottom plot, obtained interpolating spatially the deviation of the 3 S-HIS retrieved temperature profiles (closest in space to the dropsonde) from their mean, shows the same vertical structure of the top plot. This comparison clearly shows the capability of S-HIS to provide valuable information about spatial atmospheric structures at high vertical resolution.

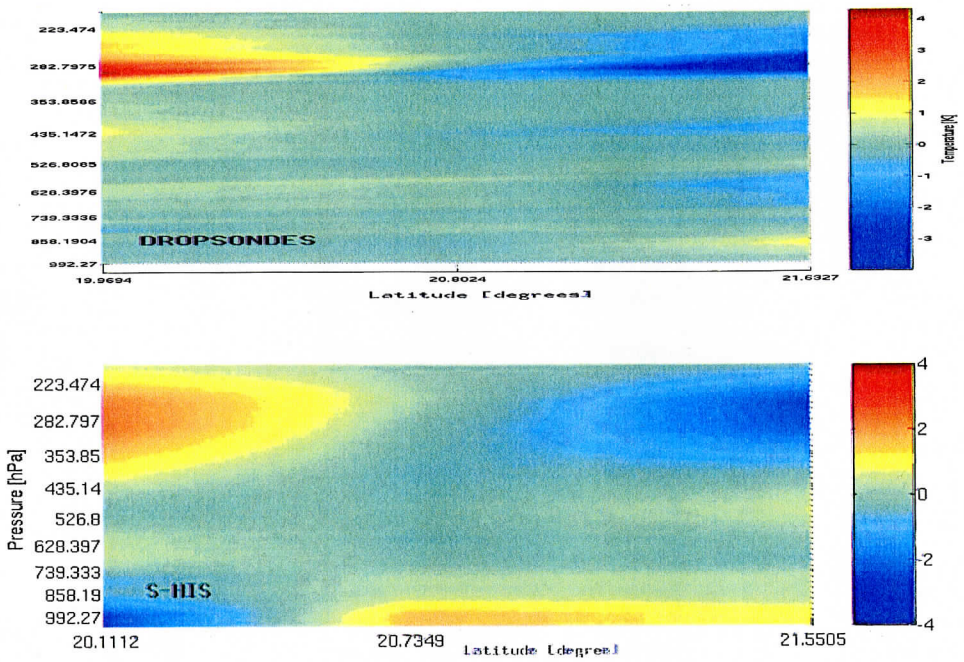

Figure 4: VCS of temperature deviation from the mean. The plots have been obtained interpolating spatially the deviation of 3 dropsonde temperature profiles from their mean (top) and 3 S-HIS retrieved temperature profiles (closest in space to the dropsonde) from their mean (bottom). They both show an horizontal temperature gradient of about 7 K at 250 hPa. The agreement between the images shows the S-HIS capability of accurately *observing* spatial temperature gradients.

Inter-comparison S-HIS, NAST-I

The VCS of the temperature deviation, derived from S-HIS observations, has been also compared to the NAST-I one (courtesy of the NAST-I NASA Langley group). In figure 5 the vertical structures shown in the two cross sections are similar. Both the instruments were able to *observe* the vertical temperature inversion at 12.5 Km of altitude and the strong horizontal temperature gradient ($\sim$ 7 K) at 10 and 15 Km of altitude. But the cross sections still show differences that, considering the similarities between the two instruments, are not expected and have to be further investigated.

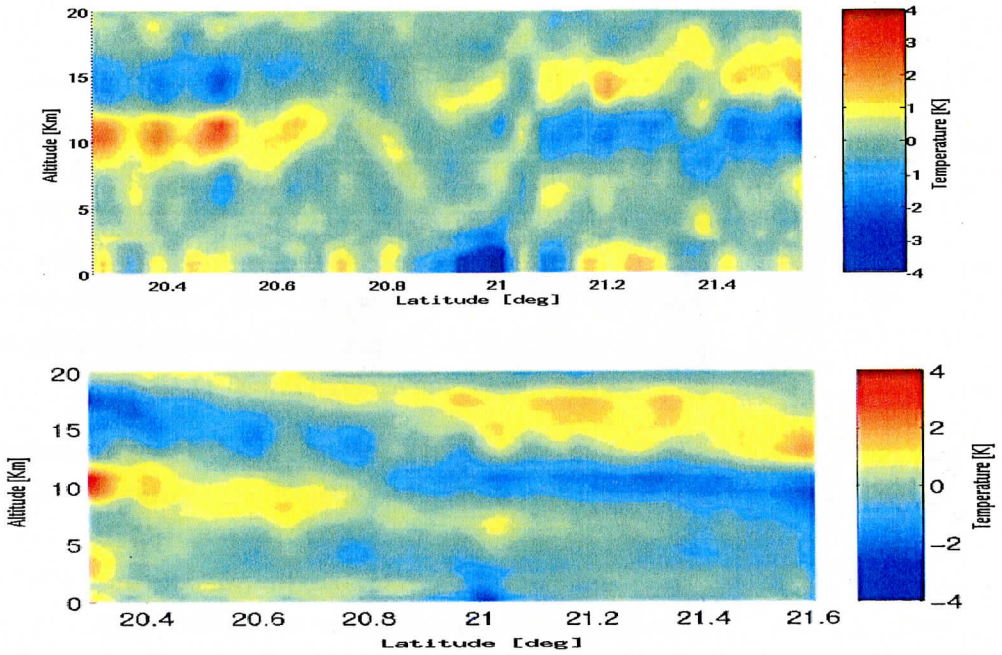

Figure 5: VCS of temperature deviation from the mean. The plots show the VCS as observed by S-HIS (top) and NAST-I (bottom) at full spatial resolution. The comparison of the two cross section shows similarities between the two spatial structures. Both the instruments were able to catch the vertical temperature inversion at 15.5 Km and the horizontal gradient at the same temperature. The plots also show differences that have to be further investigated.

Conclusions

The goal for this paper was to address the issues related to observational capabilities of S-HIS, in terms of vertical and horizontal resolution, and how they compare to the capabilities of other instruments involved in PTOST. With regard to the first question, S-HIS temperature retrievals for the selected case study, have been proved to be in good agreement with radiosonde data (figure 3). They have also been proved to be in good agreement with the profiles measured by the dropsondes released by the G-4. More important S-HIS showed the capability of observing real spatial structures of the atmospheric temperature field that could represent a valuable source of information for NWP models. The S-HIS retrieved temperature field was found to be in good agreement with the NAST-I retrieved field. But the comparison between the temperature retrievals obtained from the two interferometers showed also some differences that were not expected and that should be further investigated.

References

[Revercomb et al. 1996] Revercomb, H.E.; Smith, W.L.; Best, F.E.; LaPorte, D.D.; Knuteson, R.O.; Werner, M.W.: Anderson, J.R.; Ciganovich, N.N.; Ellington, S.D., and Dedecker, R.G.: *Airborne and ground-based Fourier transform spectrometers for meteorology - HIS, AERI and new AERI-UAV.* Optical Instruments for Weather Forecasting, Proceedings of the Conference, Denver, CO, 8-9 August 1996. Bellingham, WA: Society of Photo-Optical Instrumentation Engineers, 1996. (SPIE Proceedings volume 2832). Pp106-117.

[Smith et al., 1999] Smith, W.L.; Larar, A.; Hinton, B.; Howell, H.B.; Revercomb, H.E.; DeSlover, D.H.; Sisko, C.A.; Tobin, D.C.; Cousins, D.; Mooney, D.; Gazarik, M., and Mango, S., 1999: *The NPOESS Airborne Sounder Testbed-Interferometer (NAST-I): The validation of results from a new and revolutionary airborne remote sensing tool.* In: Conference on Atmospheric Radiation: A Symposium with tributes to the works of Verner E. Suomi, 10th, Madison, WI, 28 June-2 July 1999 (preprints). Boston, MA: American Meteorological Society; 1999. Pp548-551.

[Cousin and Gazarick, 1999] Cousins, D. and M.J. Gazarick 1999: *NAST Interferometer Design and Characterization.* Final Report, MIT Lincoln Laboratory Project Report NOAA-26, July 13,1999.

[Revercomb et al., 1988] Revercomb, Henry E.; Buijs, H.; Howell, Hugh B.; LaPorte, D.D.; Smith, William L., and Sromovsky, L.A. 1988: *Radiometric calibration of IR Fourier transform spectrometers: Solution to a problem with the High-Resolution Interferometer Sounder.* Applied Optics 27(15), 1 August 1988, pp3210-3218.

[Zhou et al. 2002] D. K. Zhou, W. L. Smith, J. Li, H.B. Howell, G.W. Cantwell, A.M. Larar, R.O. Knuteson, D.C. Tobin, H.E. Revercomb, and S. A. Mango 2002: *Thermodynamic product retrieval methodology and validation for NAST-I.* Applied Optics Vol. 41, No. 33

[Huang and Antonelli] Hang H-L, P. Antonelli, 2001: *Application of Principal Component Analysis to High-Resolution Infrared Measurements Compression and Retrieval.* Journal of Applied Meteorology, 40, 365-388

Vibration Induced Tilt Error Model for Aircraft Interferometer Data

E. R. Olson, H. E. Revercomb, R. O. Knuteson, H. B. Howell, D. D. LaPorte, S. D. Ellington, M. W. Werner, R. K. Garcia, F. A. Best

University of Wisconsin-Madison, Madison, WI

ABSTRACT

The Scanning High-resolution Interferometer Sounder (S-HIS) instrument is a cross track scanning Fourier-transform interferometer with 0.5 wavenumber resolution. It uses three detectors to cover the upwelling earth spectrum over the range from 3.3 to 17 microns. Vibration experienced during flight on aircraft platforms can cause a significant level of spectrally correlated noise in the calibrated spectra. To allow this interferometric noise to be removed by analysis, a wavefront tilt measurement system that monitors vibration induced optical tilts has been incorporated into the S-HIS instrument. This two-axis tilt measurement system records small changes in wavefront alignment during the data collection of both scene and blackbody interferograms. In general, both amplitude-modulation and sample-position errors can result from these tilts. Here we show that the modulation errors that dominate the interferometric noise in the S-HIS shortwave band can be significantly reduced by using the wavefront tilt measurements to model and remove the interferometric errors. The validation of our vibration induced tilt error model with blackbody data demonstrates a correction technique applicable to correcting all types of scene data.

1. INTRODUCTION

The Scanning High-resolution Interferometer Sounder (S-HIS) instrument flies on a number of aircraft platforms including the NASA ER-2, the NASA DC-8 and soon the Proteus as well (Revercomb, et al., 1996, 1998). These platforms provide a variety of vibration conditions that introduce interferometric errors that can be as large or even larger that detector noise equivalent radiance. Data from the S-HIS instrument is well suited for analysis of vibration induced tilt effects because the angular tilt between the wavefronts from the two legs of the interferometer is measured in parallel with the interferogram data collection. Vibration induces two types of errors into interferometer data. This work focuses on the verification of the theory for amplitude modulation errors. The treatment of vibration induced sample position errors will be covered in future publications.

In fully processed earth-viewing data modulation errors are detectable in regions where the atmospheric and surface properties are uniform. For the vibration spectrum experienced by the S-HIS, modulation errors dominantly cause a correlated fractional error in the raw signal across the shortwave band. Because of the unusual aperature sharing design of the S-HIS, the long- and mid-wave bands are dominated by sample position errors that are not addressed here. Understanding tilt induced errors is important, not only for correcting S-HIS data, but also for the potential application of the correction to future spaceflight instruments. The next generation of operational weather satellites include FTIR systems similar to the S-HIS instrument, but with very different vibration environments. The detailed understanding of vibration-induced tilt errors in aircraft prototype instruments is being used to improve the instrument designs of future satellite instruments and to develop correction routines for on-board or ground based processing. The list of Michelson interferometer instruments planned for deployment in the next ten years include the Crosstrack Infrared Sounder (CrIS) for the U.S. National Polar-orbiting Operational Environmental Satellite System (NPOESS), the Infrared Atmospheric Sounding Interferometer (IASI) for Europe's first polar-orbiting satellite dedicated to operational meteorology (MetOp1), and the Geosynchronous Imaging Fourier Transform Spectrometer (GIFTS) for demonstration and infusion of technology into the U.S. GOES program.

2. THEORY

A modulation error results when the wavefronts from the two legs of a Michelson interferometer are out of alignment (non-parallel) with each other (Figure 1). One of the primary concerns is the signal reduction of the interferogram near zero path difference (ZPD). This causes a visible drop in spectral radiances for all wavelengths.

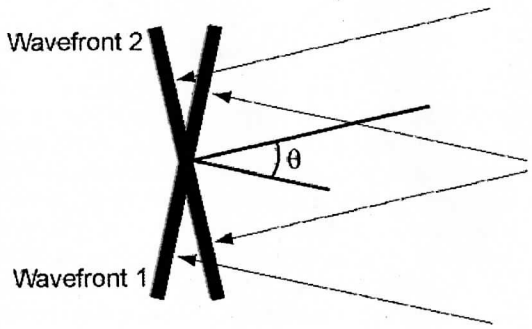

Figure 1. One dimensional diagram of the modulation error geometry. The theta angles involved are on the order of microradian, but have been exaggerated in this figure to make the effect more obvious.

In addition to the time varying relative tilt between the fixed and moving Michelson mirrors, a time invariant static tilt is also present. The static tilt is caused by the wavelength dependent refraction effects of a mismatch between the wedges in the beamsplitter and the compensator substrates. The interferometer optics effectively contain a small prism which causes the optics to be out of alignment for IR wavenumbers while in alignment for the laser wavenumber. The combined dependence on wavenumber and optical path difference (OPD) needs to be handled carefully in the mathematical treatment of these effects.

To model the modulation error we need to calculate what the detector measures in the case of a misaligned wavefront. Consider first a square interferometer beam of width $2R$, defined for easy comparison to the circular beam result. The interferogram signal can be described as the summation of sinusoidal waves with complex amplitude C at each wavenumber ν

$$F_{ideal}(x) = \int_{-\infty}^{\infty} C(\nu) e^{i2\pi\nu x} d\nu \qquad (1)$$

For a wavefront misalignment θ, the exponential in Equation 1 is replaced by an integral of the varied OPDs across the interferometer beam given by

$$e^{i2\pi\nu x} = \frac{1}{A}\int\int_{-R}^{R} e^{i2\pi\nu(x+r\tan\theta)} ds\, dl \qquad (2)$$

where s and l represent the Cartesian coordinates of the square beam, r is the radial distance from the beam center perpendicular to the axis of the tilt, and A is the area of the beam in the interferometer. The $r\tan\theta$ phase shift represents the relative delay due to the wavefronts being out of alignment. Definitions of the s and l axes are arbitrary. By choosing the axes so that theta is along one axis and using the small angle approximation of tan θ, the equation simplifies to:

$$e^{i2\pi\nu x} = \frac{1}{2R}\int_{-R}^{R} e^{i2\pi\nu(x+r\theta)} dr \qquad (3)$$

Solving the integral yields:

$$e^{i2\pi\nu x} = e^{i2\pi\nu x}\frac{\sin(2\pi\nu R\theta)}{2\pi\nu R\theta} \tag{4}$$

For a square beam, the modulation reduction factor is a sinc function of $z = 2\pi\nu R\theta$, which can be approximated by the following series

$$\frac{\sin(z)}{z} \cong 1 - \frac{z^2}{6} + \frac{z^4}{120} \tag{5}$$

In the case of a circular beam, the modulation reduction factor is

$$\frac{2J_1(z)}{z} \cong 1 - \frac{z^2}{8} + \frac{z^4}{192} \tag{6}$$

where J_1 is the first bessel function. Therefore, by substituting the first two terms of Equation 6 in Equation 1 and replacing the wavenumber with the band average wavenumber $\bar{\nu}$, an approximation for the basic effect of tilt on the S-HIS shortwave (circular beam) interferogram is

$$F(x,\theta) \approx [1 - \tfrac{1}{2}(\pi\bar{\nu}R\theta)^2]\, F(x,\theta = 0) \tag{7}$$

Having introduced the basic concept of tilt amplitude modulation, we should define the tilt more carefully. Due to the way the system measures tilt it makes sense to break the total theta, θ_t, into the stable part θ_o and the variable part θ. These are referred to as the static tilt and the jitter tilt respectively. Since θ_t is also two dimensional, there are four parts to the total tilt:

$$\begin{aligned}\theta_t &= \sqrt{(\theta_{xo} + \theta_x)^2 + (\theta_{yo} + \theta_y)^2} \\ &= \sqrt{A + B + 2(\theta_{xo}\theta_x + \theta_{yo}\theta_y)}\end{aligned} \tag{8}$$

where $A = \theta_{xo}^{\ 2} + \theta_{yo}^{\ 2}$ is the 2-dimensional static tilt and $B = \theta_x^{\ 2} + \theta_y^{\ 2}$ is the 2-dimensional jitter tilt.

The total tilt is a function of both wavenumber and OPD. The static tilt is produced by optical refraction and is therefore constant over the time scale of the interferogram, independent of OPD, and dependent on wavenumber. The jitter tilt is produced by variable mirror misalignments (geometrical) and is therefore dependent on OPD, but independent of wavenumber.

Correcting for variable amplitude modulation is complicated by the wide range of wavenumbers contributing to each interferogram point. However, handling this effect rigorously is very similar to correcting for self-apodization. Both effects cause a mixed wavenumber and OPD dependence that disrupts the fundamental relationship that the radiance spectrum is the Fourier transform of the interferogram. For the S-HIS instrument, the measured interferogram is expressed by the relationship

$$F(x) = \int d\nu \left\{1 - \frac{1}{2}\left[\pi\nu R\theta_t(x,\nu)\right]^2\right\} C_c e^{i2\pi\nu x} \tag{9}$$

where C_c is the correct complex spectrum (numerical filtering removed) that would result without tilt errors. The term in curly brackets is the factor by which the tilt-induced modulation changes the interferogram. Note that, as it stands, the

interferogram is not a pure Fourier transform of the complex spectrum, because of the mixed wavenumber and delay dependence of the tilt modulation factor. However, because the tilt angles are small, this mixed wavenumber and delay dependence is mathematically separable, making it possible to write Equation 7 in terms of Fourier transforms. That is, using Equation 8 the first small term of the Taylor series expansion of the tilt modulation factor can be represented as

$$-\frac{1}{2}\left[\pi\nu R\theta_t(x,\nu)\right]^2 = -\frac{1}{2}(\pi R)^2\left[\nu^2 A(\nu)+\nu^2 B(x)+2\nu^2\theta_{xo}(\nu)\theta_x(x)+2\nu^2\theta_{yo}(\nu)\theta_y(x)\right]$$
$$\equiv -\frac{1}{2}(\pi R)^2\sum G_i(\nu)H_i(x) \qquad (10)$$

where

$$G_1 = \nu^2 A(\nu) = \nu^2\left[\theta_{xo}{}^2(\nu)+\theta_{yo}{}^2(\nu)\right]$$
$$G_2 = \nu^2$$
$$G_3 = 2\nu^2\theta_{xo}(\nu)$$
$$G_4 = 2\nu^2\theta_{yo}(\nu)$$
$$H_1 = 1$$
$$H_2 = B(x) = [\theta_x{}^2(x) + \theta_y{}^2(x)]$$
$$H_3 = \theta_x(x)$$
$$H_4 = \theta_y(x)$$

Substituting Equation 10 into Equation 9 gives a useful relationship in terms of Fourier transforms

$$F(x) = \int d\nu\, C_c e^{i2\pi\nu x} - \frac{1}{2}(\pi R)^2\sum\left[H_i(x)\int d\nu\, G_i(\nu)C_c e^{i2\pi\nu x}\right]$$
$$= \mathbf{FT}(C_c) - \frac{1}{2}(\pi R)^2\sum\left[H_i(x)\mathbf{FT}\left(G_i(\nu)C_c\right)\right] \qquad (11)$$

where Fourier transformation is indicated by "**FT**" and can be accomplished using FFTs. We can solve for the corrected complex spectrum C_c by taking the Fourier transform of Equation 11 and rearranging to yield

$$C_c = C_o + \frac{1}{2}(\pi R)^2\sum\mathbf{FT}\left[H_i(x)\mathbf{FT}\left(G_i(\nu)C_c\right)\right]$$
$$\cong C_o + \frac{1}{2}(\pi R)^2\sum\mathbf{FT}\left[H_i(x)\mathbf{FT}\left(G_i(\nu)C_o\right)\right] \qquad (12)$$

The term C_o is the direct Fourier transform of the uncorrected interferogram, F(x). The final expression is given completely in terms of C_o, by replacing C_c with C_o in the second term. This is justified because the second term is a reasonably small correction (mathematically, the justification can be proven by iteratively substituting the expression for C_c into itself, creating an infinite series with the indicated first two terms). Equation 12 is the basis for our correction algorithm. The steps in the correction are similar to what is done to remove the self-apodization effects, so the final implementation will probably combine these two corrections for efficiency.

To demonstrate the nature of tilt magnitude errors on calibrated spectra, we have performed a simulation based on an example of measured interferogram and tilt spectra. A sample hot blackbody interferogram that had very little modulation error was chosen for a noise free signal. A separate set of high frequency tilt measurements of average magnitude was also selected. The correction term in Equation 11 was used to produce interferograms with modulation error. These noisy interferograms were then processed to produce calibrated spectra. Figure 2 shows how a tilt of representative magnitude as well as three times as large, affect the final calibrated spectra. The top plot is for the case of no static tilt and the bottom plot shows spectra for a static tilt originally found in S-HIS data. As shown, the effect of tilt jitter is strongly dependent on the size of the static tilt. To minimize the static tilt, the capability to electrically offset the laser-defined alignment has been implemented on S-HIS.

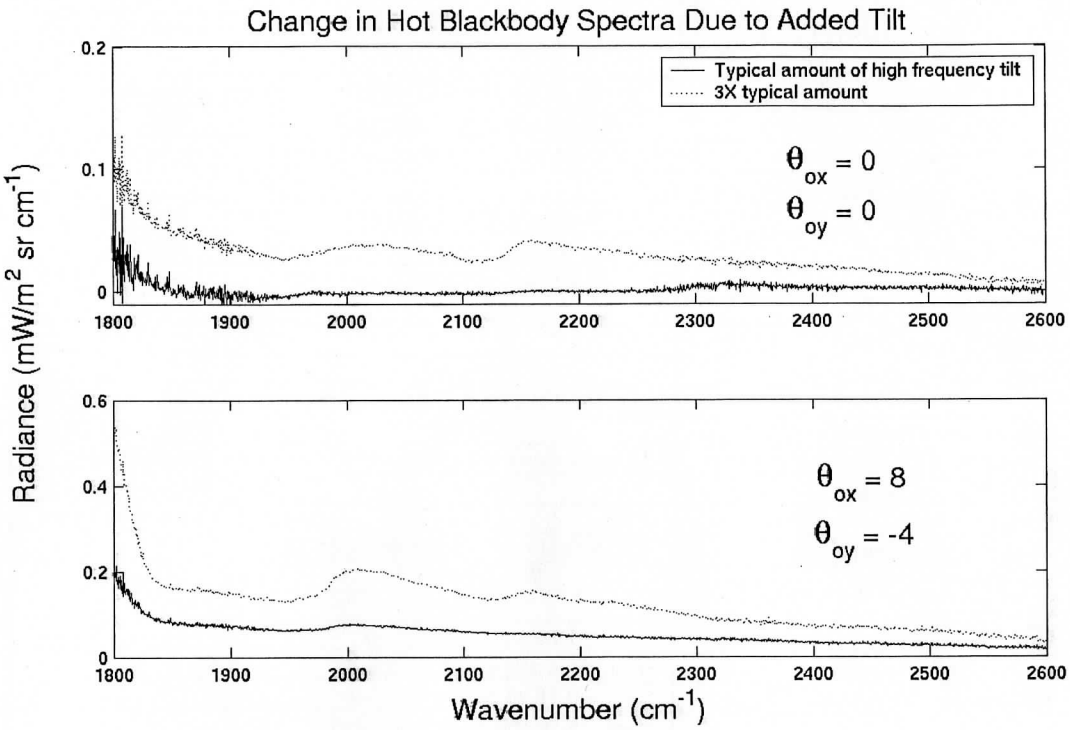

Figure 2. Simulations showing examples of the radiance effect of various levels of tilt noise added to a sample S-HIS hot blackbody spectra. Curves are the difference between calibrated blackbody spectra for interferograms with tilt noise added and those with no tilt noise. Static tilt values are in microradians.

3. INSTRUMENTATION

The S-HIS was initially designed to fly aboard an unmanned aircraft vehicle (UAV) with limited payload capacity. Therefore, it is small and light-weight, and has low power requirements. The S-HIS uses a dynamically aligned Fourier-transform interferometer with laser-controlled sampling produced by Bomem of Quebec, Canada. Due to the initial design constraints on size, the S-HIS instrument uses a mechanically cooled "3-color" detector with a shared focal plane, eliminating the need for multiple detectors and their associated dichroic beamsplitters and coolers. The S-HIS design and performance parameters are given in Table 1.

Table 1. S-HIS Instrument Specifications.

Interferometer:		
Type:	Voice Coil Dynamically Aligned Plane mirror (Custom Bomem DA-5)	
Beam Diameter	4.5 cm	
Fringe Counting	¼ wave quadrature, continuous	
Optical path drive	Flex Pivot Porch Swing	±1.037 cm; 4 cm/s
OPD sampling reference	HeNe laser w/ white light at startup	
Angular FOV	40 mrad (full)	
Scan Time	0.5 s (2 spectra per spot)	
Spectral Coverage:		
Four Band Option (3–25 μm):	Coverage	Material
Longwave	10–17 μm, 580–1000 cm^{-1}	HgCdTe
Midwave	5.5–10 μm, 1000–1800 cm^{-1}	HgCdTe
Shortwave	3–5.5 μm, 1800–3000 cm^{-1}	InSb
Three Band Option (3–16 μm)		
Longwave	9–16 μm, 620–1100 cm^{-1}	HgCdTe
Midwave	5.5–9.9 μm, 1100–1800 cm^{-1}	HgCdTe
Shortwave	3–5.5 μm, 1800–3000 cm^{-1}	InSb
Spectral Resolution:	0.5 cm^{-1}	
Spatial Field-of-view:		
Instrument Field-of-view	100 mrad	
	(nadir: 2 km from 20 km altitude)	
Cross Track Scan Step	0.15 rad	Programmable
Number of IFOV per scan	11 earth views + 2 calibration views	Programmable
Dwell time per spot	1 s	Programmable
Total scan time	15 s	Programmable
Cooler/Temperature:	0.6 W Stirling Cooler (Litton), 68 K	
Mass/Size:	70 kg; 0.05 m^3	
Power:	225 W	
Onboard processing:	DSP numerical filters	
RMS noise (per spot):	generally <0.5K at 260 K	
Radiometric Calibration:	<0.1K at 260 K; absolute	
	<0.2K at 260 K; reproducibility	

The S-HIS 45° scene mirror executes a sequence consisting of multiple views of the earth and two calibration sources, one at ambient and another controlled to a fixed temperature (typically 310 K). The raw interferograms from each view are compressed in real time to reduce the volume of data. A numerical filter is applied using a digital signal processor (DSP), while a second DSP is used for controlling the instrument. The S-HIS uses calibration techniques that were developed for the HIS and AERI (Revercomb, et al., 1988). The retrieval and spectroscopic applications of the S-HIS data require high radiometric accuracy.

To monitor wavefront tilts, the S-HIS system records wavefront phase differences between pairs of separated laser beams for both the x- and y- axes of the dynamic alignment system. These phase differences are both sampled for every eighth HeNe laser fringe (8.4 KHz sampling rate). This gives a tilt measurement with one-to-one correspondence to every point of the stored intererferograms (numerically filtered) for each band. While the phase error sampling system has a Nyquist frequency of 4.2 kHz, the system is filtered to a 2 kHz cut-off to suppress noise aliasing. The highest resonant frequencies normally observed occur in the region 1.2–1.4 kHz. The primary resonances are largely contained between 290 and 650 Hz.

The jitter tilt angles θ_x and θ_y can be obtained from the phase angle measurements ϕ_x and ϕ_y using the relationship

$$\theta = \frac{\phi}{360^\circ}(s\nu_1)^{-1} \tag{13}$$

for each orthogonal axis, where ν_1 is the laser wavenumber (15799.6 cm^{-1}) and s is the distance separating the pairs of laser beams used to detect x- and y- axis phase differences (3 mm).

4. TEST DATA AND RESULTS

To validate the modulation error model and demonstrate the correction, we focused on a subset of S-HIS data from two field experiments in 2000. The first experiment, WISC-T2000, was based in the Midwest US during the winter. The second, the SAFARI experiment, was based in South Africa. Between the two experiments, the original porch-swing Michelson moving mirror mechanism was replaced with a mechanism based on linear bearings to reduce sensitivity to aircraft vibrations. As mentioned earlier, we focused on shortwave data where the amplitude modulation effects dominate the interferometric noise.

The blackbody interferograms provide a unique testing dataset because they are easily modeled. In the case of the hot blackbody, which is servo controlled to a fixed temperature, the data should be relatively consistent over short time periods. Figure 3 plots the ZPD values of the hot blackbody interferograms for a section of data from February 27, 2000. The dashed straight line is an estimate of what the ZPD values would have been without any modulation error or noise. Since the modulation error can only reduce amplitudes, the predicted ZPD values are chosen to bound the maximum values. This estimate is slightly high, because the best estimate should also take the presence of random noise into account. The slope of the predicted ZPD values is caused by the changing temperature of the inside of the interferometer and its background contribution to the measured signal.

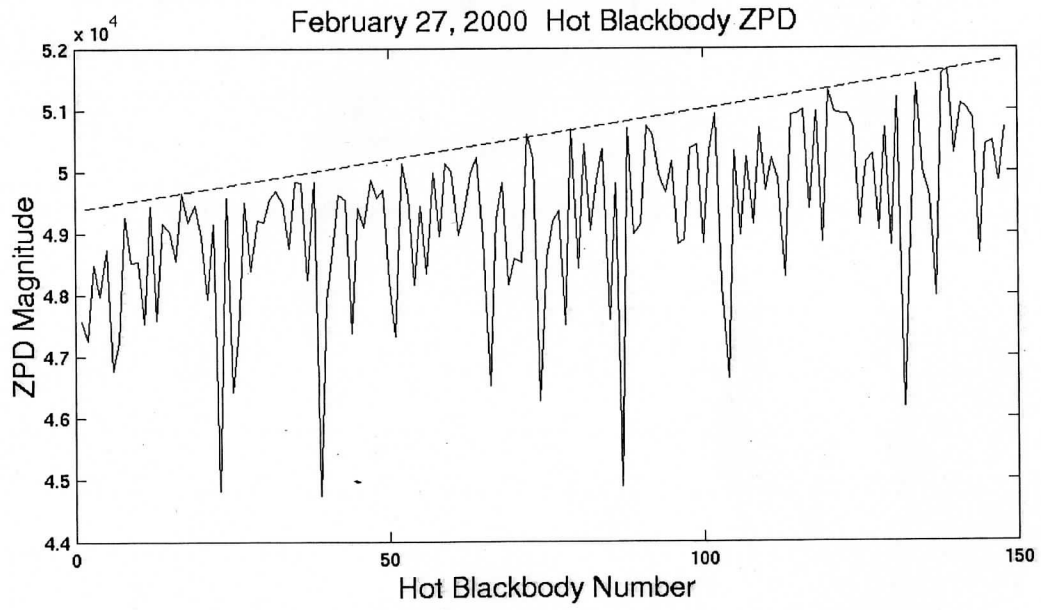

Figure 3. Hot blackbody uncalibrated ZPD values for February 27, 2000 case (solid) along with initial estimates of ZPD values without modulation error (dashed).

The modulation factor at ZPD can be calculated from the model discussed in Section 3. From Equation 7 the approximate relationship between measured ZPD values and the estimate for $\theta = 0$ is

$$F(x=0,\theta) \approx [1 - \tfrac{1}{2}(\pi \bar{\nu} R\theta)^2]\, F(x=0,\theta=0) \qquad (14)$$

Although it is not rigorous to use an average value for the wavenumber, it is a reasonable approximation for testing the fundamental soundness of our tilt measurements and this formulation. Figure 4 demonstrates the excellent agreement between the measured modulation factor and the factor modeled from Equation 15 using meaured tilt data. Because an independent determination of the static tilt is not possible, static tilt parameters are determined by solving for the values that minimize the difference shown in Figure 4. Figure 5 demonstrates the same excellent agreement with expectations as a function of total tilt.

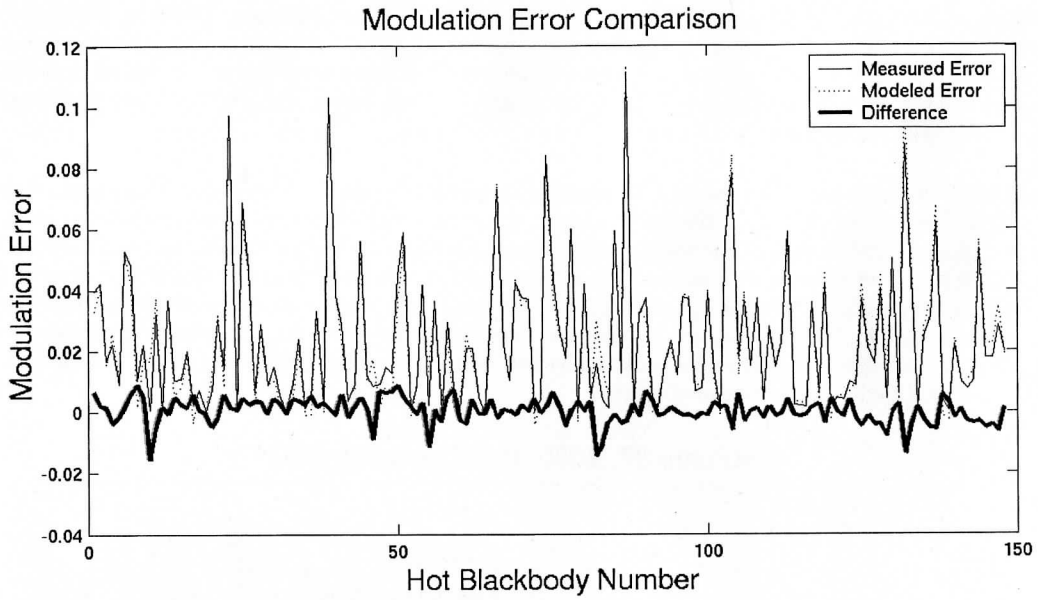

Figure 4. Comparison between the modulation error estimated from the ZPD values and the modulation error calculated from the tilt noise model.

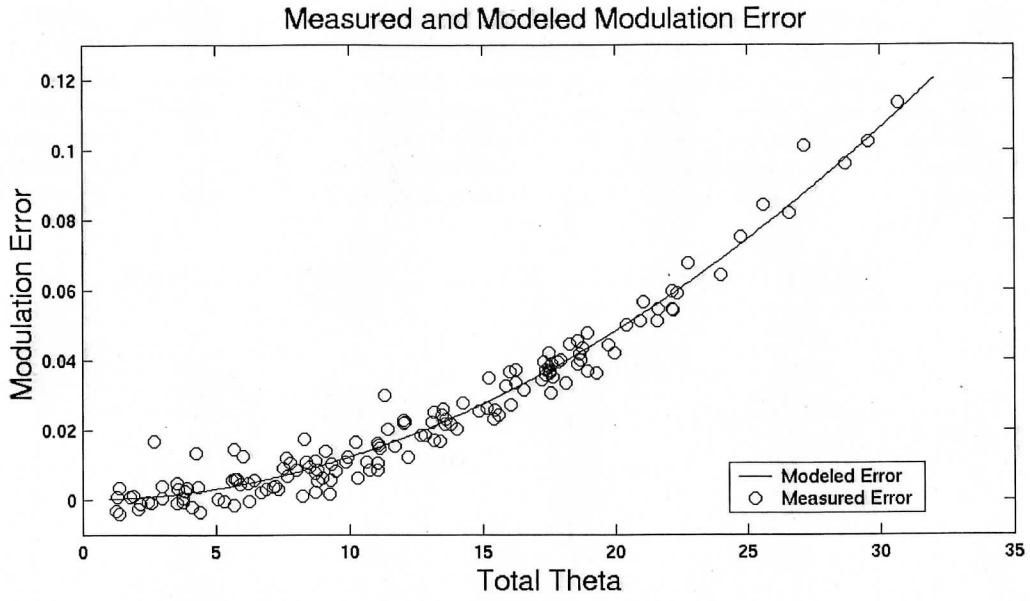

Figure 5. Same data as Figure 5 showing how well the model agrees with the data as a function of total wavefront tilt.

5. CORRECTION AND NOISE REDUCTION

The next step is to apply the formalism of Equation 12 to remove the modulation effects and to evaluate the effect on calibrated spectra. When the data is initially taken, a complex numerical filter is convolved with the raw laser-sampled interferogram to reduce the data volume without information loss or noise aliasing. Doing the modulation correction involves first reconstructing an approximation to the original interferogram. Since the numerical filter convolution is equivalent to multiplication by a real, asymmetric function in the spectral domain, the filter effects can be removed by the following steps:

A. Fourier transform to spectral domain (complex interferogram to complex spectrum).
B. Divide the spectrum by the spectral equivalent of the numerical filter (real, but asymmetric).
C. Condition the bounds of the spectra to reduce ringing,
D. Place the unfiltered spectrum into a wavenumber scale zero-filled out to the original Nyquist wavenumber.
E. Make the complex spectrum symmetric about $\nu = 0$.
F. Fourier transform to original interferogram (real and asymmetric).

The correction described by Equation 12 can now be applied to the resulting interferogram.

Applying the correction involves solving for some constants. As described earlier, a series of jitter tilt measurements is recorded for each interferogram point, but due to differences in electronic response times the delay between the interferogram data and the tilt data needs to be estimated. The constant in the series expansions of Equations 5 and 6 will likely vary slightly from the theoretical value (beam shape not exactly circular). The static tilt angles also need to be determined as discussed in connection with the results shown in Figure 4. The four quantities θ_{xo}, θ_{yo}, the series expansion coefficient, and the offset between the tilt and interferogram measurements are expected to be very stable from mission to mission. This allows us to solve for these constants by minimizing the difference between the expected blackbody spectra and the corrected blackbody spectra.

Figure 6 shows uncorrected and corrected spectral magnitudes averaged over a large spectral region (1875 – 2275 wavenumbers) for the two test datasets. The data is separated into the forward and backward scan directions because the uncalibrated data varies significantly depending on scan direction. The RMS variation for the 27 February 2000 data is reduced by about an order of magnitude and clearly demonstrates the success of this correction. However, the initial tilt-induced noise is so large for this earlier data set (order 10%) that it is not a very subtle test of the ultimate sensitivity of the correction. The original tilt-induced noise for the 6 August 2000 data is much lower (1-2 %). While it also shows a clear improvement, the residual random noise makes it difficult to quantify the improvement based on this result alone.

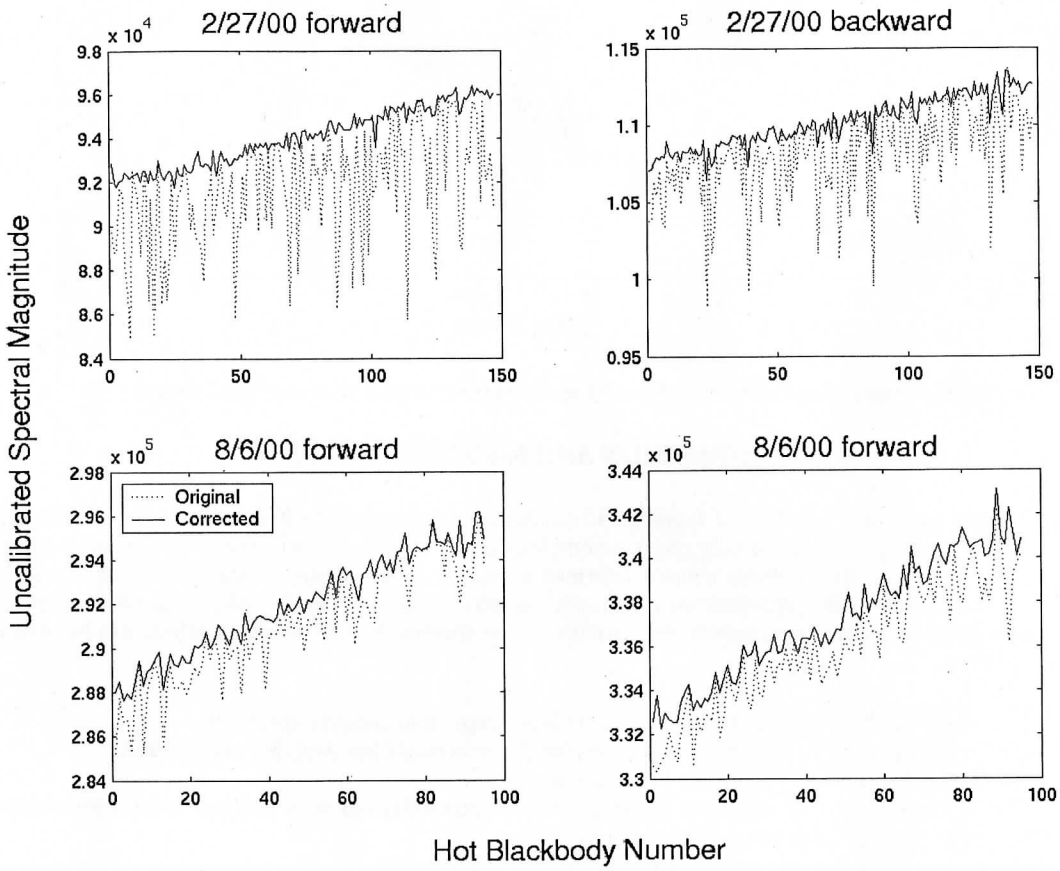

Figure 6. Corrected and original spectral magnitudes for 2/27/00 and 8/6/00. Separated by scan direction since magnitudes are uncalibrated.

To examine the 6 August results more quantitatively, the next step is to process the corrected data to calibrated radiances. To show that the correction has a major positive effect on the final data, we compare the correlated noise spectra for the original and corrected data. Tilt-induced interferometric noise for the S-HIS is strongly correlated with wavenumber, while the other sources of noise are not correlated with wavenumber. The correlated noise is separated from the random noise by convolving the spectra with a broad boxcar (50 cm^{-1} wide). This process averages away most of the random noise and the residual random contribution is removed by calculation. Figure 7 shows the random and correlated errors for the August 6, 2000 case of forward direction scans. Over most of the spectrum, the correction reduces the residual correlated noise following correction to significantly lower levels than the random detector noise. Also, over much of the spectrum, the correlated noise is reduced by factors of between 5 and greater than 10.

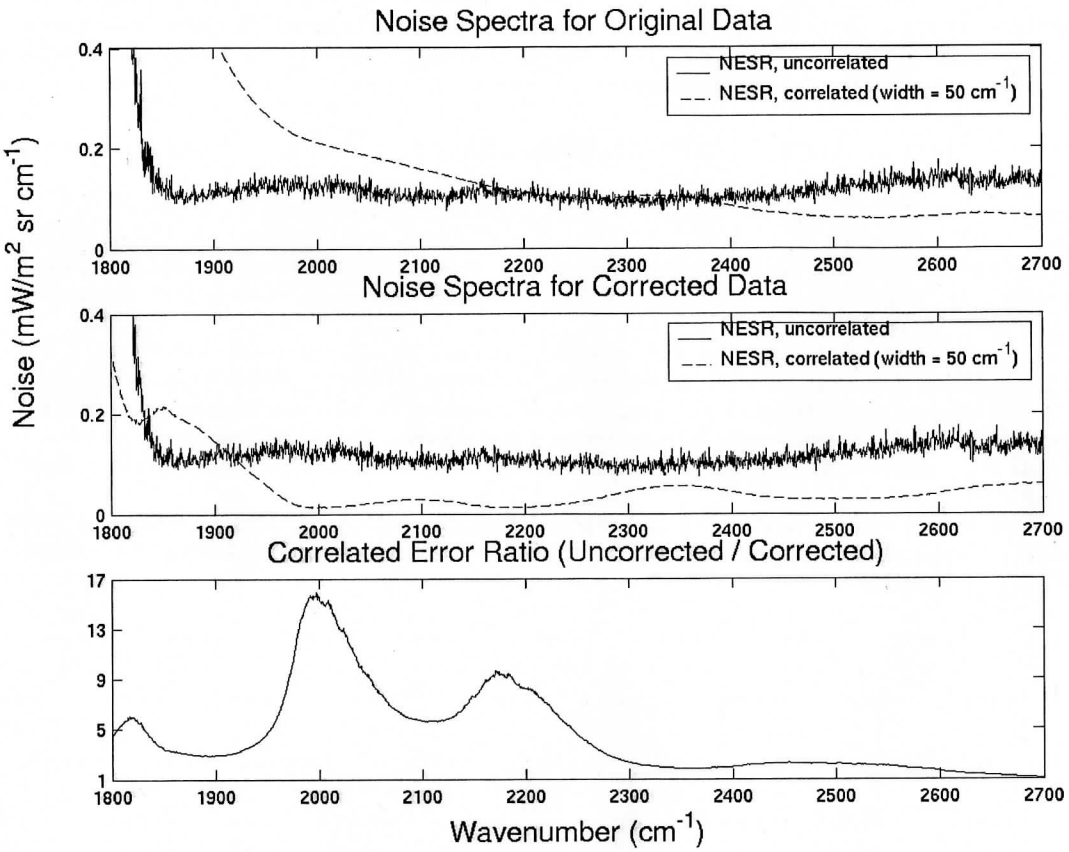

Figure 7. Reduction of correlated noise in the hot blackbody with the modulation error correction. The top plot is the random and correlated errors for the uncorrected data while middle plot shows the same thing for the corrected data. The bottom plot is the factor by which the correction improves the correlated errors.

6. CONCLUSIONS

We have shown that vibration induced tilt modulation errors in a Michelson interferometer can be corrected in post processing using tilt angles measured during an interferogram scan. The tilt correction has been shown to remove most of the tilt induced modulation error and to reduce the correlated errors by a factor of five for much of the spectrum and by as much as 15 at some wavenumbers.

Not included here are corrections for the sample-position errors that can result from tilts for interferometers in which the signal beam is not centered about the laser beam that controls interferogram sampling. Using similar techniques, we have defined corrections for the sample position errors resulting from mirror tilts and are in the process of applying them to S-HIS data. Preliminary exploration of the sample-position error model suggests that the corrections should also work very well.

ACKNOWLEDGEMENTS

We gratefully acknowledge the support for this work and for the installation of the S-HIS tilt monitoring system along with many other instrument improvements by the NPOESS Integrated Project Office (IPO) under contract number 50-SPNA-1-00039. Other substantial support for the S-HIS has been provided by the NASA EOS program and by the DOE Atmospheric Radiation Measurement (ARM) program.

REFERENCES

1. Revercomb, H. E., W. L. Smith, F. A. Best, J. Giroux, D. D. LaPorte, R. O. Knuteson, M. W. Werner, J. R. Anderson, N. N. Ciganovich, R. W. Cline, S. D. Ellington, R. G. Dedecker, T. P. Dirkx, R. K. Garcia, and H. B. Howell, 1996: Airborne and ground-based Fourier transform spectrometers for meteorology: HIS, AERI and the new AERI-UAV. Proceedings SPIE Optical Instruments for Weather Forecasting, edited by G.W. Kamerman, 2832, 106-117.
2. Revercomb, H.E., V.P. Walden, D.C. Tobin, J. Anderson, F.A. Best, N.C. Ciganovich, R.G. Dedecker, T. Dirkx, S.C. Ellington, R.K. Garcia, R. Herbsleb, R.O. Knuteson, D. LaPorte, D. McRae, and M. Werner, 1998: Recent results from two new aircraft-based Fourier transform interferometers: The Scanning High-resolution Interferometer Sounder and the NPOESS Atmospheric Sounder Testbed Interferometer, 8th International Workshop on Atmospheric Science from Space using Fourier Transform Spectrometry (ASSFTS), Toulouse, France, 16-18 November 1998.
3. Revercomb, H.E., H. Buijs, H.B. Howell, D.D. LaPorte, W.L. Smith, and L.A. Sromovsky: Radiometric calibration of IR Fourier transform spectrometers: solution to a problem with the High-Resolution Interferometer Sounder. *Appl. Opt.*, *27*, 3210-3218, 1988

ITSC-XIII: Ste. Adele, Canada, 29 October - 4 November 2003

Validation of Satellite AIRS LST/LSE Products Using Aircraft Observations

Robert O. Knuteson, Brian J. Osborne, Henry E. Revercomb, and David C. Tobin
University of Wisconsin Space Science and Engineering Center, Madison, WI, USA

William L. Smith, Sr.
NASA Langley Research Center, Hampton, VA, USA

Introduction

Weather satellites have shown positive impact on forecast models for data collected over the world's oceans. However, the use of weather satellite data over land areas has been limited. One of the problems faced by users of broadband infrared measurements is the inability to separate the effect of land surface temperature (LST) from natural variations in land surface emissivity (LSE). A new generation of infrared sounders has been developed for obtaining improved profiles of atmospheric temperature, water vapor, and trace gas concentrations. A characteristic of these advanced sounders is the use of spectrometers with nearly continuous coverage of the 8-14 micron infrared window region with resolving powers of 1000 or greater. These high spectral resolution sounders have the advantage of being able to resolve individual absorption lines of water vapor and carbon dioxide and thereby provide a number of transparent "microwindows" that require a smaller atmospheric correction than broad-band instruments. In addition, it has been recognized that high spectral resolution infrared observations have another important advantage over broad band measurements in that they allow an effective surface temperature to be determined simultaneously with an effective land surface emissivity. A method for emissivity – temperature separation using high spectral resolution infrared observations has been developed at the University of Wisconsin Space Science and Engineering Center (UW-SSEC) in conjunction with NASA Langley Research Center (LaRC). The algorithm has been applied to UW-SSEC's ground-based Surface-Atmospheric Emitted Radiance Interferometer (S-AERI), the UW-SSEC Scanning High-resolution Interferometer Sounder (S-HIS) aircraft instrument, and the NPOESS Atmospheric Sounder Testbed – Interferometer (NAST-I) operated by NASA LaRC. Recently data from the NASA Atmospheric InfraRed Sounder (AIRS) satellite instrument have been compared with measurements from these ground-based and high altitude aircraft over the U.S. Department of Energy Atmospheric Radiation Measurement (ARM) Southern Great Plains (SGP) site in north central Oklahoma, USA. The lessons learned from this analysis have implications for the future operational use of data from the NPOESS CrIS and the METOP IASI sensors.

This paper includes the results of a ground-based survey of the validation site, results of a simulation of top of atmosphere upwelling infrared radiance observations at high spectral resolution, analysis of aircraft observations over the ground site, and comparison with results derived from the AIRS satellite instrument.

ARM Site Survey

The UW-SSEC conducted a ground-based survey of the DOE ARM SGP site in north central Oklahoma (USA) over a period of several years (1996-2003). This survey includes both a characterization of the land cover/land use in the vicinity of the ARM SGP central facility and

detailed measurements of the surface emissivity of selected land types. One of the co-authors developed the methodology shown in Figure 1 for the classification of the land cover (Osborne et al. 2003). The upper panel shows the 8x8 mile grid used in the ground-based survey of land cover while the lower pie chart shows the percentage occurrence of each class. The land cover is a mixture of permanent grassland pasture intermixed with fields of winter wheat and/or bare soil. The density of the wheat grass in each field leads to a change in the vegetation fraction during the growing season (from 0 to 100%). Figure 2 presents the results of the ground-based surface emissivity survey with the UW-SSEC S-AERI instrument (Knuteson et al. 2003). The key result from the emissivity survey is that the wheat field measurements can be represented as a linear combination of measurements of "pure" scene types; vegetation (grass) and bare soil (quartz mineral).

Simulated High Altitude Observations

This paper will follow the theory outlined in Knuteson et al. (2004). The cloud-free radiative transfer equation, neglecting solar radiation and scattering effects, for a downlooking infrared sensor viewing a homogeneous surface is given by the following equation

$$I_\nu = \int_0^Z B_\nu[T(z)]\frac{\partial \tau_\nu(z,Z)}{\partial z}dz + \varepsilon_\nu \cdot B_\nu(T_S)\cdot \tau_\nu(0,Z) + (1-\varepsilon_\nu)\cdot \tau_\nu(0,Z)\int_\infty^0 B_\nu[T(z)]\frac{\partial \tau_\nu(z,Z)}{\partial z}dz,$$

where I_ν, ε_ν, B_ν, T_s, $\tau_\nu(z_1,z_2)$, Z, and T(z) are observed spectral radiance, spectral emissivity, spectral Planck function, the surface temperature, spectral transmittance at wavenumber ν from altitude z_1 to z_2, sensor altitude, and air temperature at altitude z, respectively. The first term of the equation is the emission from the atmosphere above the surface, the second term is the direct emission from the surface that reaches the sensor, and the third term is the downwelling atmospheric emission reflected off the ground under the approximation of a lambertian surface. The emissivity can be formally expressed (below) where R^{OBS} is the observed upwelling radiance,

$$\hat{\varepsilon}_\nu = \frac{[R_\nu^{OBS} - \mathrm{N}_\nu^{\uparrow}] - \tau_\nu \overline{\mathrm{N}}_\nu^{\downarrow}}{\tau_\nu B_\nu(\hat{T}_S) - \tau_\nu \overline{\mathrm{N}}_\nu^{\downarrow}}$$

$$\frac{de_\nu}{e_\nu} = \frac{-B_\nu(T_S)}{B_\nu(T_S) - \overline{N}_\nu^{\downarrow}} \bullet \frac{dB_\nu(T_S)}{B_\nu(T_S)}$$

N^{UP} represents the upwelling emission from the atmosphere only and N^{DN} represents the downwelling flux at the surface. The ^ symbol denotes "effective" quantities as defined in Knuteson et al. (2004). The fractional change in emissivity is shown to vary on and off of spectral emission lines according to the reflected infrared radiance.

Figure 3 shows the result of a simulation of upwelling infrared radiance at 20 km altitude for the spectral resolution of the S-HIS instrument (0.5 cm^{-1} unapodized). The atmospheric pressure, temperature and water vapor are obtained from the combination of a Vaisala RS80H radiosonde, a Radiometrics microwave radiometer, and the CART Raman Lidar (CRL). The magnitude of the reflected contribution to the upwelling radiance is shown for each of three surface emissivity assumptions. Figure 4 illustrates the technique for the determination of the effective surface temperature by the minimization of the spectral variance in the derived surface emissivity spectrum. This "optimum" surface temperature is then used to compute the final derived effective emissivity spectrum. This technique is used for ground-based data where both the up and down welling radiance are measured, but it has also been successfully applied to aircraft and satellite measurements where the atmospheric contributions have been calculated using a line-by-line radiative transfer program.

temperature variations in the vicinity of the ARM SGP central facility at the spatial scales needed for validation of satellite products. Figure 5 illustrates the spatial scale of the Scanning HIS field of view (2 km) compared with that of AIRS (about 15 km). Observations from a NASA ER-2 flight of 31 March 2001 were analyzed by averaging the S-HIS footprints over a spatial dimension similar to that expected from the AIRS instrument. The result of the analysis directly over the ARM SGP central facility shows that the effective emissivity derived from the spatially averaged S-HIS data can be approximately represented as a linear combination of the pure scene types measured in the ground-based survey. A case study over the same validation site has been analyzed with AIRS satellite data collected on 16 November 2002. The broader spatial coverage of the satellite data is illustrated in Figure 6, which shows the observed brightness temperature at 12 μm over north central Oklahoma and southern Kansas. The symbols mark the central facility (diamond) and the boundary facilities (triangles). After application of the "online/offline" technique the distribution of surface temperature and emissivity assumes a very reasonable pattern. The cooler temperatures are associated with the high emissivity vegetation corresponding to the permanent grassland in the southeastern corner of the domain. The warmer (daytime) temperatures correspond to the "wheat belt" where at this time of year more of the bare soil is exposed. The central facility is in the wheat-growing zone but quite near the transition region. Figure 7 highlights some of the emissivity spectra derived from AIRS radiance observations near the ARM SGP central facility.

Conclusions

The high spectral resolution structure of the infrared surface reflection can be used to determine the effective value of Ts for which ε_v is constant across spectral absorption/emission lines. Using ground-based measurements at the ARM SGP site, area averaged emissivity can be accurately represented using a single parameter (vegetation fraction) and two pure scene types; vegetation (grass) and bare soil (quartz signature). The results of ground-based, aircraft-based, and satellite-based infrared observations are shown to provide a consistent representation of the surface emissivity in the vicinity of the ARM Southern Great Plains site. These research products will be used in the validation of the AIRS "standard" land surface products.

Acknowledgements

We gratefully acknowledge the support of the Integrated Project Office (IPO), contract 50-SPNA-1-00039. This work also was supported through the NASA AIRS science team and the U.S. DOE ARM science team projects of H. Revercomb (1990-2003).

References

Knuteson, R. O., F. A. Best, D. H. DeSlover, B. J. Osborne, H. E. Revercomb, W. L. Smith, Sr., 2004: Infrared land surface remote sensing using high spectral resolution aircraft observations, *Adv. Space Res.*, Vol. 33, 2004 (in press).

Knuteson, R. O., R. G. Dedecker, W. F. Feltz, B. J. Osborne, H. E. Revercomb, D. C. Tobin, 2003: Infrared Land Surface Emissivity in the Vicinity of the ARM SGP Central Facility, Proc. of the Thirteenth ARM Science Team Meeting, Broomfield, CO, March 31–April 4, 2003.

Osborne, B. J., R. O. Knuteson, H. E. Revercomb, J. F. Short, and D. C. Tobin, 2003: Ground truth measurements for validation of AIRS land surface temperature and emissivity products at the Southern Great Plains validation site, in Fourier Transform Spectroscopy, OSA Technical Digest (Optical Society of America, Washington DC, 2003), Quebec City, 3–6 February 2003.

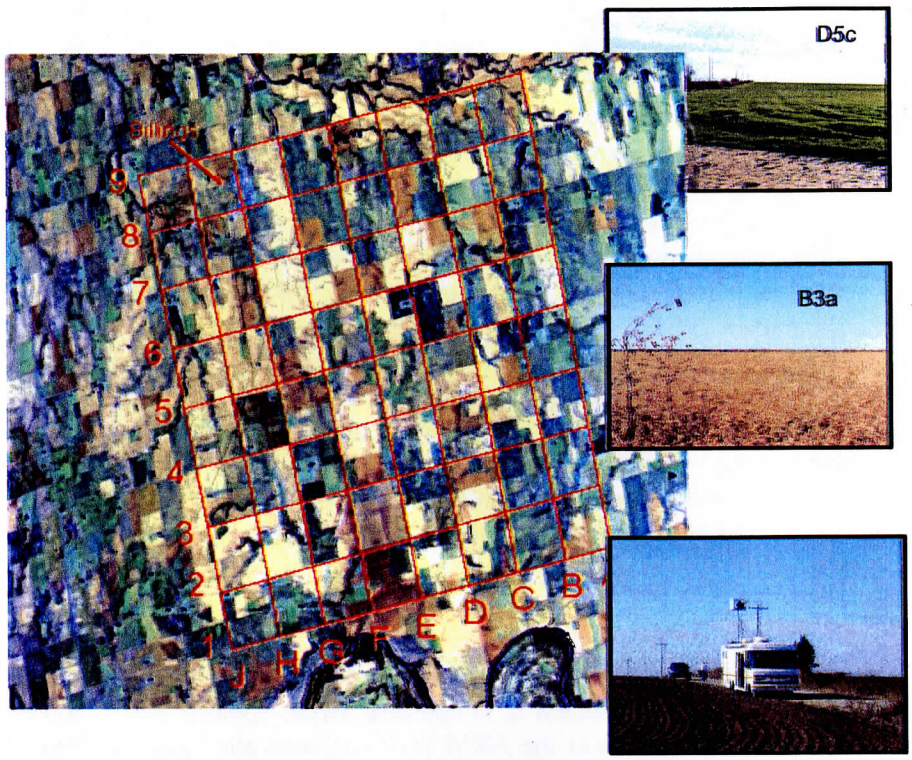

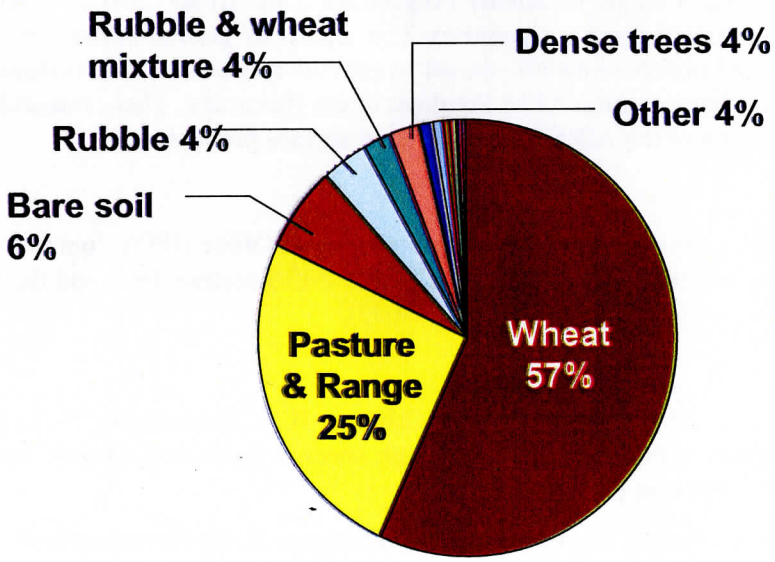

Fig. 1: The upper panel shows the 8x8 mile grid used in the ground-based survey of land cover in the vicinity of the DOE ARM SGP central facility. Land cover surveys were conducted by UW personnel in 2001, 2002, and 2003 at different times of the year. The results of the November 2002 survey are shown in the pie chart. The category "Pasture and Range" is composed of permanent grassland while the "Wheat" category is a mixture of wheat grass and bare soil which changes fraction during the growing season.

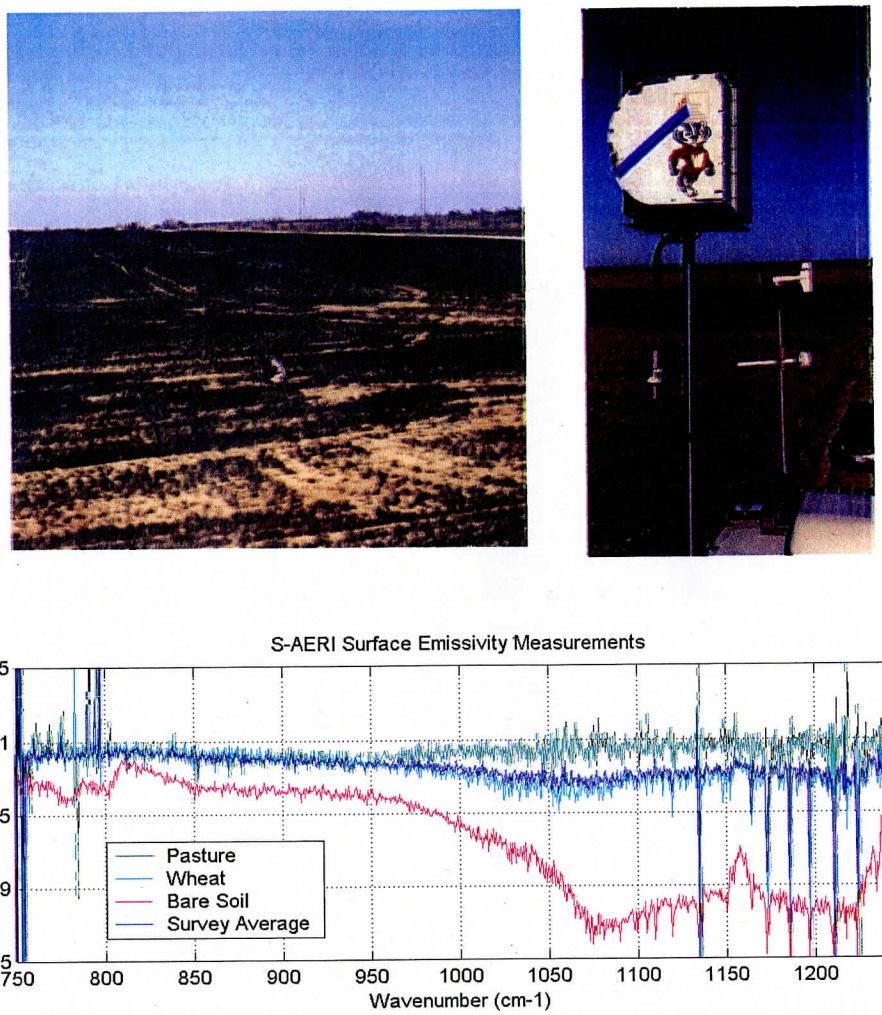

Fig. 2: UW ground-based emissivity survey conducted at the DOE ARM SGP central facility. The upper left photo shows a farm field in the early stages of winter wheat growth (March 2001). Notice the bare soil is visible between the small wheat plants at this time of year. The Scanning AERI, shown in the upper right, was used to measure the emissivities shown in the lower panel. The curve indicated as "wheat" in the plot is the measurement from the field shown above. The importance of this measurement is that the wheat measurement is very similar to the linear combination of "pure" scene types (grassland pasture and bare soil) obtained by the land cover survey. This suggests that the primary variable that determines the spectral contrast in surface emissivity is the fraction of vegetation in the instrument field of view. This result is true at all scales from the half meter scale of the ground-based Scanning AERI, to the 2 km scale of the Scanning HIS aircraft instrument, and the 15 km scale of the AIRS satellite instrument.

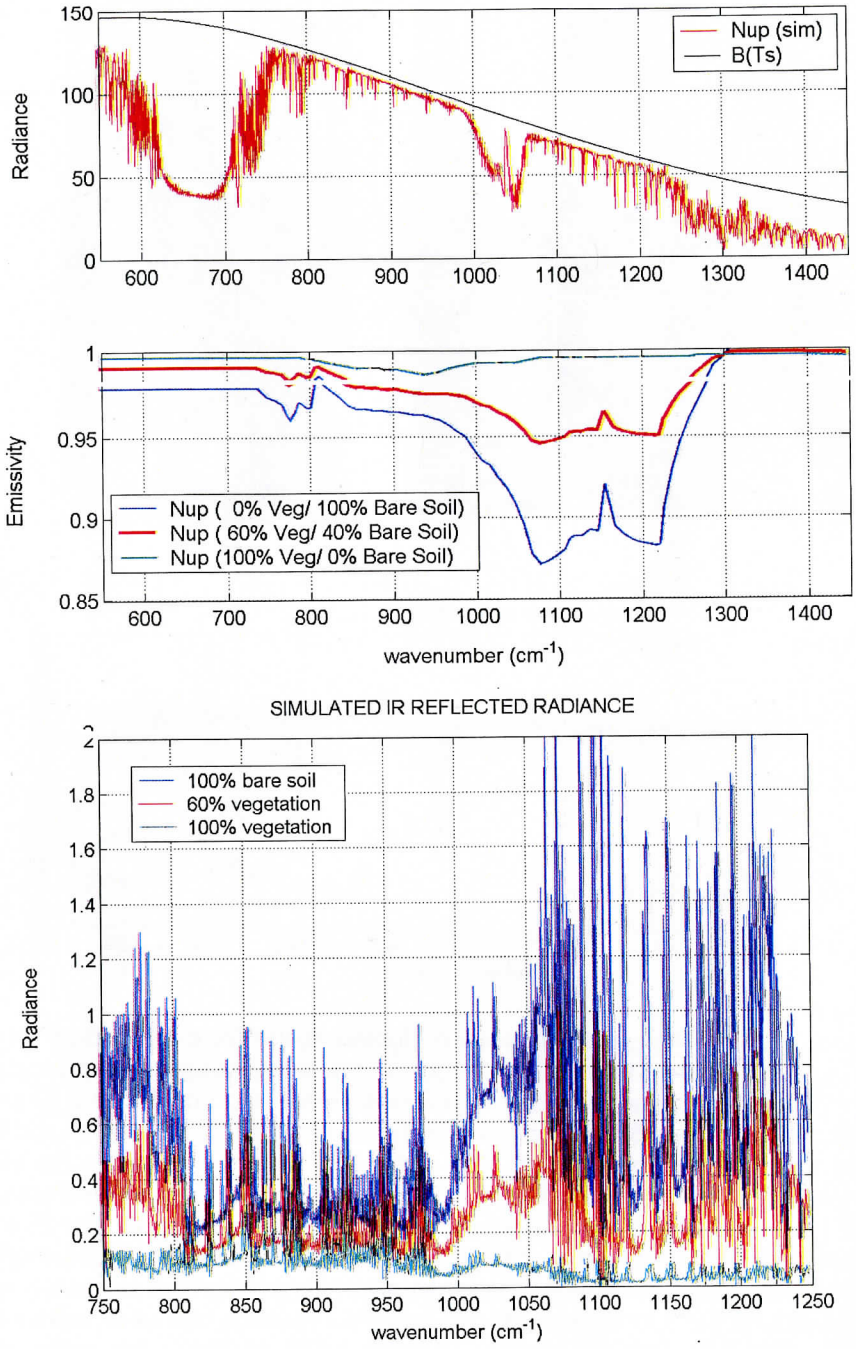

Fig. 3: Simulation of upwelling radiance at high spectral resolution (0.5 cm^{-1}) for an observer at 20 km (upper panel). This simulation uses the emissivity of pure scene types measured in the vicinity of the DOE ARM SGP central facility site and a linear combination suggested by the ground based survey (center panel). The lower panel shows the size of the infrared reflected radiance for each of the three emissivity curves.

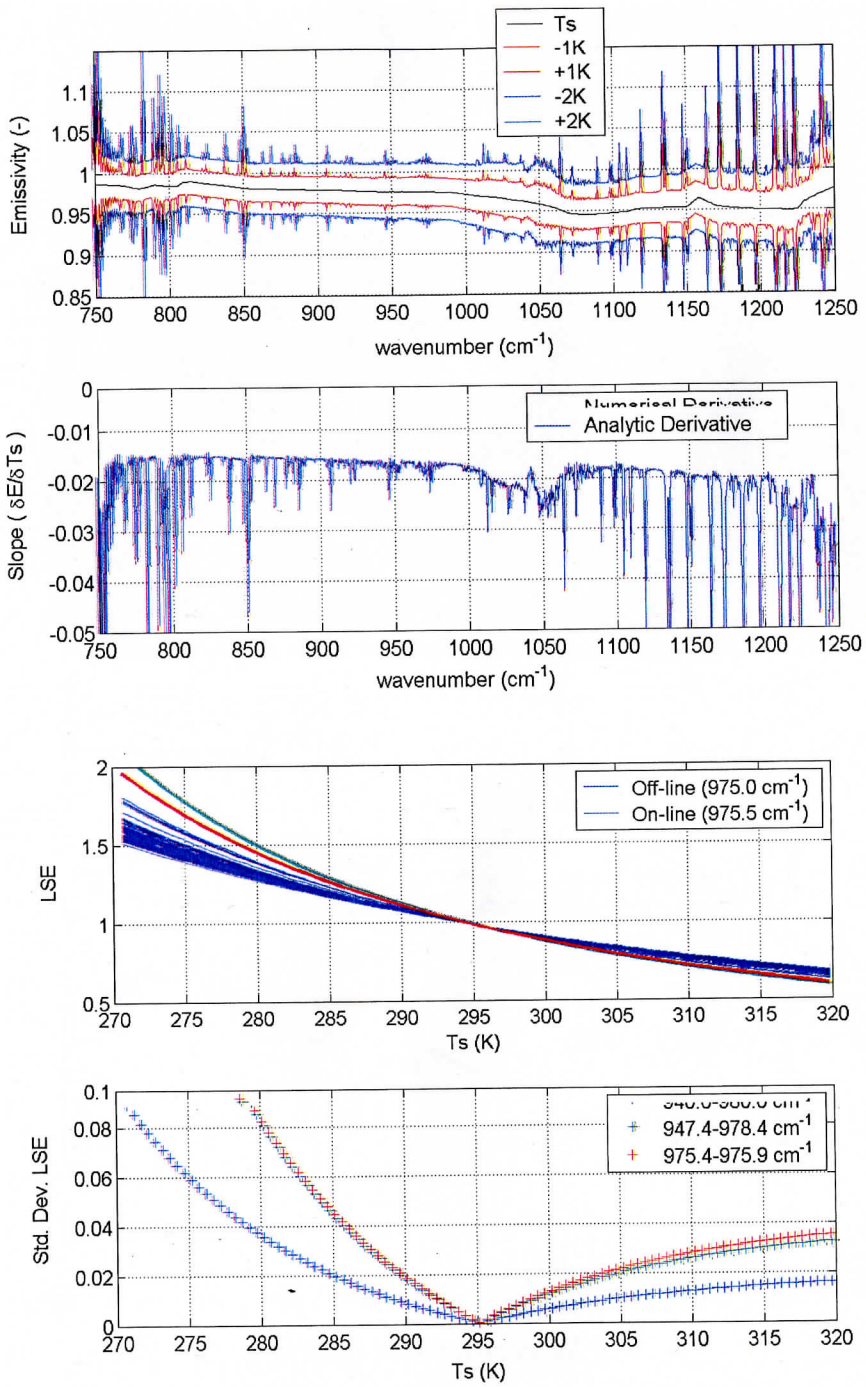

Fig. 4: Simulation of the derived emissivity as a function of land surface temperature. The top panel is the derived emissivity versus wavenumber for a range of surface temperatures. The second panel is the ratio of the change in emissivity for a change in surface temperature. The third panel shows on-line (red & green) versus off-line (blue) channels. The lower curve shows the true surface temperature is the minimum of the wavenumber standard deviation of emissivity as a function of surface temperature.

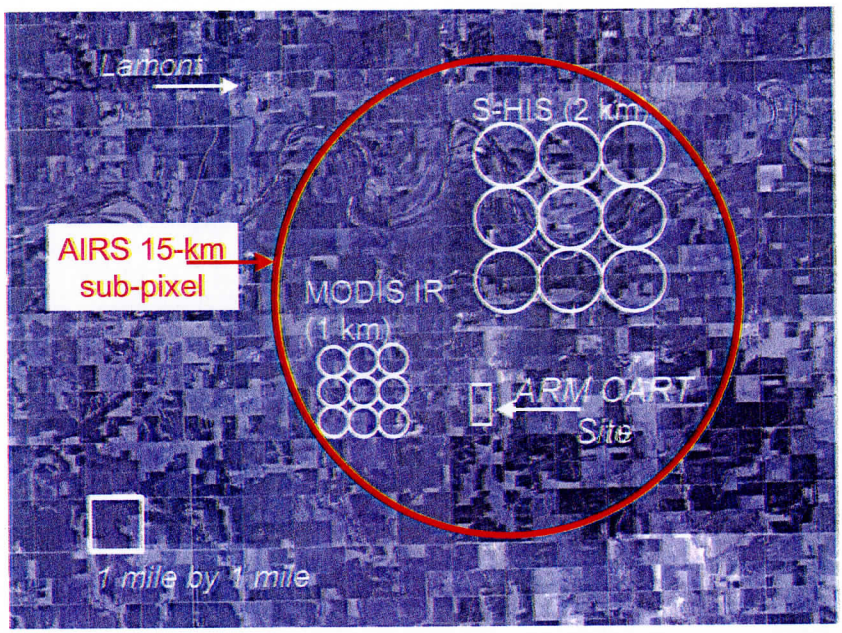

Aerial photo from http://terraserver.homeadvisor.msn.com/

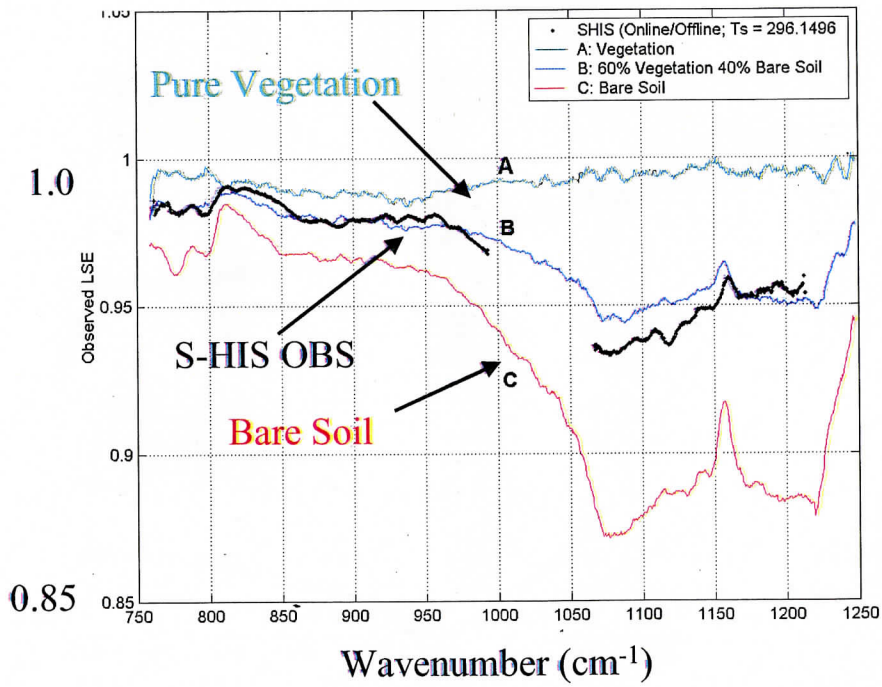

Fig. 5: The upper panel shows the approximate field of view sizes of AIRS, Scanning HIS, and MODIS instruments over an aerial photograph of the vicinity of the DOE ARM SGP central facility site. The lower panel shows that the effective land surface emissivity derived from Scanning HIS observations from 31 March 2001 18:45 UTC (averaged over 15 km) can be approximated by a linear combination of pure scene types (grass and bare soil). The best fit to these observations is 60% vegetation and 40% bare soil.

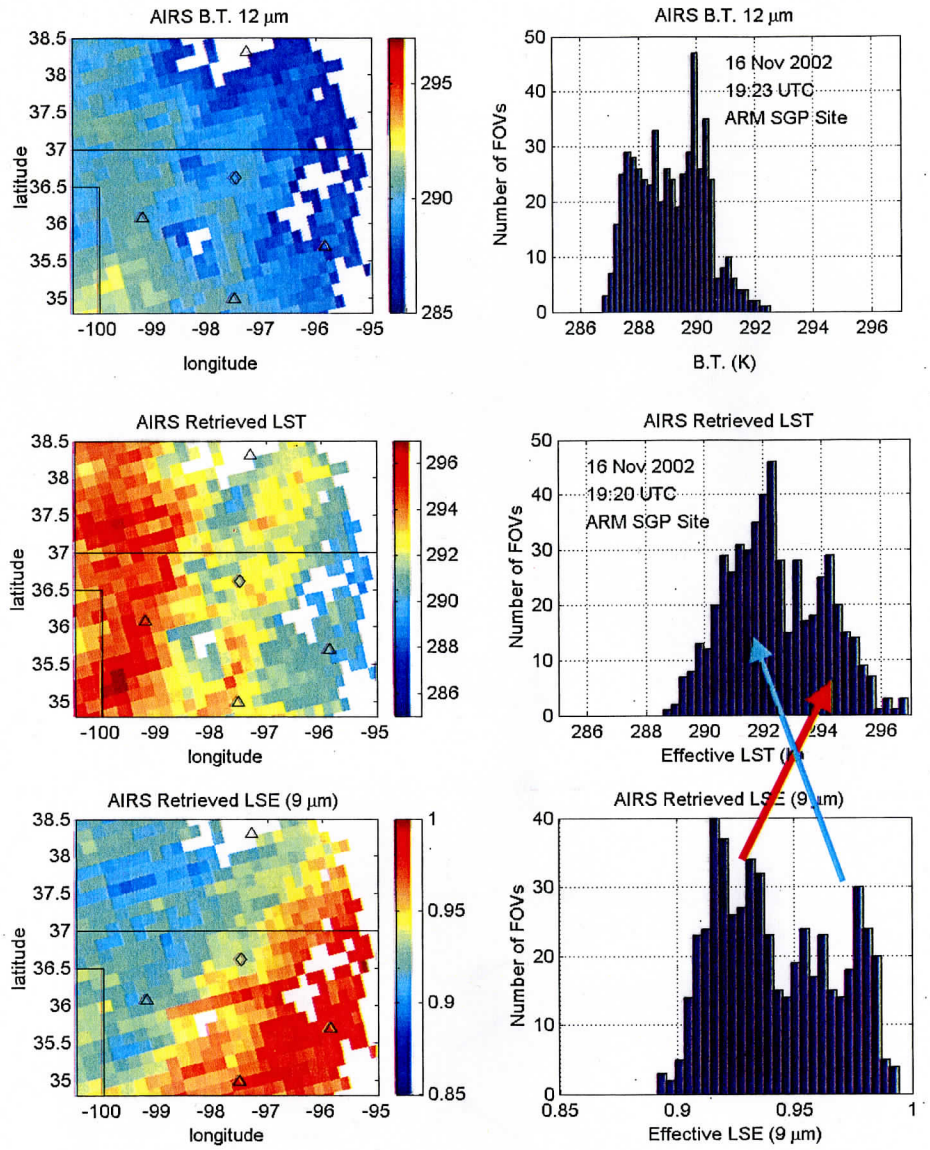

Fig. 6: The observed AIRS brightness temperature at 12 μm over the DOE ARM SGP site in north central Oklahoma, USA (16 Nov 2002 19 UTC) is shown in the upper panels as a brightness temperature map and as the corresponding histogram. The center panels show the land surface emissivity derived from the AIRS observations using the methodology described in the text. Note that the single brightness temperature distribution shifts to warmer temperatures and becomes two distinct distributions. The effective land surface emissivity derived simultaneously with the land surface temperature is shown in the lower panels. Lower emissivity values (at 9 μm) correspond to regions of higher surface temperaure. The results are consistent with the land cover survey which indicates that the central facility (indicated by the diamond symbol) is near the transition between high emissivity grassland (100% vegetation) to the southeast and wheat farming (mixed vegetation) with more low emissivity bare soil exposed.

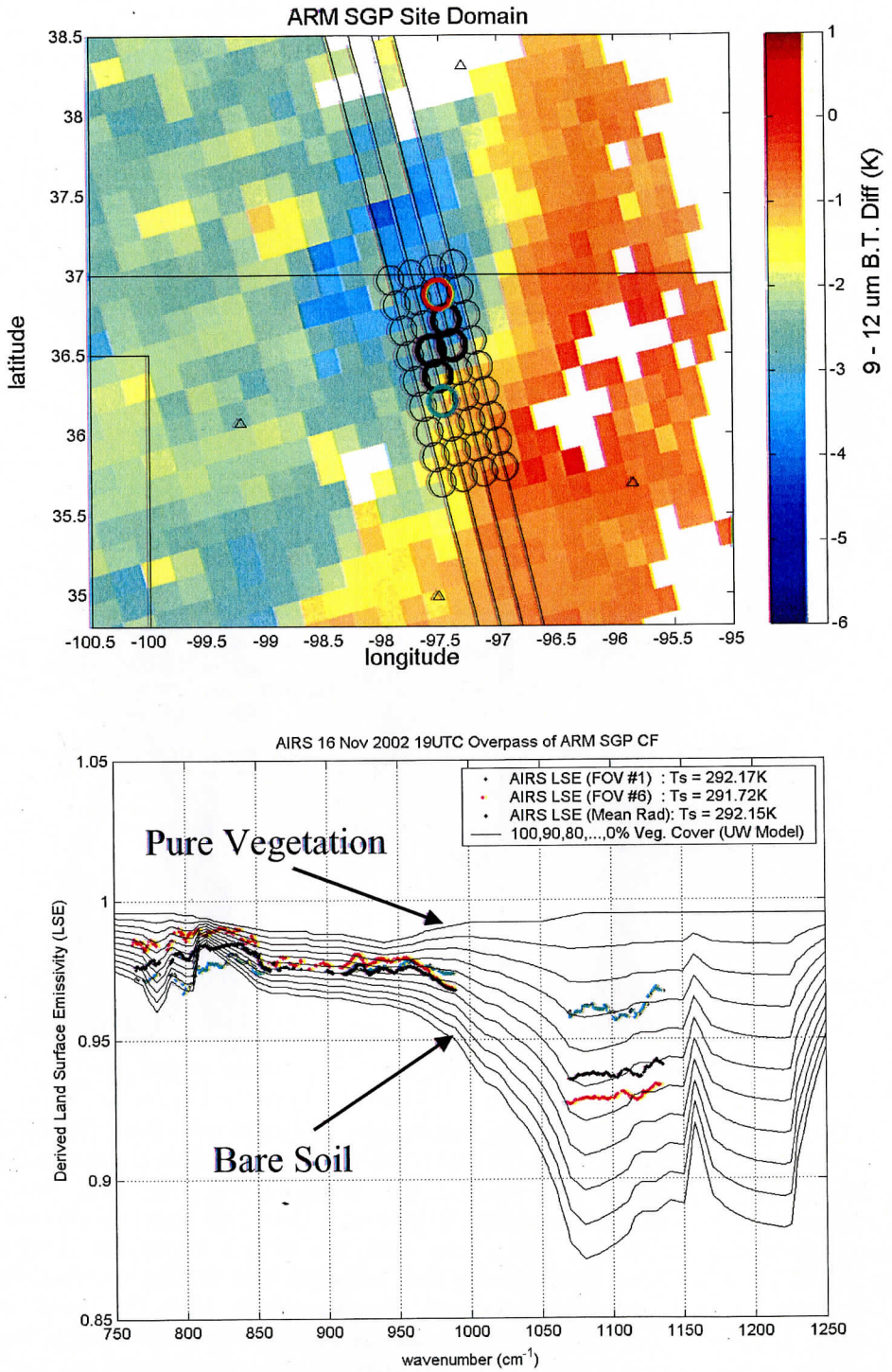

Fig. 7: Highlighted AIRS fields of view in the region near the DOE ARM SGP central facility (upper panel) show considerable variability in the effective emissivity (lower panel) derived from the AIRS radiances (16 Nov 2002 19 UTC). [UW Research Product]

Appendix C: Bibliography

Literature supported fully or in part by NPOESS/IPO Contract 50-SPNA-1-00039 is included here. A more extensive list of related efforts can be obtained at http://nimbus.ssec.wisc.edu/~davet/docs/.

2001 (Sept.-Dec. only)

DeSlover, Daniel H.; Nasiri, Shaima; Knuteson, Robert O., and Revercomb, Hank E. Measurement of cirrus cloud optical properties from ground- and aircraft-based high spectral resolution interferometry. *Remote Sensing of Clouds and the Atmosphere VI*, Toulouse, France, 17-20 September 2001. Bellingham, WA, International Society for Optical Engineering, (SPIE), 2001, pp1-7. Reprint #3358.

Huang, Hung-Lung; Wu, Xiangqian; Li, Jun; Antonelli, Paolo; Knuteson, Robert O.; Olson, Erik R.; Baggett, Kevin C., and Osborne, Brian J. Simultaneous retrieval of cloud height and effective emissivity from hyperspectral radiance measurements. *Conference on Satellite Meteorology and Oceanography, 11th*, Madison, WI, 15-18 October 2001 (preprints). Boston, MA, American Meteorological Society, 2001, pp496-499. Reprint #2986.

Knuteson, Robert; Osborne, Brian; Revercomb, Henry; Tobin, David, and Smith, William L. Infrared land surface emissivity retrieval from high-spectral resolution upwelling radiance. *Conference on Satellite Meteorology and Oceanography, 11th*, Madison, WI, 15-18 October 2001 (preprints). Boston, MA, American Meteorological Society, 2001, pp688-691. Reprint #2998.

Tanamachi, Robin L.; Walden, Von P.; Ackerman, Steven A., and Knuteson, Robert O. Quality control and preliminary data analysis of the Interferometric Monitor for Greenhouse gases (IMG) data set. *Conference on Satellite Meteorology and Oceanography, 11th,* Madison, WI, 15-18 October 2001 (preprints). Boston, MA, American Meteorological Society, 2001, pp692-695. Reprint #3095.

Vinson, Kenneth; Revercomb, Henry; Howell, H. Ben, and Knuteson, Robert. CO and CH4 column retrieval from the Scanning High-resolution Interferometer Sounder (S-HIS). *Conference on Satellite Meteorology and Oceanography, 11th,* Madison, WI, 15-18 October 2001 (preprints). Boston, MA, American Meteorological Society, 2001, pp666-669. Reprint #2996.

2002

DeSlover, DH, RO Knuteson, DD Turner, DN Whiteman, and WL Smith. 2002. "AERI and Raman Lidar Cirrus Cloud Optical Depth Retrieval to Validate Aircraft-Based Cirrus Measurements." In *Proceedings of the Twelfth ARM Science Team Meeting*, Ed. by D. Carrothers, U.S. Department of Energy, Richland, WA.

DeSlover, Daniel H.; Knuteson, Robert O.; Osborne, Brian; Zhou, Daniel K., and Smith, William L. Validation of aircraft-measured land surface emissivity. *Optical Remote Sensing of the*

Atmosphere and Clouds III, Hangzhou, China, 25-27 October 2002. Bellingham, WA, International Society for Optical Engineering, (SPIE), 2003, pp384-391. Reprint #3475.

DeSlover, D. H., D. D. Turner, D. N. Whiteman, and W. L. Smith (2002): Ground-based measurement of cirrus cloud optical properties as validation to aircraft- and satellite-based cloud studies. In *Proceedings from the 9th International SPIE Symposium on Remote Sensing: Remote Sensing of the Clouds and Atmosphere VII*, Crete, Greece.

DeSlover, D. H., D. D. Turner, D. N. Whiteman, and W. L. Smith (2002): Ground- and aircraft-based cirrus cloud measurements using lidar and high spectral resolution FTS during the AFWEX 2000 field campaign. In *Proceedings from the 47th Annual SPIE meeting: Atmospheric Radiation Measurements and Applications in Climate*, Seattle, WA.

Knuteson, Robert O.; DeSlover, Dan H.; Larar, Allen M.; Osborne, Brian; Revercomb, Henry E.; Short, John F.; Smith, William L., and Tanamachi, Robin. Infrared land surface remote sensing using high spectral resolution observations. Multispectral and Hyperspectral *Remote Sensing Instruments and Applications*, Hangzhou, China, 25-27 October 2002. Bellingham, WA, International Society for Optical Engineering, (SPIE), 2003, pp24-35. Reprint #3606.

Mitchell, D. L., R. P. d'Entremont, D. H. DeSlover, and W. P. Arnott (2002): Multispectral thermal retrievals of size distribution shape, effective size, ice water path and photon tunneling contribution. In *Proceedings of the 12th ARM Science Team Meeting*, St. Petersburg, FL.

Olson, E. R.; Revercomb, H. E.; Knuteson, R. O.; Howell, H. B.; LaPorte, D. D.; Ellington, S. D.; Werner, M. W.; Garcia, R. K., and Best, F. A. Vibration induced tilt error model for aircraft interferometer data. *International Symposium on Remote Sensing, 9th*, Athens, Greece, 2 September 2002 (proceedings). *Within the Sensors, Systems, and Next Generation Satellites Conference, 8th* (proceedings). Bellingham, WA, SPIE-The International Society for Optical Engineering, 2002. Reprint #3197.

Revercomb, Henry E.; Knuteson, Robert O.; Best, Fred A.; Tobin, David C.; Smith, William L.; Feltz, Wayne F.; Petersen, Ralph A.; Antonelli, Paolo; Olson, Erik R.; LaPorte, Daniel D.; Ellington, Scott D.; Werner, Mark W.; Dedecker, Ralph G.; Garcia, Ray K.; Ciganovich, Nick N.; Howell, H. Benjamin; Vinson, Ken, and Ackerman, Steven A. Applications of high spectral resolution FTIR observations demonstrated by radiometrically accurate ground-based AERI and Scanning HIS aircraft instruments. *Multispectral and Hyperspectral Remote Sensing Instruments and Applications*, Hangzhou, China, 25-27 October 2002. Bellingham, WA, International Society for Optical Engineering, (SPIE), 2003, pp11-23. Reprint #3605.

Zhou, Daniel K.; Smith, William L.; Li, Jun; Howell, Hugh B.; Cantwell, Greg W.; Larar, Allen M.; Knuteson, Robert O.; Robin, David C.; Revercomb, Henry E., and Mango, Stephen A. Thermodynamic product retrieval methodology and validation for NAST-I. *Applied Optics* v.41, no.33, 2002, pp6957-6967. Reprint #3244.

Vinson, Kenneth H.; Revercomb, Henry E.; Howell, H. Benjamin; Knuteson, Robert O., and Smith, William L. Carbon monoxide and methane column retrieval from the Scanning High Resolution Interferometer Sounder (S-HIS) and National Polar-orbiting Operational

Environmental Satellite System Airborne Sounder Testbed- Interferometer (NAST-I). *Optical Remote Sensing of the Atmosphere and Clouds III*, Hangzhou, China, 25-27 October 2002. Bellingham, WA, International Society for Optical Engineering, (SPIE), 2003, pp472-482. Reprint #3474.

Wang, Z., D. Whiteman, K. Sassen, B. Demoz, and D. DeSlover (2002): Mixed phase cloud properties derived from Raman lidar and depolarized lidar measurements: A case study. In *Proceedings from the 21st ILRC*, Quebec, Canada.

2003

Ackerman, Steven A.; Tobin, D.; Knuteson, R.; Antonelli, P.; Revercomb, H., and Vinson, K. Fire detection and properties from high-spectral resolution infrared observations. *Conference on Satellite Meteorology and Oceanography*, 12th, Long Beach, CA, 9-13 February 2003 (preprints). Boston, MA, American Meteorological Society, 2003.

Antonelli, P. et al., 2003: Validation and Comparison of S-HIS and NAST-I Retrievals for THORPEX-2003, *Intl. TOVS Study Conference - XIII*, Ste. Adele, Canada, 29 October - 4 November 2003.

DeSlover, D. H., D. D. Turner, and R. O. Knuteson (2003): AERI measured cirrus cloud optical depth and particle size. In *Proceedings from the 13th ARM Science Team Meeting*, Denver, Colorado.

Feltz, W. F., D. D. Turner, D. H. DeSlover, R. G. Dedecker, R. O. Knuteson (2003): Rapid scan AERI observations during CRYSTAL FACE and Texas 2002: Analysis and benefits. In *Proceedings from the 13th ARM Science Team Meeting*, Denver, CO.

Ivanova, D. C., D. L. Mitchell, G. M. McFarquhar, and D. H. DeSlover (2003): Tropical cirrus parameterization for bimodal ice size spectra. In *Proceedings from the 13th ARM Science Team Meeting*, Denver, CO.

Knuteson, R., F. Best, D. DeSlover, B. Osborne, H. Revercomb, and W. Smith, Sr., 2004: Infrared land surface remote sensing using high spectral resolution aircraft observations, *Adv. Space Res.*, Vol. 33, 2004 (in press).

Knuteson et al., 2003: Aircraft Measurements for Validation of AIRS Land Surface Temperature and Emissivity Products at the Southern Great Plains Validation Site, *Optical Society of America ORS/FTS Topical Meeting*, Quebec-City, 3-6 February, 2003

Knuteson, RO, RG Dedecker, WF Feltz, BJ Osborne, HE Revercomb, and DC Tobin. 2003. "Infrared land surface emissivity in the vicinity of the ARM SGP central facility." In *Proceedings of the Thirteenth Atmospheric Radiation Measurement (ARM) Science Team Meeting*, Ed. by D. Carrothers, Department of Energy, Richland, WA.

Knuteson, R., B. Osborne, H. Revercomb, W. Smith, and D. Tobin, 2003: Validation of Satellite AIRS LST/LSE Products Using Aircraft Observations, *Intl. TOVS Study Conference - XIII*, Ste. Adele, Canada, 29 October - 4 November 2003.

Knuteson, R., H. Revercomb, D. Tobin, B. Osborne, 2003: Land Surface Product Validation Using the DOE ARM Southern Great Plains Site, *Eos Trans. AGU*, 84(46), Fall Meet. Suppl., Abstract B21E-0751, 2003.

Knuteson, R., P. Antonelli, F. Best, S. Dutcher, W. Feltz, and H. Revercomb, 2003: Scanning High-resolution Interferometer Sounder (S-HIS) measurements during the International Water-Vapor Project (IHOP), *Proceedings of the 6th International Symposium on Tropospheric Profiling: Needs and Technologies*, September 14-20, 2003, Leipzig, Germany.

Mlawer, E. J., S. A. Clough, D. C. Tobin, 2003: The MT_CKD Water Vapor Continuum: A Revised Perspective Including Collision Induced Effects, *ASSFTS (Atmospheric Science from Space using Fourier Transform Spectrometry) 11 Workshop*, Bad Wildbad (Black Forest), Germany, 8-10 October 2003.

McMillan, W. W.; McCourt, M. L.; Revercomb, H. E.; Knuteson, R. O.; Christian, T. J.; Doddridge, B. G.; Hobbs, P. V.; Lukovich, J. V.; Novelli, P. C.; Piketh, S. J.; Sparling, L.; Stein, D.; Swap, R. J., and Yokelson, R. J. Tropospheric carbon monoxide measurements from the Scanning High-Resolution Interferometer Sounder on 7 September 2000 in southern Africa during SAFARI 2000. *Journal of Geophysical Research* v.108, no.D13, 2003, pp(SAF 28-1)-(SAF 28-13). Reprint #3554.

Mitchell, D. L., D. DeSlover, R. P. d'Entremont (2003): Remote sensing of small ice crystal concentrations. In *Proceedings from the 13th ARM Science Team Meeting*, Denver, CO.

Mitchell, D. L., R. P. d'Entremont, D. H. DeSlover, and W. P. Arnott (2003): Multispectral Thermal Retrievals of Size Distribution Shape, Effective Size, Ice Water Path and Photon Tunneling Contribution. In *Proceedings from the 83rd AMS Annual Meeting*, Long Beach, CA.

Moeller, Christopher C.; Revercomb, Henry E.; Ackerman, Steven A.; Menzel, W. Paul, and Knuteson, Robert O (2003). Evaluation of MODIS thermal IR and L1B radiances during SAFARI 2000. *Journal of Geophysical Research* v.108, no.D13, 2003, (SAF 30-1)-(SAF 30-12). Reprint #3553.

Revercomb et al., 2003: Atmospheric Infrared Sounder (AIRS) validation with the Scanning High resolution Infrared Sounder (SHIS), *Optical Society of America ORS/FTS Topical Meeting*, Quebec City, 3-6 February, 2003.

Revercomb et al., 2003: Scanning-HIS Aircraft Instrument Calibration and AIRS Validation, *CALCON 2003, Characterization and Radiometric Calibration for Remote Sensing*, Space Dynamics Laboratory / Utah State University, Logan, Utah, 15-18 September 2003.

Revercomb, H. E. D. Tobin, R. Knuteson, F. Best, W. Smith, P. van Delst, D. LaPorte, S. Ellington, M. Werner, R. Dedecker, R. Garcia, N. Ciganovich, H. Howell, S. Dutcher, and J. Taylor, 2003: Validation of AIRS Spectral Radiances with the Scanning HIS Aircraft, *Intl. TOVS Study Conference - XIII*, Ste. Adele, Canada, 29 October - 4 November 2003.

Revercomb, H. E., 2003: Steps to Producing Calibrated Radiances and SDR Input Parameters, CrIS Calibration/Validation Working Group Meeting, ITT, Fort Wayne, IN, 9 December 2003.

Tjemkes, S. A.; Patterson, T.; Rizzi, R.; Shephard, M. W.; Clough, S. A.; Matricardi, M.; Haigh, J. D.; Hopfiner, M.; Payan, S.; Trotsenko, A.; Scott, N.; Rayer, P.; Taylor, J. P.; Clerbaux, C.; Strow, L. L.; DeSouza-Machado, S.; Tobin, D., and Knuteson, R. The ISSWG line-by-line inter-comparison experiment. *Journal of Quantitative Spectroscopy and Radiative Transfer* v.77, no.4, 2003, pp433-453. Reprint #3439.

Tobin et al., (2003): On-orbit Spectral Calibration of the Geosynchronous Imaging Fourier Transform Spectrometer (GIFTS), *CALCON 2003, Characterization and Radiometric Calibration for Remote Sensing*, Space Dynamics Laboratory / Utah State University, Logan, Utah, 15-18 September 2003

Whiteman, D, B. Demoz, Z. Wang, C. Barnet, R. Hoff, W. McMillan, I. Veselovskii, K. McCann, F. Russo, A. Gambacorta, K. Lightner, E. Maddy, J. Comer, N. Kolb, D. DeSlover, G. Jedlovec, M. Cadirola (2003): Use of Raman lidar for validation of Aqua retrievals and the study of AIRS radiances. In *Proceedings from IGARSS 2003*, Toulouse, France.

2004

Antonelli, Paolo; Cherubini, T.; Revercomb, H.; Businger, S.; Knuteson, R.; Posselt, D., and Ackerman, S. Comparison of S-HIS temperature and water vapor retrievals to MM5 derived fields for THORPEX 2003. *Symposium on Integrated Observing and Assimilation Systems for Atmosphere, Oceans, and Land Surface, 8th*, Seattle, WA, 11-15 January 2004 (preprints). Boston, MA, American Meteorological Society, 2004.

Dutcher, Steven T.; Garcia, Ray K.; Dedecker, Ralph G.; Knuteson, Robert O.; Smuga-Otto, Maciek; Hackel, Denny J.; Nasiri, Shaima, and Antonelli, Paolo. Hyperspectral data storage: Prototype implementation using the 2003 Pacific THORPEX dataset. *International Conference on Interactive Information and Processing Systems (IIPS) for Meteorology*, Oceanography, and Hydrology, 20th, Seattle, WA, 11-15 January 2004 (preprints). Boston, MA, American Meteorological Society, 2004, Paper P2.30. Reprint #3648.

Revercomb, Henry E.; Ackerman, S. A.; Best, F.; Dedecker, R.; Feltz, W.; Garcia, R. K.; Huang, H.-L.; Knuteson, R. O.; Li, J.; Tobin, D.; Velden, C. S., and Smith, W. L. The path to high spectral resolution IR observing: Looking backward and forward as a new era begins with AIRS. *International Conference on Interactive Information and Processing Systems (IIPS) for Meteorology*, Oceanography, and Hydrology, 20th, Seattle, WA, 11-15 January 2004 (preprints). Boston, MA, American Meteorological Society, 2004, manuscript not available for publication.